

NPS ARCHIVE
1966
EDWARDS, R.

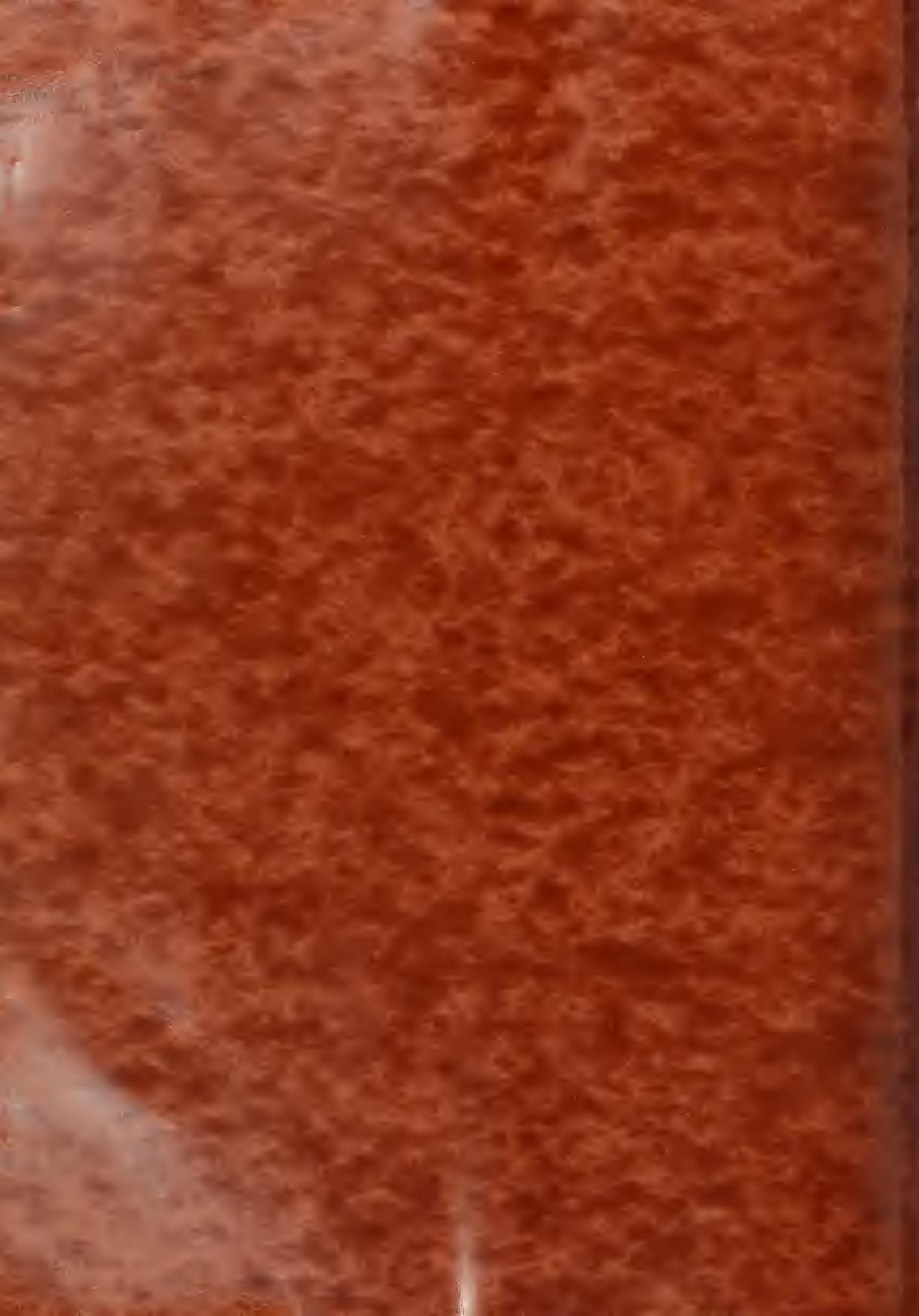
LT. RODERICK YERKES EDWARDS , JR., USCG

XIII A

PREDICTION OF BOUNDARY LAYER EFFECTS

ON MARINE PROPELLER SECTIONS

Thesis
E254



-1-

PREDICTION OF BOUNDARY LAYER EFFECTS ON
MARINE PROPELLER SECTIONS

by

LT. ROBERT W. YERGEN, JR., USCG

//

SUBMITTED TO THE DEPARTMENT OF NAVAL ARCHITECTURE AND MARINE
ENGINEERING IN PARTIAL FULFILLMENT OF THE REQUIREMENTS FOR
THE MASTER OF SCIENCE DEGREE IN MECHANICAL ENGINEERING
AND THE PROFESSIONAL DEGREE, NAVAL ENGINEER

at the

MASSACHUSETTS INSTITUTE OF
TECHNOLOGY

May, 1966

Signature of Author
Department of Naval Architecture and
Marine Engineering, May 20, 1966

Certified by
Thesis Supervisor

Certified by
Thesis Supervisor

Accepted by
Chairman, Departmental Committee
on Graduate Students

ABSTRACT

PRESENTATION OF BOUNDARY LAYER EFFECTS ON
MARINE PROPELLER SECTIONS

by

Lt. Frederick Veritas Edwards, Jr., USCG

Submitted to the Department of Naval Architecture and Marine Engineering on May 20, 1966 in partial fulfillment of the requirements for the Master of Science Degree in Mechanical Engineering and the Professional Degree, Naval Engineer.

Heretofore viscous corrections used in the design of thin marine propeller and hydrofoil sections have been based upon data obtained from experiments with relatively thick sections. In an attempt to improve this process, the viscous effects on the lift of an extremely thin, low camber airfoil section were studied experimentally.

An airfoil of small thickness and low camber was constructed and instrumented for the measurement of pressure distribution along the chord. Measurements were made of the velocity distribution normal to the surface of the foil at points along the chord for several angles of attack and two Reynolds Numbers, using "Pike" type sensors. The displacement thickness of the boundary layer along the chord was then determined. Increasing the dimensions of the actual foil by the displacement thickness and treating the resulting form as a solid body in potential flow was the method used for determining the viscous correction in this work. The result of the

THE

THE

THE

THE

THE

THE

THE

THE

THE

THE

THE

THE

THE

THE

THE

THE

THE

THE

THE

THE

THE

THE

THE

solution to potential flow about this altered body was then compared with the experimentally determined pressure distribution. Comparison of the limited amount of data with theoretical predictions is not conclusive, but suggests that with improved instrumentation, this relatively straightforward procedure will be successful.

ACKNOWLEDGMENTS

The author expresses his appreciation for the contributions of Professor J. E. Keenan, Thesis Supervisor, who first aroused my interest in viscous effects on Marine Propeller and foil design, and to Professor Hal L. Moses, for his help on the subject of boundary layers.

I am particularly grateful to Professor J. Micknell for his guidance in the wind tunnel work and to Messers, Massachusetts, Christensen, and Herbert Johnson of the various gas turbine laboratory shops, for their help in building the model.

I wish to thank Lieutenant Peter Bergen, USN, Lieutenant Willard Firebaugh, USN, Lieutenant Robert Cheney, USN, and Lieutenant Paul Amos, USN, all of whom assisted me in the wind tunnel, and without whose help I would have been unable to operate the tunnel.

Finally, I would like to thank Mrs. Joyce Edwards, Jr., who spent several weeks in the wind tunnel taking data with me at night and who has patiently deciphered my "rough drafts" in typing this thesis.

CONTENTS

1. Introduction 1
2. The problem of the origin of the universe 2
3. The problem of the origin of life 3
4. The problem of the origin of the human race 4
5. The problem of the origin of the human mind 5
6. The problem of the origin of the human soul 6
7. The problem of the origin of the human body 7
8. The problem of the origin of the human spirit 8
9. The problem of the origin of the human intellect 9
10. The problem of the origin of the human will 10
11. The problem of the origin of the human emotions 11
12. The problem of the origin of the human passions 12
13. The problem of the origin of the human virtues 13
14. The problem of the origin of the human vices 14
15. The problem of the origin of the human sins 15
16. The problem of the origin of the human crimes 16
17. The problem of the origin of the human wars 17
18. The problem of the origin of the human diseases 18
19. The problem of the origin of the human death 19
20. The problem of the origin of the human resurrection 20

TABLE OF CONTENTS

	<u>PAGE</u>
ABSTRACT	2
ACKNOWLEDGMENTS	4
TABLE OF CONTENTS	5
LIST OF FIGURES	7
I. INTRODUCTION	
A. BACKGROUND	9
B. STATEMENT OF THE PROBLEM	11
C. OBJECTIVES	12
II. PROCEDURE	
A. EXPERIMENTAL APPARATUS	14
1. FOIL DESIGN	14
2. DESIGN OF THE TEST SECTION	16
3. MEASURING APPARATUS	16
4. SET UP PROBLEMS	19
B. EXPERIMENTAL METHOD	20
C. ANALYSIS OF THE DATA	25
1. BOUNDARY LAYER COMPUTATION	25
2. CALCULATION OF THE PRESSURE COEFFICIENTS	30
III. RESULTS	
A. RESULTS OF THE BOUNDARY LAYER MEASUREMENTS	32
B. RESULTS OF THE PRESSURE COEFFICIENT MEASUREMENTS ..	34
C. RESULTS OF CORRELATED PLOTS	36
D. CARBON BLACK TRACES	37

IV.	DISCUSSION OF RESULTS	
A.	GENERAL	39
B.	BOUNDARY LAYER PROFILES	44
C.	DISCUSSION OF POTENTIAL FLOW CALCULATIONS WITH CORRECTED FORMS	46
V.	CONCLUSIONS	49
VI.	RECOMMENDATIONS FOR FURTHER STUDY	51
VII.	BIBLIOGRAPHY	53
VIII.	APPENDIX	55
A.	TABLE OF DATA	
B.	GRAPHS OF DATA	
C.	COMPUTER OUTPUTS	

LIST OF FIGURES

	<u>PAGE</u>
FIGURE 1. DETAIL OF PRESSURE TAPS	15A
FIGURE 2. DETAIL OF END WALLS	15B
FIGURE 3. BOUNDARY LAYER RAKE	17A
FIGURE 4. INCLINED MANOMETER BANK	17A
FIGURE 5. AUXILIARY BOUNDARY LAYER RAKE	17A
FIGURE 5A. AUXILIARY STATIC PROBES	17A
FIGURE 6. BOUNDARY LAYER RAKE AND MANOMETER	17A
FIGURE 7. INCLINED MANOMETER IN POSITION	20A
FIGURE 8. INDIRECT READING MANOMETER	20A
FIGURE 9A. RAKE IN POSITION SHOWING "STRIPATUBE"	20A
FIGURE 9B. RAKE POSITIONED ADJACENT TO STATIC TAPS	20A
FIGURE 10A. FOIL IN TEST SECTION SHOWING STANCHION	25A
FIGURE 10B. FOIL IN TEST SECTION SHOWING ADDITIONAL TUBES FROM AUXILIARY RAKE	25A
FIGURE 11. CARBON BLACK TRANSITION TESTS	25A
FIGURE 12. CHORD WISE DISPLACEMENT THICKNESS DEVELOPMENT .. $\alpha = 0.0^\circ$	B1
FIGURE 13. CHORD WISE DISPLACEMENT THICKNESS DEVELOPMENT .. $\alpha = 2.0^\circ$	B2
FIGURE 14. VELOCITY PROFILES FOR $\alpha = 0^\circ$, $Re = 3.67 \times 10^6$.. Top Surface	B3
FIGURE 15. VELOCITY PROFILES FOR $\alpha = 0^\circ$, $Re = 3.67 \times 10^6$.. Bottom Surface	B4
FIGURE 16. VELOCITY PROFILES FOR $\alpha = 2^\circ$, $Re = 3.67 \times 10^6$.. Top Surface	B5
FIGURE 16A. VELOCITY PROFILES FOR $\alpha = 2^\circ$, $Re = 3.67 \times 10^6$.. Bottom Surface	B6

INDEX

100	1. ROAD TO RUSSIA 1917
100	2. ROAD TO RUSSIA 1918
100	3. ROAD TO RUSSIA 1919
100	4. ROAD TO RUSSIA 1920
100	5. ROAD TO RUSSIA 1921
100	6. ROAD TO RUSSIA 1922
100	7. ROAD TO RUSSIA 1923
100	8. ROAD TO RUSSIA 1924
100	9. ROAD TO RUSSIA 1925
100	10. ROAD TO RUSSIA 1926
100	11. ROAD TO RUSSIA 1927
100	12. ROAD TO RUSSIA 1928
100	13. ROAD TO RUSSIA 1929
100	14. ROAD TO RUSSIA 1930
100	15. ROAD TO RUSSIA 1931
100	16. ROAD TO RUSSIA 1932
100	17. ROAD TO RUSSIA 1933
100	18. ROAD TO RUSSIA 1934
100	19. ROAD TO RUSSIA 1935
100	20. ROAD TO RUSSIA 1936
100	21. ROAD TO RUSSIA 1937
100	22. ROAD TO RUSSIA 1938
100	23. ROAD TO RUSSIA 1939
100	24. ROAD TO RUSSIA 1940
100	25. ROAD TO RUSSIA 1941
100	26. ROAD TO RUSSIA 1942
100	27. ROAD TO RUSSIA 1943
100	28. ROAD TO RUSSIA 1944
100	29. ROAD TO RUSSIA 1945
100	30. ROAD TO RUSSIA 1946
100	31. ROAD TO RUSSIA 1947
100	32. ROAD TO RUSSIA 1948
100	33. ROAD TO RUSSIA 1949
100	34. ROAD TO RUSSIA 1950
100	35. ROAD TO RUSSIA 1951
100	36. ROAD TO RUSSIA 1952
100	37. ROAD TO RUSSIA 1953
100	38. ROAD TO RUSSIA 1954
100	39. ROAD TO RUSSIA 1955
100	40. ROAD TO RUSSIA 1956
100	41. ROAD TO RUSSIA 1957
100	42. ROAD TO RUSSIA 1958
100	43. ROAD TO RUSSIA 1959
100	44. ROAD TO RUSSIA 1960
100	45. ROAD TO RUSSIA 1961
100	46. ROAD TO RUSSIA 1962
100	47. ROAD TO RUSSIA 1963
100	48. ROAD TO RUSSIA 1964
100	49. ROAD TO RUSSIA 1965
100	50. ROAD TO RUSSIA 1966
100	51. ROAD TO RUSSIA 1967
100	52. ROAD TO RUSSIA 1968
100	53. ROAD TO RUSSIA 1969
100	54. ROAD TO RUSSIA 1970
100	55. ROAD TO RUSSIA 1971
100	56. ROAD TO RUSSIA 1972
100	57. ROAD TO RUSSIA 1973
100	58. ROAD TO RUSSIA 1974
100	59. ROAD TO RUSSIA 1975
100	60. ROAD TO RUSSIA 1976
100	61. ROAD TO RUSSIA 1977
100	62. ROAD TO RUSSIA 1978
100	63. ROAD TO RUSSIA 1979
100	64. ROAD TO RUSSIA 1980
100	65. ROAD TO RUSSIA 1981
100	66. ROAD TO RUSSIA 1982
100	67. ROAD TO RUSSIA 1983
100	68. ROAD TO RUSSIA 1984
100	69. ROAD TO RUSSIA 1985
100	70. ROAD TO RUSSIA 1986
100	71. ROAD TO RUSSIA 1987
100	72. ROAD TO RUSSIA 1988
100	73. ROAD TO RUSSIA 1989
100	74. ROAD TO RUSSIA 1990
100	75. ROAD TO RUSSIA 1991
100	76. ROAD TO RUSSIA 1992
100	77. ROAD TO RUSSIA 1993
100	78. ROAD TO RUSSIA 1994
100	79. ROAD TO RUSSIA 1995
100	80. ROAD TO RUSSIA 1996
100	81. ROAD TO RUSSIA 1997
100	82. ROAD TO RUSSIA 1998
100	83. ROAD TO RUSSIA 1999
100	84. ROAD TO RUSSIA 2000
100	85. ROAD TO RUSSIA 2001
100	86. ROAD TO RUSSIA 2002
100	87. ROAD TO RUSSIA 2003
100	88. ROAD TO RUSSIA 2004
100	89. ROAD TO RUSSIA 2005
100	90. ROAD TO RUSSIA 2006
100	91. ROAD TO RUSSIA 2007
100	92. ROAD TO RUSSIA 2008
100	93. ROAD TO RUSSIA 2009
100	94. ROAD TO RUSSIA 2010
100	95. ROAD TO RUSSIA 2011
100	96. ROAD TO RUSSIA 2012
100	97. ROAD TO RUSSIA 2013
100	98. ROAD TO RUSSIA 2014
100	99. ROAD TO RUSSIA 2015
100	100. ROAD TO RUSSIA 2016

	<u>PAGE</u>
FIGURE 17. VELOCITY PROFILES FOR $\alpha = 0^\circ$, $Re = 5.45 \times 10^6$.. Top Surface	B7
FIGURE 17A. VELOCITY PROFILES FOR $\alpha = 0^\circ$, $Re = 5.45 \times 10^6$.. Bottom Surface	B8
FIGURE 18. WAKE SURVEYS AT 0.0°	B9
FIGURE 19. WAKE SURVEYS AT 2.0°	B10
FIGURE 20. EXPERIMENTAL PRESSURE DISTRIBUTION ALONG CHORD OF NACA 66 AIRFOIL	B11
$\alpha = 0.0^\circ$, $Re = 3.67 \times 10^6$	
FIGURE 21. TOP SURFACE PRESSURE DISTRIBUTION WITH RAKE ON THE SURFACE	B12
FIGURE 22. POTENTIAL THEORY PREDICTION FOR PRESSURE DISTRIBUTION AROUND NACA 66 AIRFOIL	B13
$\alpha = 0.0^\circ$, $Re = 3.67 \times 10^6$	
FIGURE 23. EXPERIMENTAL PRESSURE DISTRIBUTION ALONG THE CHORD OF A NACA 66 AIRFOIL	B14
$\alpha = 0.0^\circ$, $Re = 5.45 \times 10^6$	
FIGURE 24. EXPERIMENTAL PRESSURE DISTRIBUTION ALONG THE CHORD OF A NACA 66 AIRFOIL	B15
$\alpha = 2.0^\circ$, $Re = 3.67 \times 10^6$	
FIGURE 25. POTENTIAL THEORY PREDICTION FOR PRESSURE DISTRIBUTION AROUND NACA 66 AIRFOIL	B16
$\alpha = 2.0^\circ$, $Re = 3.67 \times 10^6$	
FIGURE 26. MOMENTUM THICKNESS VERSUS CHORD FOR THE TOP SURFACE	B17
$\alpha = 0.0^\circ$, $Re = 3.67 \times 10^6$	

I. INTRODUCTION

A. Background

As the design of high performance marine propellers and hydrofoils has become more exact, the desire to investigate all of the mechanisms of efficiency loss has naturally increased. One of the most evasive of these loss mechanisms is that of viscosity. It is obvious that viscosity, both molecular viscosity and the virtual or eddy viscosity arising in turbulent flow, contribute to the drag of the foil by providing for transfer of energy from the foil to the medium in which it operates, thereby increasing the power required to move the foil through this medium. A little less obvious is the fact that due to the way we have chosen to treat the motion of the foil mathematically, viscosity causes a discrepancy between the pressure distribution as we calculate it and what is actually measured in experiment.

In order to make the solution of the flow about a lifting form tractable, we choose not to solve the Navier Stokes Equations in all their glory, but rather by applying the unrealistic boundary condition of 100% slip at the boundary, we use Laplace's Equation for solving the so-called potential flow and apply the Kutta Condition at the trailing edge of the form to prevent the solution from giving results which we have observed do not occur, i.e. flow across the trailing edge. However, at the Reynolds Numbers around which these lifting surfaces operate, experiments indicate that there is a region around the foil where viscous effects are noticeable and in fact are of the same order of magnitude as the inertia forces. Thus, the existence of the boundary or shear layer around

the foil must be acknowledged if the artifice of potential theory is used to estimate flow behavior near the foil. The boundary layer is defined as the region quite near the surface of the foil where the velocity varies from zero at the surface to some high fraction of the velocity predicted by potential theory; in this thesis 0.992 has been chosen for this fraction. The flow then does not actually encounter the boundaries of the solid body as predicted by potential theory but it is assumed that it encounters boundaries which include the virtual thickness of the boundary layer, which allows no flow, i.e. displacement thickness. This change in the effective shape of the body then must change the lift since potential flow theory predicts a lift coefficient which is a function of geometry only. The boundary layer generally grows unsymmetrically about the nose-tail line of the foil and therefore moves the center of the trailing edge in the direction of the thickest surface boundary layer. This effectively changes the angle of attack of the section which the flow encounters causing an additional change in lift.

Limited experiments pursuing the determination of viscous effects on the lift of airfoil sections have been carried out by Pinkerton (1), Preston (2), Schneider (3), and Spence (4). In fact as far back as 1933, investigations were made into boundary layer development along two dimensional airfoils by Stuper (5). These experiments have been limited to foils of large thickness. However, for lack of better information, the results of these investigations have been used in the prediction of viscous effects in the design of thin marine propeller and hydrofoil sections, if viscous effects on the lift of these devices is considered

at all. Leopold (6), suggests that the above procedure is fallacious and proposes that since the boundary layer development on the surface of a foil is strongly dependent on the pressure distribution ($\frac{dp}{dx}$) and chord-wise Reynolds Number, the effects of thickness and Reynolds Number must indeed be incorporated in any consideration of lift alteration due to viscosity. Leopold recommends that the boundary layer on the surface of the foil be calculated using an approach developed by Moses (7), which has been programmed to accept the surface velocities predicted by potential theory, then the displacement thickness, $\delta^* = \int_0^{\delta} (1 - \frac{v}{V}) dy$ around the section is incorporated in the linear theory to predict the lift of the section in viscous flow. The concluding sections of Leopold's work recommend experimental work oriented toward establishing the validity of this approach.

B. STATEMENT OF THE PROBLEM

A proposed theory then exists for the determination of viscous lift correction which would be useful in the design of all foil sections but which is particularly applicable to foils used in Marine designs. However, no experimental work is available to uphold the theory. Errors may exist due to the difficulty in exactly stipulating the behavior of turbulent boundary layers in pressure gradients, and it is by no means clear that the pressure distribution around a body in viscous flow can be exactly modeled by the pressure distribution resulting from calculating the potential flow around the body "corrected" by δ^* . This method is, at best, an iterative approximation to the complicated Navier-Stokes Equations. The problem then, is first, to determine whether the measured

boundary layer thickness or more correctly, displacement thickness, when added to the dimensions of a foil, produces a shape whose potential flow solution for pressure distribution conforms to the measured pressure distribution. Second, since most algorithms for solving the turbulent boundary layer problem are accurate only for particular types of flow, i.e. (some breakdown in strong adverse pressure gradients, others in favorable gradients), the applicability of the boundary layer calculation chosen by Leopold must be checked in this particular physical situation. Perhaps the most elusive factor is the effect of the location of laminar-turbulent transition on both surfaces. The position of transition is extremely difficult to predict and is dependent on such parameters as surface roughness, turbulence level of the oncoming flow, and perturbations caused by vibration, in addition to the parameters which we feel we have reasonable ability to predict (dp/dx and Re_x). The thickness of the boundary layer toward the trailing edge and its effect on the angle of attack of the adjusted form is highly dependent on the transition point on each surface as well as on the relative transition points on the top and bottom surfaces.

C. OBJECTIVES

The objective of this thesis was to build and instrument a model of an extremely thin, low camber two dimensional section of a marine propeller or hydrofoil, measure the pressure distribution at reasonably high Reynolds Numbers and simultaneously measure the velocity distribution normal to the surface at points along the chord on both the pressure and suction sides. The dimensions of the foil were then to be

increased by the value of ζ^* gotten from the experimental results. Now, with the offsets of this altered form, the pressure distribution around it was to be calculated, using the most convenient and accurate potential theory type calculation. The computer program organized by T. Brockett (8) was used for this purpose, rather than linear theory as recommended by Leopold (6). The pressure distribution obtained from this calculation was then to be compared with that which was experimentally determined. The boundary layer measurements were to be compared with results of the calculations due to Moses (7), as modified by Leopold (6).

II. PROCEDURE

A. EXPERIMENTAL APPARATUS

The primary requirement of this experiment was to be able to measure accurately, (1) the chord-wise pressure distribution and (2) the velocity distribution in the boundary layer. These items were to be obtained at as high a Reynolds Number as is experienced by the 0.7 radius section of a marine propeller. This Reynolds Number is approximately 10^7 . The requirement for the test piece was that it be a reasonable model of a standard two dimensional foil section used in the design of propellers and hydrofoils.

1. FOIL DESIGN

The foil chosen was a NACA 66 modified nose and tail airfoil. The thickness ratio was to be 0.0333. A 1.0 mean line with 2% camber with a chord length of 60 inches was planned. Strength calculations were made, based on uniform lift along a 7 foot span with simple supports, and the results appeared marginal. The span was originally chosen to fit the vertical dimension of the test section of the Wright Brother's Wind Tunnel. Since it appeared that conventional foil construction methods would result in danger of structural failure at high Reynolds Numbers and high angles of attack as well as excess flexibility which might permit fluttering vibrations, it was decided to construct the foil of solid Honduras Mahogany reinforced in the span-wise direction by steel tubes. For reasons of economy, the span was reduced to four feet. Even with this modest span, robust construction was still necessary. Static pressure taps were installed in the upper and lower

surfaces by drilling down to the span-wise tubes and filling the holes with Epoxy. After the surface of the Epoxy was finished flush with the surface of the foil, 0.035 inch holes were drilled into the Epoxy normal to the surface and down into the tubes. The leading and trailing edges were milled out of solid aluminum, and fitted into the wooden part of the foil with steel keys.

The method of getting the pressure readings out of the wing as originally planned, appeared simple but, did not work out satisfactorily (Fig. 1). The center of each span-wise tube was plugged; effectively dividing each one into two tubes. The pressure taps were drilled down offset from the center of the span so that the upper and lower taps entered the tubes on either side of the plugs. This arrangement would allow the suction side pressures to be taken from one side of the foil and the pressure side from the other, thereby obtaining twenty-six pressure readings with only thirteen tubes. Unfortunately rendering the center plugs in the tubes air tight turned out to be impossible, and an alternate plan was used.

Galvanized steel sheet end plates were bolted to the ends of the foil. The ends of the pressure take-off tubes were threaded and used as fastenings for the end plates. The plates were used to cover the openings in the end walls of the test section which were required to allow the pressure tubes to swing in a 10° arc. They also served the purpose of housing bolts to hold the foil in position at various angles of attack (Fig. 2).

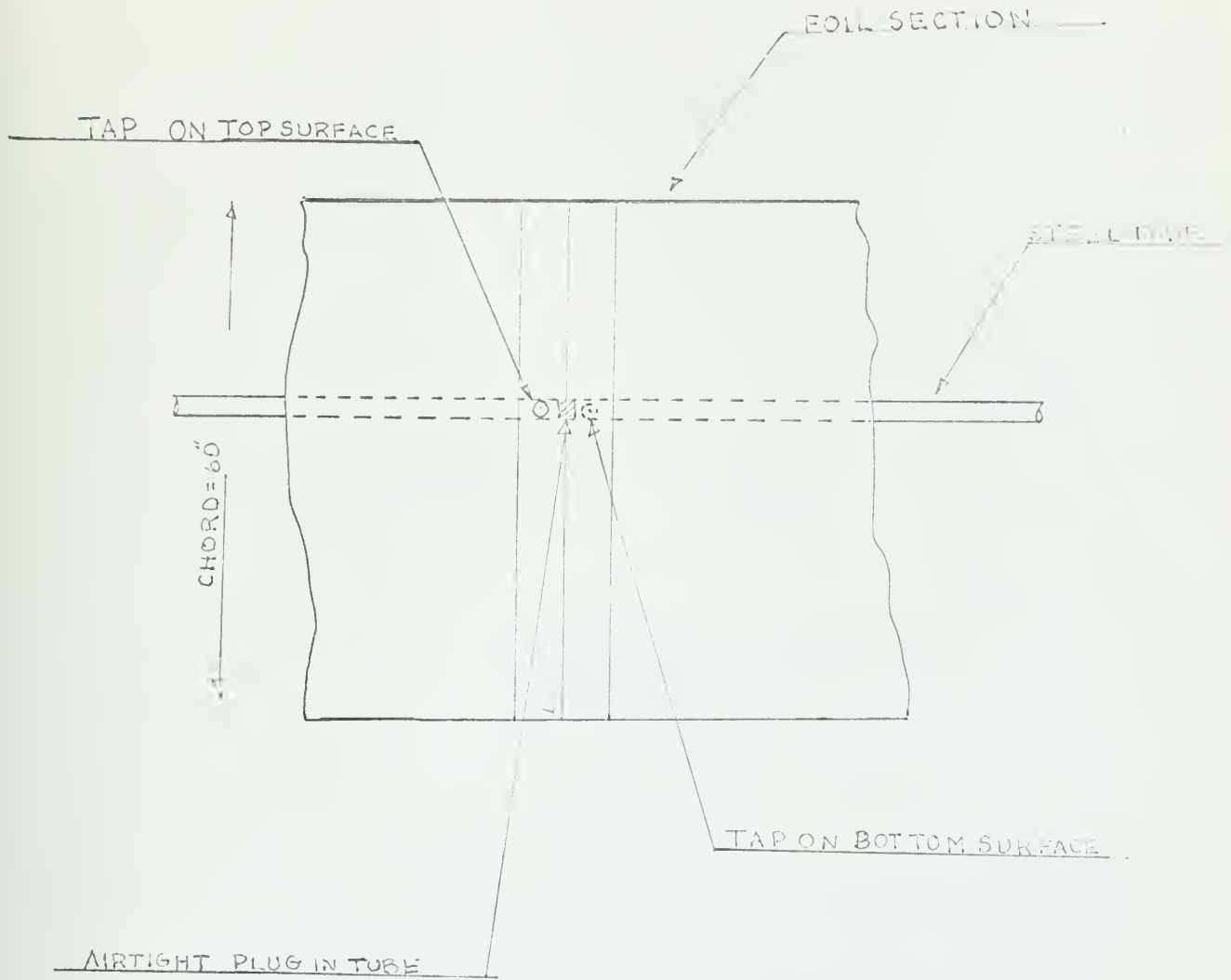


FIG. 1
DETAIL OF PRESSURE TAPS

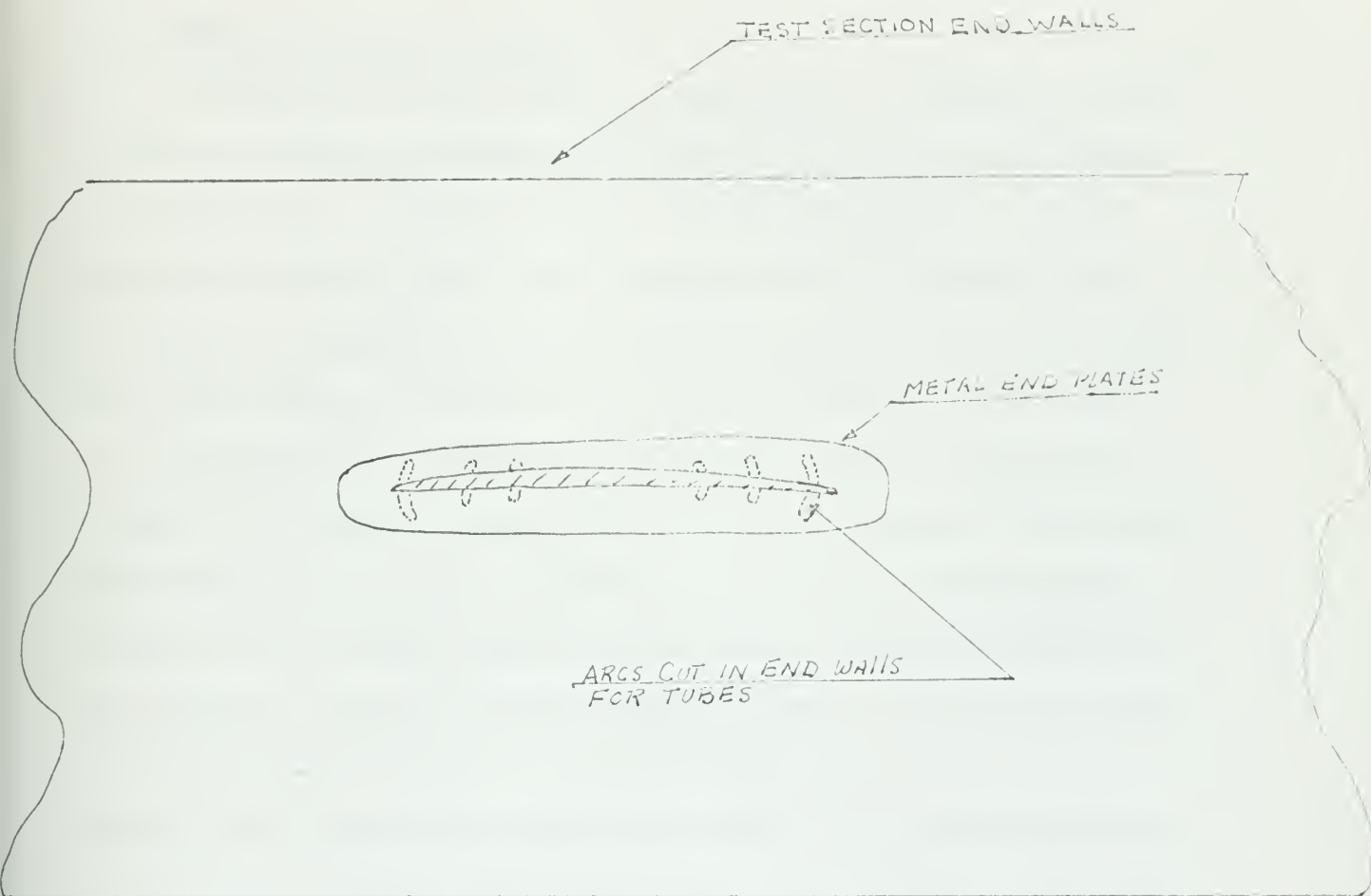


FIGURE 2.
END PLATES AND END WALLS

2. DESIGN OF THE TEST SECTION

The originally planned seven foot span would have enabled the test section of the Wright Brothers Wind Tunnel to be used without significant alteration. However, when the four foot span section was built instead, an elaborate test section was necessitated. The foil was to be placed horizontally in the tunnel between end walls which would span the entire length and height of the tunnel test section. These walls were fabricated from sections of fibre board fastened to foundations bolted to the tunnel overhead. The center of the fabricated test section had circular arcs cut into it which would allow all of the protruding pressure tubes to swing freely when the angle of attack of the section was changed. The part of the end walls into which the foil was fitted was given additional bracing, and metal bearing plates were bolted to them to accept the pivotal tube of the airfoil. The overall dimensions of the test section were $7\frac{1}{2}$ ft. high by 16ft. long with 4ft. between the end walls. The walls were toed out at the trailing edge by $\frac{3}{8}$ in. on each side to compensate for the nozzle effect caused by the development of a boundary layer along the test section. The amount of toe-out was determined by a simple flat plate turbulent boundary layer calculation for 5^* .

3. MEASURING APPARATUS

As mentioned in section 1, airtight plugging of the centers of the pressure tubes was not successful, therefore, the neoprene tubing from both sides of these tubes was connected to "T" joints and single tubes from the "T"s were connected to thirteen of the openings of a twenty-four

tube inclined manometer bank. Top and bottom pressures were measured on separate runs. When not in use, the holes of either suction or pressure sides were covered with a single long strip of very fine transparent tape.

The total pressure readings in the boundary layer on the surface of the foil were taken using a ten tube rake, built by the Aerodynamics Projects Laboratory (Fig. 3). The top tube of this rake was a static tube; the remaining nine tubes were total pressure tubes ranging in distance from the surface from 0.02in. to 1.0in. The tubes had elliptical openings to aid resolution. The dimensions of the tube openings were: major axis 0.03in., minor axis 0.01in. The major axis was parallel to the surface. The tubes connecting the rake to the manometer are called by the brand name "Stripatube" and the ten tubes come in a single strip with overall dimensions $1/8$ " by $2\frac{1}{2}$ " wide. The strip was led aft over the trailing edge down to a stanchion mounted on the tunnel floor, down the stanchion, along the tunnel floor and thence out of the test section to ten of the tubes on the inclined manometer bank (Fig. 4). The purpose of the stanchion was to reduce the angle at which the Stripatube fell away from the foil surface, thereby reducing drag on the tubing and hence eliminating the possibility of having the rake removed from the surface in the middle of a run. An additional total pressure rake was used in regions where the boundary layer thickness exceeded 0.8 inches. It consisted of two total pressure tubes approximately 1.25 inches and 1.50 inches above the surface. These tubes also had elliptical openings with the major axis parallel to the surface of the foil (Fig. 5).



FIG. 3
BOUNDARY LAYER RAKE

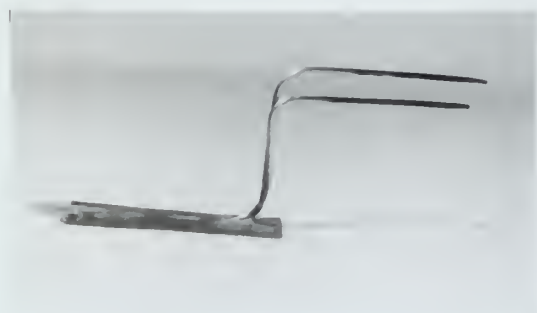


FIG. 5
AUXILIARY BOUNDARY LAYER RAKE



FIG. 5A
AUXILIARY STATIC PROBES



FIG. 4
INCLINED MANOMETER



WAKE SURVEY RAKE AND VERTICAL
MANOMETER

FIG. 6

A pitot-static tube was mounted in the test section about five feet ahead of the foil. The tubes were led to an indirect reading manometer at the control board of the wind tunnel. A tee joint was placed in the static pressure tubing from the probe and a tube was led from it to the inclined manometer table so that the tunnel static pressure ($P_{stat \infty}$) could be readily compared with the static pressures along the surface of the foil, which are also displayed on the inclined manometer bank.

Surveying the boundary layer just aft of the trailing edge required the use of an additional rake. This one consisted of alternating groups of three total pressure tubes and one static tube (Fig. 6). Only twenty of the tubes were read. The entire rake was moved up and down, traversing the wake in intervals of 0.1 to 0.2 inches. The tubes from this rake were led to a vertical manometer in the tunnel control room. This rake was simply bolted to the floor of the tunnel just behind the foil and adjusted by hand between runs.

An inclined manometer obtained from the Gas Turbine Laboratory was set up at an angle with the floor of 14.5° , giving an amplification factor of 4.0 to the readings (Fig. 7). The fluid used was Meriam Oil with a specific gravity of 0.827 at 60°F . The columns on the inclined manometer are numbered 1 thru 13 for the thirteen static taps. "S" is the tunnel static lead and numbers 1 thru 10 are the leads from the rake. The indirect reading manometer was of the inclined type with a vernier scale for adjusting the height of the inclined section (Fig. 8). It was filled with alcohol whose specific gravity was 0.806. The vertical manometer used for the wake survey also used alcohol of the same specific gravity (Fig. 6).

4. SET UP PROBLEMS

The main difficulty rested in the design of the foil section. The experiment would not be particularly meaningful if the section tested were not a "thin" section. Also, large span was considered necessary to remove the possibility of end effects disturbing the boundary layer at the center section. The combination of large span and small cross sectional moment of inertia introduced a considerable strength problem. In addition, the small thickness introduced obvious construction difficulties. After conversing with several sheet metal fabricators, the idea of building the foil in a manner similar to a conventional wing, using ribs and frames with sheet metal covering, was abandoned by the author. This was unfortunate, since excellent instrumentation of this type of model could have been obtained. The method of building the foil of chord-wise strips of mahogany fitted over steel tubes was adopted. The installation of the pressure tubes seemed simple and foolproof. However, the finished surfaces of the Epoxy plugs were unsatisfactory in many instances due to the inclusion of small bubbles, and no amount of wet sanding seemed to help. Drilling the 0.035 holes through the plugs, regardless of how carefully done, heated some of the plugs enough to cause them to bulge slightly above the surface of the foil. Any small discontinuity in the surface can obviously make static pressure measurements inaccurate.

The foil itself, when returned by the model maker had several discrepancies. The foil did not conform to the template supplied by the author. It was in fact, drastically thinner and had greater camber.

The exact dimensions of the foil were obtained by the author, using a clay impression. It had been planned to leave the center section of the three sections of the leading and trailing edges unattached to the foil except by the key. This was to enable the author to further instrument the leading and trailing edges. Unfortunately the model maker misunderstood and returned the foil solidly together in all aspects. As a result, a rather crude job was done in getting pressure readings from the leading and trailing edges.

B. EXPERIMENTAL METHOD

With the model set up in the tunnel at the desired angle of attack, the rake was attached to the surface of the foil using pieces of tape. The leading edges of the tape were blended to the foil surface using fine Scotch Tape. The rake was always positioned with the openings of its static tube on the same chord-wise line as a surface static tap (Fig. 9). This facilitated comparison between the surface static pressure and the static pressure at the edge of the boundary layer. In regions of separated flow or where large streamline curvature existed, no significant correlation was expected. The total pressures and static pressures from the rake, the static pressures on the foil surface and the tunnel static pressure upstream of the wing were read on the inclined manometer. The tunnel velocity head was measured on the indirect reading manometer.

Twelve runs were made on each foil surface, coinciding with twelve of the thirteen surface taps. The rake could not be placed far enough back on the trailing edge to get a run for a position corresponding to number thirteen surface tap.



FIG. 7
INCLINED MANOMETER IN POSITION

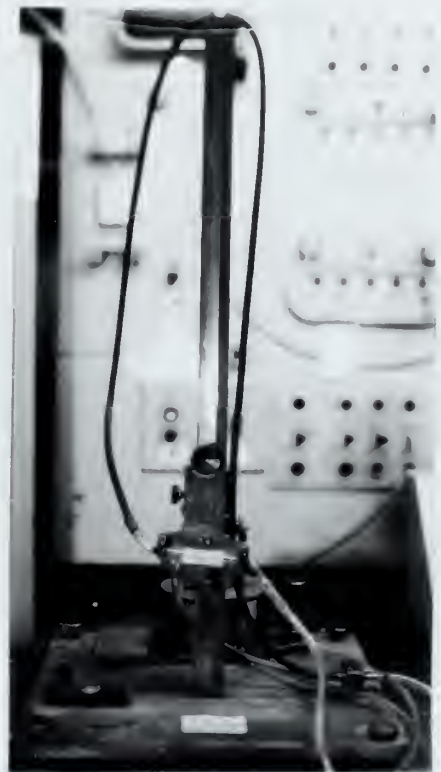


FIG. 8
INDIRECT READING MANOMETER
FOR MEASURING TUNNEL VELOCITY



FIG. 9A
RAKE IN POSITION ON PILE
SHOWING "STRIP TUBES"



FIG. 9B
RAKE POSITIONED ADJACENT TO
STATIC TAPS

Each of the runs actually were made at slightly different Reynolds Numbers, since the tunnel velocity would not return to the same value after the tunnel was shut down for repositioning the rake for the next run.

However, the difference in the velocity head for the various runs amounted to, at most, 0.06 inches of fluid of specific gravity 0.806, which is equivalent to 1.1 feet per second. This, obviously has little effect on Reynolds Number and therefore no loss in accuracy of the measurements of viscous phenomena is expected.

The runs were to be made on both surfaces of the foil. And the original plan was to take measurements at five different angles of attack and at two Reynolds Numbers. This amounts to 240 runs. Since, the total pressure tubes on the boundary layer took close to thirty-five minutes to steady down, and since it was necessary to measure the heights of the rake tubes above the foil surface and carefully reposition the rake after each run, bringing the total "run time" to about forty-five minutes, it was not possible to make nearly the number of measurements originally planned. When it was necessary to leave the wind tunnel, the following information had been obtained:

a.) At zero angle of attack:

1. Total head profiles at 23 stations
(11 on the suction side and 12 on the pressure side,
at a Reynolds Number of 3.67×10^6)
2. Total head profiles at 12 stations
(6 on the suction side and 6 on pressure side,
at a Reynolds Number of 5.45×10^6)

3. Wake surveys of total and static pressures at both Reynolds Numbers
4. Static pressures at the surface of the foil for both Reynolds Numbers.
5. Rough ideas of the location of transition from laminar to turbulent flow using lampblack traces.

b.) At $+2^\circ$ angle of attack

1. Same as number (1.) above
2. Wake survey at a Reynolds Number of 3.67×10^6
3. Static pressure at the surface for Reynolds Number of 3.67×10^6 .

c.) At $+5^\circ$ and -4° angle of attack

1. Only total head profiles on the top surface of the foil at Reynolds Number of 3.67×10^6 at 12 stations

At zero angle of attack, surface pressures on the foil were recorded every time a total pressure profile was measured. This was necessary only to determine how positioning of the rake along the chord affected the chord-wise pressure distribution. It was found that, with the rake in position on the foil, the pressure distribution was slightly greater in magnitude and shifted along the chord toward the trailing edge. But the differences between the distributions were small and the slopes were essentially the same, so no noticeable effects on the boundary layer development were expected. This practice was then discontinued since it was time consuming and did not produce any additional meaningful data. It should be noted that the effect of moving the rake along the foil was

extremely small and differences were noticed only between the conditions of the rake on or the rake off, regardless of position.

The surface static pressure readings on the leading and trailing edge sections were measured using a variety of small probes since only the top surface tap on the trailing edge was airtight. A small 0.035 O.D. tube, with an 81 gage hole drilled into its surface was designed in such a way that it would have the same curvature as the leading edge, and its orifice would be in the same position as the proposed surface tap. It was placed on the leading edge and fastened to the surface with tape. Before using it, the probe was placed on the same chord-wise line as several other of the static taps and the readings were compared. Agreement of the readings obtained using the two different sources was good. The measured differences were of the order of 0.025 inches of Meriam Oil, with a total reading of 4.00 inches.

A similar tube was used to obtain the static pressures around the trailing edge. The only difference was, that the probe used on the trailing edge had a 90° angle bend close to the end so that readings could be taken within 1.0 inches of the trailing edge without having a plastic tube projecting beyond the foil. These readings did not seem to be steady and reliable and as a result, were not exploited. This was unfortunate, since after plotting the resulting pressure coefficients, the ones obtained with this probe seemed to fair in nicely with other data. More information about the trailing edge static pressures would have helped make a more intelligent explanation of the observed boundary layer development in this region.

[illegible]

For further information, please contact:

© 2004 Blackwell Publishing Ltd *Journal of Internal Medicine* 255: 255–262

doi:10.1017/S0022292411000606

Received 10 May 2006; accepted 17 July 2006

and 80% reduction in 12 months in the case of the 100% reduction in the number of cases.

Source: Government of India, Ministry of Health and Family Welfare, 1997.

2000 was derived from 1995 and 1996 data available publicly and is based on

A brief review of the overall procedure is as follows:

1. Test the system for leaks.
2. Position the rake adjacent to a static tap.
3. Light-off the wind tunnel and obtain the desired speed.
4. Read the inclined manometer when steady.
5. Read indirect reading manometer for tunnel velocity upstream.
6. Shut down tunnel.
7. Measure and record the rake tube heights.
8. Reposition the rake.
9. Repeat this until top and bottom surfaces have been traversed at the required angle of attack.
10. Change the angle of attack and repeat items 1. through 9. Checks were made for leaks on the static tubes after changing the angle of attack because the static pressure leads were often disturbed by the tubes swinging through the area cut in the end walls.
11. After obtaining all the desired total pressure surveys on the surface, remove the rake and Stripatube support stanchion. Install wake survey apparatus.
12. Read total and static pressure in the wake on vertical manometer.
13. Reposition rake vertically. Repeat readings until reasonable coverage of a region 2.0 inches above and below the foil is obtained.
14. Obtain surface static pressure readings for both surfaces at required angles of attack using the surface tap and probes and

reading the results on the inclined manometer. These readings were taken without any tubes or other apparatus on the foil surface.

C. ANALYSIS OF THE DATA

1. BOUNDARY LAYER COMPUTATION

The previous section outlines the general data which was obtained by the end of the experiment. The information on the foil at 0.0° angle of attack was most important. At each of the stations on both surfaces (the stations coincide with the surface taps) there is a series of ten or twelve total head measurements at various distances from the surface of the foil. There were two static pressures available for obtaining the dynamic head in these profiles. One of these was read on the top tube on the rake and the other measured at the adjacent surface static tap. After plotting the pressure coefficients along the chord obtained from both the rake and the static taps, and noting that the difference between the coefficients was small, it was decided to use the reading on the rake static tube for boundary layer calculations. The foil has such low curvature that it is doubtful that any appreciable pressure drop across the boundary layer $dp/dr = \rho V^2/R$ is to be expected except right on the leading edge, and no attempt was made to obtain total head measurements very close to the nose of the foil. In computing the dynamic heads in the boundary layer then, a constant local h static was subtracted from the measured total pressure: $h(\text{dynamic}) = h \text{ total} - h(\text{stat local})$.

To insure that the top probes of the boundary layer rake were indeed out of the layer, the total head measured at the topmost total head

...and the

... ..

... ..

... ..

... ..

... ..

... ..

... ..

... ..

... ..

... ..

... ..

... ..

... ..

... ..

... ..

... ..

... ..

... ..

... ..

... ..

... ..

... ..

... ..

... ..

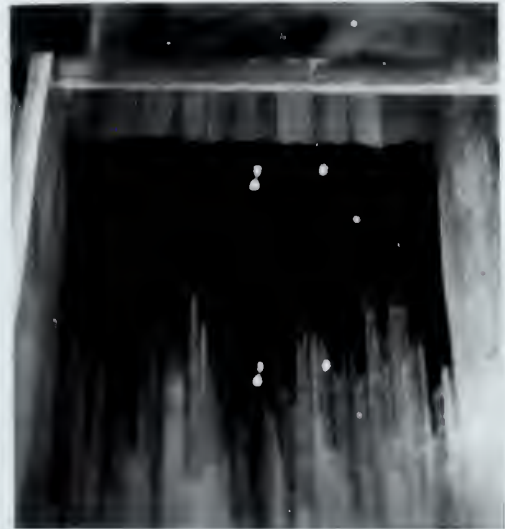


FIG. 10A
FOIL IN TEST SECTION SHOWING STANCHION



FIG. 10B
FOIL IN TEST SECTION SHOWING ADDITIONAL
TUBES FROM AUXILIARY RAKE

FIG. 11
CARBON BLACK TRANSITION TESTS



$\alpha = 2.0^\circ$ $Re = 3.67 \times 10^6$



$\alpha = 0.0^\circ$ $Re = 5.45 \times 10^6$

tube on the rake was compared with the total head of the stream upstream of the foil section. This was accomplished by converting the dynamic head upstream of the foil (measured on the vertical indirect reading manometer) to the same scale as the inclined manometer. First the inclination must be considered and then of course the difference in specific gravities as follows:

$$h(\text{ind}) \times \frac{\text{spg. of fluid in ind. read. man.}}{\text{spg. of fluid in incl. man.}} \times \frac{1}{\sin(\theta \text{ line})} = h(\text{inclined}) \quad (1)$$

Now with both upstream dynamic head and local total head in the same measurement system, the upstream static head read on the inclined manometer was subtracted from upstream dynamic head. If the total pressure tubes in the top section of the wake are out of the shear layer and in a region of essentially potential flow, then from Bernoulli, $H_{\text{total}} = C$ thus the two readings must be the same. In this experiment the agreement between the total pressures was usually quite good. Differences of a few hundredths of an inch as read on the inclined manometer were most frequently encountered. The maximum disagreement was 0.15 inches on the inclined manometer. And this amounts to an error of about one percent in the ratio of $h_{\text{dynamic}}(\text{boundary layer})$ to $h_{\text{dynamic}}(\text{potential})$.

After all of the total pressure readings had been corrected for manometer zeros, etc., they were compared with the potential flow dynamic head as follows:

$$\frac{h_{\text{dynamic}}(\text{B.L.})}{h_{\text{dynamic}}(\text{Potential})} = \frac{h_{y \text{ total}} - P_{\text{stat}}(\text{local})}{H - P_{\text{stat}}(\text{local})} \quad (2)$$

v/V was then computed by taking the square root of this ratio.

$$v/V = \left[\frac{h_{y \text{ total}} - P_{\text{stat}}(\text{local})}{H - P_{\text{stat}}(\text{local})} \right]^{1/2} \quad (3)$$

After this calculation is carried out for each total pressure tube reading across the boundary layer, it is possible to plot the non-dimensional boundary layer velocities against distance y . This was accomplished for all of the stations on the top and bottom surface of the foil at 0.0° and $+2.0^\circ$ angle of attack.

In order to proceed further into the numerical analysis of the boundary layer, a limit for v/V must be defined which will be, for the purpose of calculation, the outer edge of the boundary layer. 0.992 has been chosen. This figure is usually applied to the laminar boundary layer where a clear boundary between the viscous and inviscid flow does not exist. Depending on roughness, however, the turbulent layer may have a reasonably distinct boundary. Nonetheless, the figure 0.992 for v/V was used as an outer limit for both turbulent and laminar layers for no other reason than to standardize the limits of the graphical integration of the velocity profiles.

Since the primary purpose of the experiment was to determine the effect of the boundary layer on the pressure loading of the foil, a quantity must be obtained from the velocity distribution in the shear layer which represents the distance the potential flow streamlines are displaced in "moving around" the low velocity region of the boundary layer. It has been stated earlier that this quantity is called δ^* and is defined as

$$\delta^* = \int_0^{\delta} (1 - v/V) dy. \quad (b)$$

We call the boundary layer thickness, the region in which v/V is less than 0.992. We then define δ^* as equal to the height which when

subtracted from the actual height of the layer, results in a height which if multiplied by the free stream velocity gives the same flow per unit width as the boundary layer permits.

$$V(\delta - \delta^*) = \int_0^{\delta} v \, dy \quad (5)$$

$$-V\delta^* = -V\delta + \int_0^{\delta} v \, dy \quad (6)$$

$$V\delta^* = \int_0^{\delta} (V - v) \, dy \quad (7)$$

Giving:

$$\delta^* = \int_0^{\delta} (1 - v/V) \, dy \quad (8)$$

To obtain δ^* , the velocity profiles were plotted to a large scale on sheets of millimeter cross section paper. The height scale was twenty times the actual height of the boundary layer and the scale for v/V was spread out over a twenty inch abscissa. The resulting profiles were then mechanically integrated using a planimeter to obtain δ^* .

The series of total pressure heads and static readings obtained in the wake survey were treated in a similar manner, and a value for δ^* was obtained for the regions of the wake either side of a center line extending back from the center of the trailing edge parallel to the tunnel floor. The values of δ^* along the chord of the foil and at the point in the wake, $x/c = 1.023$, were plotted versus cord-wise distance/cord length.

The behavior of the boundary layer at the trailing edge was not determined experimentally due to limitations in the measuring devices and is not entirely known but judging from the pressure gradient measured in that region, it must continue to grow rapidly to the trailing edge

... and ...

... and ...

$$(1) \quad \dots$$

$$(2) \quad \dots$$

$$(3) \quad \dots$$

$$(4) \quad \dots$$

$$(5) \quad \dots$$

$$(6) \quad \dots$$

$$(7) \quad \dots$$

$$(8) \quad \dots$$

$$(9) \quad \dots$$

$$(10) \quad \dots$$

$$(11) \quad \dots$$

$$(12) \quad \dots$$

$$(13) \quad \dots$$

$$(14) \quad \dots$$

$$(15) \quad \dots$$

$$(16) \quad \dots$$

$$(17) \quad \dots$$

$$(18) \quad \dots$$

$$(19) \quad \dots$$

$$(20) \quad \dots$$

$$(21) \quad \dots$$

$$(22) \quad \dots$$

$$(23) \quad \dots$$

$$(24) \quad \dots$$

$$(25) \quad \dots$$

and then fall as the flow around the trailing edge causes the pressure to drop. The wake point indicates that some discontinuity exists in the slope of the ψ versus x/chord curve at the trailing edge. With this in mind the ψ curve was extrapolated back to the trailing edge, and values for ψ were obtained from the plots at points on the abscissa corresponding to the required ordinates of the computer program for the potential flow calculation. Ref. (8).

The actual shape of the foil was obtained using a clay impression and the dimensions were listed at the "required ordinates". The displacement thickness values were then added to the dimensions of the foil and an intermediate form determined. The foil dimensions by definition, are symmetrical about the nose tail line at the trailing edge. The boundary layer however, is not, and after adjusting the shape of the foil by δ we have a foil which is unsymmetrical about the original nose tail line. The new center of the trailing edge was then determined and the new nose-tail line defined. The end of the nose-tail line now passes through a point whose relative distance to the original center of the leading edge is given by

$$e = \frac{\psi_{\text{top}} - \psi_{\text{bottom}}}{2} \quad (8)$$

The angle of attack used to enter the numerical conformal mapping program must be adjusted accordingly. One additional correction is necessary. The nose-tail line, once shifted due to the unsymmetrical trailing edge thickness, changes the value of the ordinates once again, so all of the dimensions must be corrected by

$$y = x \tan \alpha \quad (9)$$

$$\begin{aligned} y &= x \quad c/c = x/c \cdot c \cdot c/c \\ y &= c \quad x/c \end{aligned} \quad (10)$$

Whether y is to be added or subtracted from the ordinates depends, of course, on which ordinates we are altering and the sign of the angular change. The ordinates of this thrice corrected foil and corrected angle of attack are then entered as inputs to a numerical conformal mapping program, (Ref. 5), for the solution of flow around arbitrary profiles. The output of this program is primarily the chord-wise pressure distribution of the foil in question. The results of this program were to be compared with the pressure distribution obtained in the experiment.

2. CALCULATION OF THE PRESSURE COEFFICIENTS

Both the static pressure at the head of the test section and the static pressures sensed by the top tube on the boundary layer rake and the surface taps were measured on the inclined manometer. The computation of the pressure coefficients $c_p = \frac{p - p_\infty}{\frac{1}{2} \rho V^2}$ was then a matter of applying the corrections to compensate for the tilt of the manometer table not in the plane of inclination and subtract h static at the head of the tunnel from the local static head measured with the rake or the taps. The dynamic head observed on the indirect reading manometer was again converted to the same scale as the inclined manometer and the resulting quantity

$$\begin{aligned} h(\text{inclined}) &= \frac{0.806}{0.827} \times \frac{1}{\sin 14.5^\circ} h(\text{indirect}) \\ h(\text{inclined}) &= 3.93 h(\text{indirect}) \end{aligned} \quad (1)$$

is divided into the static head difference.

the same way as the other two cases.

Let us now consider the case $\alpha = 1$.

For $\alpha = 1$, the function $f(x)$ is defined by the formula

$f(x) = \frac{1}{2} \left(1 + \frac{x}{\sqrt{1+x^2}} \right)$ for $x \geq 0$ and $f(x) = 0$ for $x < 0$.

It is easy to see that $f(x)$ is a non-decreasing function of x .

Let us now consider the case $\alpha = 2$.

For $\alpha = 2$, the function $f(x)$ is defined by the formula

$f(x) = \frac{1}{3} \left(1 + \frac{x}{\sqrt{1+x^2}} + \frac{x^2}{(1+x^2)^{3/2}} \right)$ for $x \geq 0$ and $f(x) = 0$ for $x < 0$.

It is easy to see that $f(x)$ is a non-decreasing function of x .

Let us now consider the case $\alpha = 3$.

For $\alpha = 3$, the function $f(x)$ is defined by the formula

$f(x) = \frac{1}{4} \left(1 + \frac{x}{\sqrt{1+x^2}} + \frac{3x^2}{(1+x^2)^{3/2}} + \frac{x^3}{(1+x^2)^{5/2}} \right)$ for $x \geq 0$ and $f(x) = 0$ for $x < 0$.

It is easy to see that $f(x)$ is a non-decreasing function of x .

Let us now consider the case $\alpha = 4$.

For $\alpha = 4$, the function $f(x)$ is defined by the formula

$f(x) = \frac{1}{5} \left(1 + \frac{x}{\sqrt{1+x^2}} + \frac{6x^2}{(1+x^2)^{3/2}} + \frac{4x^3}{(1+x^2)^{5/2}} + \frac{x^4}{(1+x^2)^{7/2}} \right)$ for $x \geq 0$ and $f(x) = 0$ for $x < 0$.

It is easy to see that $f(x)$ is a non-decreasing function of x .

Let us now consider the case $\alpha = 5$.

For $\alpha = 5$, the function $f(x)$ is defined by the formula

$f(x) = \frac{1}{6} \left(1 + \frac{x}{\sqrt{1+x^2}} + \frac{10x^2}{(1+x^2)^{3/2}} + \frac{10x^3}{(1+x^2)^{5/2}} + \frac{5x^4}{(1+x^2)^{7/2}} + \frac{x^5}{(1+x^2)^{9/2}} \right)$ for $x \geq 0$ and $f(x) = 0$ for $x < 0$.

It is easy to see that $f(x)$ is a non-decreasing function of x .

Q.E.D.

$$f(x) = \frac{1}{2} \left(1 + \frac{x}{\sqrt{1+x^2}} \right) \quad \text{for } x \geq 0 \quad \text{and} \quad f(x) = 0 \quad \text{for } x < 0$$

It is easy to see that $f(x)$ is a non-decreasing function of x .

Let us now consider the case $\alpha = 2$.

$$\frac{h_{\text{stat local}} - h_{\text{stat upstream}}}{3.93 h(\text{indirect})} = C_p \quad (11)$$

The only slight difficulty which arises, is when the pressure coefficients are calculated from the measurements taken on the rake static probe. Each measurement is made at slightly different tunnel speed and so each calculation involves different dynamic and static pressures. The pressure coefficients fall into five categories:

- (a.) Those determined from surface static tap readings with no apparatus on the foil.
- (b.) Those determined from the tap probe on the boundary layer rake with the rake on the foil, of course.
- (c.) Those determined from surface static tap readings with the rake on the foil.
- (d.) Those determined by the potential flow calculation around the real body.
- (e.) Those determined by the potential flow calculation around the corrected foil.

All five were plotted as a function of chord-wise distance/ chord length, to obtain an idea of the error caused by the presence of the rake, and to determine the agreement of the theory with experiment.

III. RESULTS

A. RESULTS OF THE BOUNDARY LAYER MEASUREMENTS

The results of the total pressure surveys made along the chord are shown in figures 10 and 11. The displacement thickness is plotted as a function of distance/chord length. The figures show the effects of the pressure gradients along the chord on the development of the boundary layer. The actual computed values of boundary layer thickness and displacement thickness are tabulated in Tables III and IV. In addition the velocity profiles at each chord-wise station are listed in Table VI. The plots of velocity distribution versus $y/$ are shown in figures 12 through 17. The original plots of v/V versus y were done on huge sheets of paper and have not been included in this report.

The displacement thickness in the wake 1.35 inches in back of the trailing edge was determined by a survey of wake total pressures. The wake surveys are tabulated in Table V and shown graphically in figures 18 and 19.

The boundary layer surveys indicate an extremely rapid thickening of the boundary layer in the presence of adverse pressure gradients toward the trailing edge. This may be seen quite clearly by observing both the measured pressure distribution in figure 20 and the curve of δ^* versus x/c , figure 10. Although this is for a nominal angle of attack of 0.0° the location of the stagnation point is indicated in figure 20 as being on the upper surface which belies an effective negative angle of attack. In figures 11 and 24, the correlation between pressure distribution and boundary layer development may also be noted.

Again referring to figure 10, what appears to be transition occurs somewhere between $x/c = 0.5$ and 0.6 . Figure 12 displaying the velocity distribution at various chord-wise points shows also a noticeable change in the shape of the velocity profile between these chord-wise points. A distinct rise in surface pressure may also be observed in figure 20, at this point. Actually this behavior does not really firmly indicate transition and other possibilities for what may be occurring here will be discussed later. The main point to observe in the boundary layer growth at nominal zero angle of attack is the fact that the behavior of the boundary layer along with the pressure distribution curve show the foil to be at some negative angle of attack. Notice that rapid boundary layer growth commences immediately on the forward portion of the bottom surface and how retarded laminar flow exists on the top surface up until the aforementioned point of suspected transition. Obviously the stagnation point is on the upper surface of the wing and the low pressure region caused by the corner flow around the nose causes the boundary layer on the bottom to separate immediately and reattach in turbulent region. On the top surface the large negative pressure gradient at the leading edge, as may be seen in figure 20, laminarizes the flow in the region; thus retarding its growth.

At an angle of attack of 2.0° the top surface growth is quite rapid and observing the velocity profiles in figures 16 and 17, we see that no distinct changes in shape occur. The pressure gradient on the top surface at 2° angle of attack is adverse all the way from $x/c = 0.10$ hence, the boundary layer and corresponding displacement thickness are quite large at the trailing edge.

The wake surveys shown in figures 15 and 19 show nothing of particular note. They were taken only to obtain a figure for displacement thickness as close to the trailing edge as possible. The points plotted on figures 10 and 11, are not a particular aid in predicting trailing edge behavior since it has been experimentally established by Stanton and Sweeting (Ref. 12), that θ^* and θ^*/δ suffer a slope discontinuity at the trailing edge. This can be observed (with imagination) in this experiment if we observe the pressure gradients and the trend of the boundary layer growth and extrapolate to the trailing edge, then proceed from this point to the wake point directly. This has been done with dotted lines in the figures.

B. RESULTS OF THE PRESSURE COEFFICIENT MEASUREMENTS

The pressure distribution curves have been mentioned in the previous section as an aid in visualizing what was happening to the boundary layer. In this respect they appear reasonable. The measured gradients seem to agree with other measured characteristics of the experiment. However, as may be seen upon comparing the measured pressure distribution (Figs. 20, 23, and 24), with the potential flow distributions obtained from T. Brockett's computer program (Ref. 8), (Figs. 22 and 25), agreement here is poor.

The pressure distribution on the unaltered foil section as predicted by potential flow shows, for the nominal 2° angle of attack, a lift coefficient of 0.127683.

The foil corrected for displacement thickness and with the resulting angle of attack change (effective angle of attack = 1.9569°) predicts a

The first of these is the fact that the system is not a simple one. It is a complex system, and the complexity is not only in the number of components, but also in the way they are connected. The second is the fact that the system is not a static one. It is a dynamic system, and the dynamics are not only in the way the components change, but also in the way they interact with each other. The third is the fact that the system is not a linear one. It is a non-linear system, and the non-linearity is not only in the way the components behave, but also in the way they interact with each other. The fourth is the fact that the system is not a deterministic one. It is a stochastic system, and the stochasticity is not only in the way the components behave, but also in the way they interact with each other. The fifth is the fact that the system is not a simple one. It is a complex system, and the complexity is not only in the number of components, but also in the way they are connected. The sixth is the fact that the system is not a static one. It is a dynamic system, and the dynamics are not only in the way the components change, but also in the way they interact with each other. The seventh is the fact that the system is not a linear one. It is a non-linear system, and the non-linearity is not only in the way the components behave, but also in the way they interact with each other. The eighth is the fact that the system is not a deterministic one. It is a stochastic system, and the stochasticity is not only in the way the components behave, but also in the way they interact with each other. The ninth is the fact that the system is not a simple one. It is a complex system, and the complexity is not only in the number of components, but also in the way they are connected. The tenth is the fact that the system is not a static one. It is a dynamic system, and the dynamics are not only in the way the components change, but also in the way they interact with each other. The eleventh is the fact that the system is not a linear one. It is a non-linear system, and the non-linearity is not only in the way the components behave, but also in the way they interact with each other. The twelfth is the fact that the system is not a deterministic one. It is a stochastic system, and the stochasticity is not only in the way the components behave, but also in the way they interact with each other. The thirteenth is the fact that the system is not a simple one. It is a complex system, and the complexity is not only in the number of components, but also in the way they are connected. The fourteenth is the fact that the system is not a static one. It is a dynamic system, and the dynamics are not only in the way the components change, but also in the way they interact with each other. The fifteenth is the fact that the system is not a linear one. It is a non-linear system, and the non-linearity is not only in the way the components behave, but also in the way they interact with each other. The sixteenth is the fact that the system is not a deterministic one. It is a stochastic system, and the stochasticity is not only in the way the components behave, but also in the way they interact with each other. The seventeenth is the fact that the system is not a simple one. It is a complex system, and the complexity is not only in the number of components, but also in the way they are connected. The eighteenth is the fact that the system is not a static one. It is a dynamic system, and the dynamics are not only in the way the components change, but also in the way they interact with each other. The nineteenth is the fact that the system is not a linear one. It is a non-linear system, and the non-linearity is not only in the way the components behave, but also in the way they interact with each other. The twentieth is the fact that the system is not a deterministic one. It is a stochastic system, and the stochasticity is not only in the way the components behave, but also in the way they interact with each other.

lift coefficient of 0.1116. The measured pressure distribution when mechanically integrated results in a lift coefficient of 0.335. This would correspond to an angle of attack of about 1.15 degrees. At this angle of attack the pressure distribution was plotted on figure 25. The points were also displayed in figure 24 for comparison. Reasonable agreement can be seen right up to within $x/c = 0.992$ for the top surface. At this point the influence of the corner on the square trailing edge causes the potential calculation to predict very low pressures. Since no data was obtained for this region, no adequate comparison can be made. The bottom surface data however, agrees with the predicted pressure distribution only in general trend up to within a few percent to the trailing edge. The magnitude is greater by 100%.

The results of the potential flow calculations around the body corrected by displacement thickness and with angle of attack adjusted by the arctan of the ratio of displacement thickness difference to chord length at the trailing edge, agrees with the potential theory for the mid chord area but, at the leading edge the small angle of attack change shows up and at the trailing edge the thickness effects become apparent and the corrected foil pressures in the region of $x/c = 0.75$ to $x/c = 1.00$ flatten out and then fall rapidly at the trailing edge due to the accelerating flow.

It appears then that there are three sources of disagreement. First, the pressure distribution as predicted by potential theory does not agree well with the experimental data. Second, the pressure distribution around the corrected form does not agree with the experimental data.

Third, the pressure distribution around the corrected form not only does not agree with the potential theory but it predicts a correction which although is the logical result of the input is just the opposite of the result which is sought.

Figure 23 displays the pressure distribution around the foil at a Reynolds Number of 5.15×10^6 . Considering the scale of the plot, it agrees well with the measurements obtained at $Re = 3.57 \times 10^6$. There was some slight change in the boundary layer behavior (Fig. 19) at the two Reynolds Numbers but nothing which would "cause" significant difference in the pressure distribution except perhaps due to movement of the transition points.

C. RESULTS OF CORRECTED FORMS

Table II lists the original dimension of the foil which was tested. It is not a NACA 66 with a 1.0 mean line nor does it have the originally desired thickness ratio of 0.033. It is thinner and has more camber. Table II also lists the displacement thickness at the required ordinates of Ref. 8 and, the correction in the offsets for adjusted angle of attack and finally the completely corrected foil dimensions for 0.00 and 2.00 angle of attack. These forms were used as inputs to the computer program and the results of these computations have been outlined in the previous section. The potential flow results for both the corrected and uncorrected foils have been plotted in figures 22 and 25. Noting the large disagreement, an attempt was made to find the angle of attack for which the experimental foil was tested. The computer results were obtained for a range of angle from -2.50° to $+2.00^\circ$ at small intervals. At angles

...and

... ..

... ..

... ..

... ..

... ..

... ..

... ..

... ..

... ..

... ..

... ..

... ..

... ..

... ..

... ..

... ..

... ..

for which the lift coefficient due to theory agreed with that of experiment, the resulting pressure distribution was plotted. At 2° nominal angle of attack, reasonable agreement was gotten between measured and calculated pressure distribution for the top surface at 1.20° but the bottom surface was considerably off. At 0.0° nominal angle of attack, the program output agreed somewhat with the top surface data at an angle of attack of -0.10° , and here the bottom surface data disagreed in magnitude. In fact the experiment gave small negative pressure coefficients where theory predicted small positive ones as may be seen on comparing figure 20 and 22.

The results of the measurements of the pressure distribution with the rake on the surface is shown in figure 21. Comparison of this graph with figure 20 indicates little difference in the distribution obtained with the rake on and off the surface.

D. CARBON BLACK TRACER

Two photographs depicting the use of carbon black on the foil surface are shown in figure 9. Usually carbon black and oil is used to predict separation. However, since the structure of turbulent flow is quite different from that of laminar, the author felt that some insight might be gained into the location of transition as well as separation, if any, by using carbon black. At zero angle of attack and Reynolds Number $= 3.67 \times 10^6$ the flow of the carbon black flow pattern changed completely between stations 7 and 8 which corresponded roughly to $x/c = 0.5$ and 0.6 . On the bottom surface the same behavior was observed

between stations 3 and 4. Figure 9³ shows the behavior of the carbon black at an incidence of 2.0° and indicates transition near station four. There is no reinforcement of this behavior in the plot of ϵ for 2° as shown in figure 11.

IV. DISCUSSION OF RESULTS

A. GENERAL

A brief review of the experimental results is in order at this point.

First, the foil is obviously not at the angle of attack measured in the wind tunnel. Some rough comparison with the data for some fifty odd angles of attack gotten from potential theory, indicate that the foil may be below the measured angles of attack anywhere from 0.1 to 0.8 degrees. The measured pressure distributions for nominal zero and 2.0° angles of attack produce lift coefficients of 0.145 and 0.335 respectively. Both of these figures are well below those predicted by the potential theory calculations; 0.268 and 0.414 for 0.0° and 2.0° respectively. The values from theory were obtained by mechanically integrating the pressure distributions obtained from the program output. The C_l listed by the program depends upon a given ideal angle of attack and lift slope. Since these values were not available exactly for the foil used in the experiment, it was necessary to check the program results in this manner.

Secondly, even when pressure distributions obtained from the program at angles of attack, which gave the same lift as experimental data predicted were compared with the data, the pressure distributions did not agree particularly well. In addition, attempts were made to find angles of attack for which pressure distributions on one of the surfaces agreed with theory, and then compare the pressure distribution on the other surface as well as the lift coefficient. For an angle of attack

of 1.2° the top surface data agree reasonably with the computed pressure distribution whereas the computed bottom surface pressures are much higher than those for the experiment. The trend of the computed pressures is however, essentially the same but the lift coefficient is slightly higher.

After unsuccessfully attempting to come up with an angle of attack at which the potential flow calculations resembled the experimental results, it was decided to figure what experimental error was responsible for the mismatching. The first thought was that, perhaps the sign of the static head on the inclined manometer may have been read wrong but, since for example, on the readings at zero angle of attack for the bottom, the static pressure was so close to zero on the manometer board that a difference in sign would not make any difference (at most 0.01"). However, if the pitot-static tube at the head of the tunnel were in error, say, ten percent, then the readings obtained with it as a reference would be seriously in error. This is true since both P_{stat} and q_{∞} are obtained from this instrument. This can be illustrated by the assuming that total pressure is known accurately and that the static taps are perfect. If a pressure coefficient of 0.1 were being measured and

$$\frac{h_{stat} - h_{stat \infty}}{q_{\infty}} = 0.1$$

if q_{∞} is around 12, as in this experiment, then $h_{stat} - h_{stat \infty} = 1.2"$. Then suppose the pitot static tube was in error by 10% or 1.2". If h_{total} is known, and it usually is known quite accurately, then $p_{stat \infty}$

changes by 1.2", therefore for readings this close to the zero a change of 1.2" if in the right direction could double the pressure coefficient and change its sign. In general, the effect of not knowing dynamic pressure exactly can change the scale of the pressure distribution scale as well as shifting the axis because it is q_{∞} and h_{static} that we are uncertain of in this equation

$$C_p = \frac{h - h_{static}}{q_{\infty}} \quad .$$

The static pressure readings were not taken at the same time on both surfaces which adds to the difficulty of putting a finger on the problem. The bottom surface readings were taken toward the end of the experiment and the pitot-static tube and its associated lines and manometers may well have developed an error between the measurements of the two distributions. However, the data for the top surface at 2° nominal angle of attack was obtained in between bottom surface readings for zero and 2.0° angles of attack and both top surface measurements appear to be reasonable.

If we rule out the possibility that the static tube and equipment were in error there remain only a few more reasons for the difficulty and these have to do with the effects of the walls and ceiling and the possibility of a vertical dynamic head variation. The pitot tube was mounted in the upper section of the tunnel about two feet from the overhead. The height of the tunnel is approximately 7½ feet and the foil was mounted about 3½ feet from the floor.

Glauert (Ref. 9), has obtained corrections to the effective angle of attack of a two dimensional foil in a closed jet. This was

accomplished by replacing the floor and overhead by air foil shapes and continuing until an infinite cascade was produced. The results are as follows:

$$\alpha = + \frac{1}{2} \frac{c^2}{1.8} \frac{C^2}{h} (C_1' + 1.6m' 1h)(573) \quad (12)$$

and

$$C_1 = C_1' \left(1 - \frac{c^2}{1.8} \frac{C^2}{h} \right) \quad (13)$$

where $Cm' (\frac{1}{4})$ is the moment about the quarter chord where C/h is the ratio of chord length to tunnel height. In this experiment it was equal to 0.667.

C_1' is the measured lift in the tunnel.

$$C_1 = 0.9046 C_1'.$$

At nominal values of angle of attack of 0.0° and 2.0° the true lift coefficient was then 0.1312 and 0.306 respectively.

$Cm' (\frac{1}{4})$ was estimated from the measured pressure distributions as 0.0361 at zero degrees and 0.08 for 2.0° . With these values, the correction to angle of attack becomes:

$$\alpha = 0.11^\circ \quad (0.0^\circ)$$

$$\alpha = 0.31^\circ \quad (2.0^\circ)$$

Clearly, these corrections are not sufficient to account for the poor data.

If there existed a vertical dynamic head variation in the tunnel, due to poor design of the contraction nozzle, then having the pitot-static

converges. Each one of functions f_n and f has a unique antiderivative on any interval $[a, b]$ containing the closed interval $[0, 1]$ and hence continuous on $[a, b]$.

$$(10) \quad \lim_{n \rightarrow \infty} \int_a^b f_n(x) dx = \int_a^b f(x) dx \quad \text{if } f_n \rightarrow f \text{ uniformly on } [a, b]$$

Let us apply this theorem to the functions f_n and f defined above.

$$(11) \quad \lim_{n \rightarrow \infty} \int_0^1 f_n(x) dx = \int_0^1 f(x) dx$$

Let us first prove that the limit of the integrals exists and is equal to the integral of the limit function. We have $f_n(x) = x^n$ and $f(x) = x$ for $x \in [0, 1]$. We have $f_n(x) \rightarrow f(x)$ uniformly on $[0, 1]$ and hence $f_n \rightarrow f$ uniformly on $[0, 1]$.

Therefore, by the theorem, we have $\lim_{n \rightarrow \infty} \int_0^1 f_n(x) dx = \int_0^1 f(x) dx$.

Now, let us compute the limit of the integrals. We have $\int_0^1 f_n(x) dx = \int_0^1 x^n dx = \frac{1}{n+1}$ and $\int_0^1 f(x) dx = \int_0^1 x dx = \frac{1}{2}$. Therefore, we have $\lim_{n \rightarrow \infty} \int_0^1 f_n(x) dx = \frac{1}{2}$.

Let us now prove that the limit of the integrals exists and is equal to the integral of the limit function. We have $f_n(x) = x^n$ and $f(x) = x$ for $x \in [0, 1]$. We have $f_n(x) \rightarrow f(x)$ uniformly on $[0, 1]$ and hence $f_n \rightarrow f$ uniformly on $[0, 1]$.

$$\lim_{n \rightarrow \infty} \int_0^1 f_n(x) dx = \int_0^1 f(x) dx$$

Let us now prove that the limit of the integrals exists and is equal to the integral of the limit function. We have $f_n(x) = x^n$ and $f(x) = x$ for $x \in [0, 1]$. We have $f_n(x) \rightarrow f(x)$ uniformly on $[0, 1]$ and hence $f_n \rightarrow f$ uniformly on $[0, 1]$.

Therefore, by the theorem, we have $\lim_{n \rightarrow \infty} \int_0^1 f_n(x) dx = \int_0^1 f(x) dx$.

tube in the upper section of the test section would be disastrous and p static would, of course, be correct for the upper surface and in error in the lower section. It was however, necessary to place the pitot tube in that portion of the tunnel to prevent its wake from impinging on the surface of the foil. The maximum error encountered, according to Poole (Ref. 10), is 2 to 3% of the dynamic head and the region of error is usually confined to a short distance from the floor at the entrance.

The possibility of a pressure gradient existing length-wise down the tunnel section exists but precautions were taken to remove this effect. The walls were toothed out. According to Ref. (10), this effect can also be caused by the presence of the body itself but is restricted however, to bodies such as fuselages and nacelles and is negligible for normal wings, by inference then, the effect must be even more negligible for such a thin section as the one tested in this experiment.

A simple calculation just to estimate the contraction effect of the foil on the jet entering the test section

$$\frac{V_1}{V_2} = \frac{A_2}{A_1} \quad (1b)$$

where V_1 is the velocity at the pitot tube and V_2 is the velocity, in incompressible flow, in the vicinity of the foil. This region is modeled by a section of area decreased by the cross sectional area of the foil. So, A_1 is the test section area at the pitot tube and A_2 is the effective flow area in the region of the foil.

$$C_p = \frac{v_1^2}{v_2^2} - 1$$

$$\frac{A_2}{A_1} = \frac{72 \text{ in}^2}{4320 \text{ in}^2} = 0.0166$$

$$C_p = 0.00275 - 1$$

Thus, the correction to the pressure coefficients is two orders of magnitude less than the measured ones and need not be considered.

To summarize the preceding explanation, there exists an error in static pressure readings of sufficient magnitude that only the viscous effects on the gradients of the pressures may be discussed. The experiment was considerably more delicate than the author conceived and much greater control and calibration than was exercised is necessary to make an intelligent correction to this discrepancy.

5. BOUNDARY LAYER PROFILES

The data obtained for the boundary layer profiles is good and agrees with what one would expect in the presence of the measured pressure gradients.

The profiles indicate that the flow is turbulent along the surface of the foil except for the top surface of the section tested at a nominal angle of attack of 0.0° . Here, at station 1, the shape factor is 2.290 which corresponds to a laminar boundary layer which is fairly stable. Station 1, on the top surface is, according to figure 20, in a region of intense acceleration. The shape factor has decreased to about 1.57

as we approach station 6, which seems to indicate that transition to turbulent flow has occurred, however, H drops sharply between station 6 and 7 and by station 8, has begun to rise rapidly as flow nears the trailing edge. At station 12, H has reached the value of 2.33. This type of behavior is shown in Ref. (11) by Von Doerhoff and Telrevis, in their experiments with air foil sections. The trend of which I speak is the high value of H at the leading edge, decreasing and then rising in turbulent flow.

This information then removes the certainty that what we see between station 7 and 8 on the top surface is truly transition. Poole, Ref. 10, indicates that transition can be noted by taking pressure measurements a short distance from the surface and noting that a dip in the pressure envelope will indicate transition. The rake static tube provided this type of measurement and there certainly is a dip in the C_p curve at this point. However, a shape factor which is characteristic of a turbulent boundary layer has been measured ahead of this point.

The crux of this discussion of the boundary layer profiles is that the measurements appear to be in agreement with theory and the value for * and δ can certainly be used (if the overall procedure is correct) to adjust the shape of the body.

It also may be observed that the relative location of the transition point on the top and bottom surfaces of the foil will make a distinct difference in the nature of the appearance of the adjusted trailing edge. Here roughness effects can be important. No attempt was made to stimulate turbulence on the model and the surface of the foil was

reasonably smooth along its forward portions so that the extensive length of the region of laminar boundary layer growth on the forward section is not particularly surprising.

Examination of this data leads us to the conclusion that at negative angles of attack, the boundary layer growth on the upper surface will be retarded, and the larger δ^* which would occur at the bottom of the trailing edge would effectively increase the angle of attack. Disregarding thickness effects, this would tend to increase the lift. The reverse is true for positive angles of attack where the gradients on the upper surface may be strongly adverse. The positive angle of attack also results in strong corner flow at the leading edge which causes an intense low pressure region which could well induce turbulence all along the upper surface.

Roughness of the foil surface, if its "hydraulic" diameter is sufficiently large, may influence the behavior of the turbulent layer as well as the transition point.

C. DISCUSSION OF POTENTIAL FLOW CALCULATIONS WITH THE CORRECTED FORM

As mentioned in section III, the plots of the experimental data do not agree with potential flow about the unaltered body, let alone with the form corrected for δ^* . Therefore it is possible only to make qualitative remarks on the merits of the proposed method for obtaining lift alterations due to viscosity.

In figures 21 and 22, we know that the magnitude of the bottom surface data is different than the theoretical results, however, it should be noted that there is a hump between $x/c = .4$ and $.6$ in the

experimental pressure curve. In Figure 22 we can see the same hump only in the corrected form curve. At the rear part of the foil it is extremely difficult to see which of the potential theory curves has the same slope and behavior at the trailing edge as the data. The potential flow results for the uncorrected foil section show higher value of slope at the trailing edge. This is to be expected especially when the pressure gradients are strongly adverse. The boundary layer grows rapidly on the surface in question and when the resulting δ^* is added to the foil an opposing correction results. An example will illustrate the point; using the system of corrections devised in this report. Given a two-dimensional foil section at a high angle of attack but with no separation: the boundary layer measured on the top surface will be quite large and the angle of attack will be effectively decreased. The thickening of the after section of the foil and the resulting increase in flow acceleration as well as the decreased angle of attack will contribute to reduce the strong adverse gradient. Thus, potential theory about this corrected form must predict lower adverse gradients than the flow around the unchanged body. For negative angles of attack, the lower surface will have the adverse gradients as the trailing edge is approached. δ^* will consequently be greater there and the effective angle of attack will be increased and the combined effects of added thickness and angle of attack will cause a decrease in the adverse pressure gradient.

All of the plots of potential theory solutions for the corrected forms show a rapid pressure loss at $x/c = .99$. This has been explained

in a previous section. It is worth noting here, however, that this is the largest single shortcoming of the entire philosophy of the thesis. The flow as described in this computer program sees a square tailed projectile like foil at an angle of attack, with the requirement for a stagnation point in the center of the tail. The potential flow around this form certainly will not be the analog of the actual flow. Schneider (Ref. 3), pointed out in his experiment that the displacement thickness of the boundary layer and wake joined reasonably uniformly at the trailing edge so that a better procedure would be to assume that the foil is extended a short bit by the wake and the dead air bubble which Schneider (3) observed and that it tapers to a zero thickness. This could not be attempted in this experiment without better coverage of the trailing edge region, since the point of zero thickness would be most logically chosen when the static pressure variation across the wake has fallen to some small value.

V. CONCLUSIONS

The large disagreement between the measured and calculated pressure distribution leads to the following conclusions:

In order to obtain meaningful data the experiment must be performed in a much better instrumented and controlled manner. The statement made earlier in the thesis to the effect that the wall corrections were negligible should not be taken out of context. The calculated correction did not suitably adjust my data, however, the magnitude of the wall corrections in sensitive boundary layer, drag, and lift effect experiments have led to increased work with flexible tunnel walls and ceilings to eliminate the constraints placed on streamline curvature by the jet boundaries. In section IV, I calculated this effect. It was 10% of the total lift at only 0.0° . From this, I conclude that wall effects are substantial enough to warrant rerunning the experiment with the overhead and floor of the tunnel formed to the shape of the foil.

The method which I used to apply the ϵ correction to the foil is fallacious and should be replaced with one that does not predict obviously excessive streamline defects toward the trailing edge.

I noted that along the foil not in the trailing edge region, the results of the potential flow around the corrected form show similar humps and hollows as the experimental data, but the uncorrected form often misses them. Therefore, I conclude that in regions where the displacement thickness is not unrealistically truncated as it was at the trailing edge, the streamline deflection is reasonably well predicted by this theory.

The boundary layer results show behavior which would be expected under the measured conditions and is not considered as a source of the discrepancy between theory and experiment.

The design of the foil pressure sensing devices were poor as well as the angle of attack control set up. A good deal of the uncertainty about the measured pressures would have been eliminated had efficient taps been used and more of them installed. Not really knowing the angle of attack, made real numerical comparisons impossible.

In addition to thickness, Reynolds Number and camber, the boundary layer distribution on the surface of the foil and indirectly the lift are dependent on foil roughness and free stream turbulence. For this reason it is felt that best results would be had if tunnel turbulence were reduced by employing screens and straighteners and different turbulence inception positions established using trip wire. Preston and Sweeting (12), show some of the results of work with and without turbulence stimulators on the wings they tested and the results are quite graphic.

...and the

... ..

... ..

... ..

... ..

... ..

... ..

... ..

... ..

... ..

... ..

... ..

... ..

... ..

... ..

... ..

... ..

... ..

... ..

... ..

... ..

... ..

... ..

... ..

... ..

VI. RECOMMENDATIONS FOR FURTHER STUDY

Before attempting to continue the investigation of viscous effects using the same apparatus, certain corrections must be made.

First, the airfoil section should have the leading and trailing edges removed and the key width doubled to avoid any warp due to poor joints. While they are removed, pressure taps should be installed in them. Most important is a tap in the center of the vertical back side of the trailing edge. The nose should have as many taps as possible, installed. Then the center lift in the foil should be cut down and routed out so there is a $\frac{1}{2}$ inch channel all around the wing. Taps should be installed in a flexible brass strip which will conform to the foil surface. The strip would fit into the center lift. Rather than wasting time with the steel tubes in the foil all the taps could be brought out of two channels in the foil which could be refaired.

The tunnel should be adjusted with some molded plywood to have no boundary effects on the foil behavior. For high angles of attack, this will be absolutely necessary.

To obtain a meaningful amount of data, different measuring devices must be used -- the boundary layer should be investigated using a traversing probe which could be controlled from outside the tunnel and moved both in and out of the boundary layer, and in a chord-wise direction. Conducting paint and warning lights could be used to maintain fine position control. This traversing mechanism should have accommodation for both static and total pressure tubes and also hot wire anemometers and a spherical tube with which to make detailed wake surveys.

The time constant on this system should be low. If possible, a transducer arrangement for the total pressure surveys in conjunction with an x - y plotter, should be used.

The static taps on the foil should number no less than sixty and they could be connected to a photostatic manometer bank. There is one available at N.I.T. With these modifications, data which can really be analyzed would be obtained.

This experiment provides the opportunity to "kill two birds with one stone" as it were. The work is closely related with turbulent boundary layers and it provides an opportunity to obtain some data on turbulent layers. The ability to predict the behavior of these layers depends upon having data with which the skin friction or the integral of the skin friction may be found since it is an input to the Karman integral approach. Therefore, it would behoove us to obtain skin friction data simultaneously and correlate it with some of the boundary layer parameters.

... und ...

...

...

...

...

...

...

...

...

...

...

...

...

...

...

...

...

...

...

...

...

...

...

...

VII. BIBLIOGRAPHY

- (1) Pinkerton, Robert M., "Calculated and Measured Pressure Distributions Over the Midspan Section of the NACA 11-12 Air Foil", NACA Report Number 563
- (2) Preston, J. H., "The Calculation of Lift Taking Account of the Boundary Layer", ARC Report No. 2725, Nov. 1949
- (3) Schneider, Kurt H., "Boundary Layer Effects on Airfoil Lift", Gas Turbine Laboratory Report No. 17, Sept. 1958
- (4) Spence, D. A. and Beasley, J. A., "The Calculation of Lift Slopes Allowing for Boundary Layer, With Applications to NAE 101 and 104 Airfoils", Reports and Memoranda No. 3137, Feb. 1958, London
- (5) Stuper, J., "Investigation of Boundary Layers on an Airplane Wing in Free Flight", NACA Technical Memorandum No. 751, (Translation)
- (6) Leopold, Reuben, "The Effect of Viscosity on the Lift Coefficient of Propeller Sections", Massachusetts Institute of Technology, Department of Naval Architecture and Marine Engineering Report No. 65-7, Sept. 1955
- (7) Moses, Hal L., "The Behavior of Turbulent Boundary Layers in Adverse Pressure Gradients", Gas Turbine Laboratory Report No. 73, Jan. 1961

111. The following is a list of the names of the persons who have been elected to the office of

the following is a list of the names of the persons who have been elected to the office of

the following is a list of the names of the persons who have been elected to the office of

112. The following is a list of the names of the persons who have been elected to the office of

the following is a list of the names of the persons who have been elected to the office of

113. The following is a list of the names of the persons who have been elected to the office of

the following is a list of the names of the persons who have been elected to the office of

114. The following is a list of the names of the persons who have been elected to the office of

the following is a list of the names of the persons who have been elected to the office of

the following is a list of the names of the persons who have been elected to the office of

115. The following is a list of the names of the persons who have been elected to the office of

the following is a list of the names of the persons who have been elected to the office of

116. The following is a list of the names of the persons who have been elected to the office of

the following is a list of the names of the persons who have been elected to the office of

the following is a list of the names of the persons who have been elected to the office of

the following is a list of the names of the persons who have been elected to the office of

117. The following is a list of the names of the persons who have been elected to the office of

the following is a list of the names of the persons who have been elected to the office of

the following is a list of the names of the persons who have been elected to the office of

- (8) Brockett, T., "Steady Two-Dimensional Pressure Distributions on Arbitrary Profiles", NACA Report No. 1021, Oct. 1946
- (9) Glauert, H., "The Interference on the Characteristics of an Airfoil in a Wind Tunnel of Rectangular Section; Report and Memorandum No. 1159
- (10) Pope, "Wind Tunnel Testing", John Wiley & Sons, Inc., Chapman & Hill, Limited, London, 1947
- (11) Von Doenhoff, Albert E. and Tetervin, Noel, "Determination of General Relations for the Behavior of Turbulent Boundary Layers", NACA Report No. 772, 1943
- (12) Preston, J. H. and Sweeting, W. E., "The Experimental Determination of the Boundary Layer and Wake Characteristics of a Simple Norkowski Aerofoil, with Particular Reference to the Trailing Edge Region", ARC Technical Report, Report and Memoranda No. 1993, 1943

APPENDIX A
TABLES OF DATA

TABLE II

FOIL GEOMETRY FOR $Q = 0.00$ $c = 50.07$ inches $EF_c = 3.67 \times 10^6$

x/c	y top	y bottom	δ^* top	δ^* bottom	Corrected for δ^*		$x \tan \alpha_s$		Corrected for δ^* & α	
					y top	y bottom	$x \tan \alpha_s$		y top	y bottom
1.000000	0.0665	-0.0665	0.136	0.135	0.2286	-0.2516	0.0212		0.2259	-0.2259
0.992401	0.2100	-0.0500	0.134	0.133	0.2710	-0.2330	0.0210		0.3950	-0.2090
0.959515	0.3350	0.0000	0.126	0.103	0.1610	-0.1830	0.0235		0.1315	-0.1595
0.933013	0.5700	+0.0350	0.115	0.152	0.6350	-0.1170	0.0226		0.7076	-0.1214
0.883022	0.8201	+0.0100	0.108	0.155	0.9280	-0.1150	0.0214		0.9191	-0.1236
0.821374	1.0600	-0.0200	0.103	0.130	1.1740	-0.1500	0.0199		1.1939	-0.1301
0.750000	1.3100	-0.0700	0.094	0.120	1.4010	-0.2000	0.0181		1.4221	-0.1419
0.671010	1.4600	-0.1500	0.092	0.103	1.5420	-0.2450	0.0162		1.5532	-0.2118
0.586524	1.5600	-0.2000	0.068	0.097	1.6200	-0.2970	0.0142		1.6122	-0.2328
0.500000	1.6200	-0.2200	0.034	0.085	1.6540	-0.3350	0.0121		1.6661	-0.2929
0.413176	1.6200	-0.2400	0.022	0.071	1.6420	-0.3110	0.0100		1.6520	-0.3010
0.328990	1.5100	-0.2400	0.016	0.059	1.5560	-0.2990	0.0080		1.5640	-0.2910
0.250000	1.3700	-0.2100	0.012	0.045	1.4020	-0.2350	0.0060		1.4030	-0.2790
0.178606	1.2000	-0.2400	0.010	0.036	1.2100	-0.2760	0.0040		1.2110	-0.2720
0.116976	0.9700	-0.2200	0.008	0.030	0.9750	-0.2500	0.0030		0.9610	-0.2470
0.066997	0.7300	-0.2000	0.006	0.024	0.7350	-0.2210	0.0020		0.7150	-0.2220
0.030154	0.4400	-0.1600	0.003	0.016	0.4450	-0.1750	0.0010		0.4190	-0.1750
0.007596	0.2200	-0.1200	0.008	0.014	0.2280	-0.1340	0.0000		0.2280	-0.1340
0.000000	0.0000	0.0000	0.000	0.000	0.0000	0.0000	0.0000		0.0000	0.0000

NOTE: y is measured normal to a straight line through the center of the leading edge and trailing edge.

(*) indicates distance above this line.

(-) indicates distance below this line. All above dimensions in inches.

TABLE II (cont.)

FOIL GEOMETRY FOR $\alpha = 2.0^\circ$

$$R/C = 3.67 \times 10^6$$

α_{top}	α_{bottom}	Corrected for α		x tan α	y top	y bottom
		y top	y bottom			
0.220	0.130	0.2866	-0.1966	0.0150	0.2116	-0.2116
0.210	0.126	0.1500	-0.1760	0.0146	0.1051	-0.2206
0.202	0.121	0.5320	-0.1210	0.0136	0.1581	-0.1646
0.171	0.112	0.7110	-0.1170	0.0120	0.7120	-0.1190
0.156	0.106	0.9760	-0.1160	0.0197	0.9363	-0.1557
0.129	0.098	1.1890	-0.1180	0.0370	1.1520	-0.1550
0.120	0.092	1.1300	-0.1720	0.0337	1.3963	-0.2057
0.110	0.089	1.5700	-0.2390	0.0302	1.5398	-0.2692
0.091	0.066	1.6510	-0.2660	0.0261	1.6276	-0.2921
0.093	0.057	1.7130	-0.2770	0.0255	1.6905	-0.2995
0.070	0.046	1.6900	-0.2860	0.0155	1.6715	-0.3015
0.051	0.035	1.5910	-0.2750	0.0118	1.5792	-0.2894
0.042	0.025	1.1320	-0.2650	0.0112	1.1298	-0.2762
0.031	0.019	1.2310	-0.2590	0.0080	1.2230	-0.2670
0.023	0.015	0.9930	-0.2350	0.0052	0.9878	-0.2132
0.018	0.013	0.7160	-0.2130	0.0030	0.7150	-0.2160
0.013	0.012	0.1530	-0.1720	0.0013	0.1517	-0.1733
0.010	0.010	0.2300	-0.1300	0.0003	0.2297	-0.1300

1. 凡在本公司工作之員工，其工資之計算，應以實際工作時間為準。
 2. 凡在本公司工作之員工，其工資之計算，應以實際工作時間為準。
 3. 凡在本公司工作之員工，其工資之計算，應以實際工作時間為準。
 4. 凡在本公司工作之員工，其工資之計算，應以實際工作時間為準。
 5. 凡在本公司工作之員工，其工資之計算，應以實際工作時間為準。
 6. 凡在本公司工作之員工，其工資之計算，應以實際工作時間為準。
 7. 凡在本公司工作之員工，其工資之計算，應以實際工作時間為準。

中華民國 100 年 1 月 1 日

中華民國 100 年 1 月 1 日
 (共計 11 頁)

TABLE III
BOTTOM SURFACE

ANGLE OF ATTACK = 0.0°

$RE_c = 3.67 \times 10^6$

STATION	x/c	(inches)	ξ^* (inches)
1	0.00757	0.162	0.01215
2	0.117	0.234	0.0315
3	0.1776	0.220	0.0330
4	0.2498	0.300	0.0461
5	0.3280	0.361	0.0588
6	0.4140	0.420	0.0711
7	0.4990	0.590	0.0834
8	0.5860	0.624	0.0961
9	0.6700	0.720	0.1086
10	0.7500	0.758	0.1207
11	0.8220	0.820	0.1390
12	0.9140	1.122	0.1742
WAKE	1.023	0.910	0.1780

TABLE III (cont)

TOP SURFACE

ANGLE OF ATTACK = 0.0° $RE_\phi = 3.67 \times 10^6$

STATION	x/c	ξ (inches)	ξ^* (inches)
1	0.00757	0.034	0.00894
2	0.1170		
3	0.1776	0.044	0.00964
4	0.2498	0.065	0.0121
5	0.3280	0.091	0.01445
6	0.4140	0.190	0.0225
7	0.4990	0.246	0.0354
8	0.5860	0.444	0.0678
9	0.6700	0.510	0.0781
10	0.7500	0.568	0.0956
11	0.8220	0.593	0.101
12	0.9140	0.660	0.1140
WAKE	1.023	0.790	0.1400

TABLE III (cont)

TOP SURFACE

ANGLE OF ATTACK = 0.0° $Re_c = 5.65 \times 10^5$

STATION	x/c	(inches)	η^* (inches)
1	0.00757	0.032	0.00680
4	0.24980	0.160	0.02015
6	0.41400	0.192	0.02735
8	0.58600	0.320	0.04170
10	0.75000	0.568	0.08710
12	0.91400	0.717	0.12490
WAKE	1.02300	0.810	0.16240

BOTTOM SURFACE

STATION	x/c	(inches)	η^* (inches)
1	0.00757	0.111	0.01375
4	0.24980	0.299	0.02605
6	0.41400	0.470	0.06000
8	0.58600	0.570	0.08350
10	0.75000	0.746	0.10950
12	0.91400	0.970	0.16400
WAKE	1.02300	0.850	0.15100

TABLE IV
TOP SURFACE

ANGLE OF ATTACK = 2°

$Re = 3.67 \times 10^6$

STATION	x/c	(inches)	η (inches)
1	0.03757	0.150	0.01082
2	0.11700	0.175	0.02265
3	0.17760	0.231	0.03280
4	0.26980	0.300	0.04170
5	0.32800	0.353	0.05520
6	0.41100	0.465	0.06650
7	0.49900	0.548	0.09310
8	0.58600	0.592	0.08930
9	0.67000	0.710	0.11160
10	0.75000	0.763	0.12050
11	0.82200	0.834	0.13250
12	0.91400	0.935	0.16760
WAKE	1.02300	1.085	0.20400

TABLE 1

Summary of data

Year	Country	Area	Population
1950	USA	100	150
1955	USA	100	160
1960	USA	100	170
1965	USA	100	180
1970	USA	100	190
1975	USA	100	200
1980	USA	100	210
1985	USA	100	220
1990	USA	100	230
1995	USA	100	240
2000	USA	100	250
2005	USA	100	260
2010	USA	100	270
2015	USA	100	280
2020	USA	100	290
2025	USA	100	300
2030	USA	100	310
2035	USA	100	320
2040	USA	100	330
2045	USA	100	340
2050	USA	100	350

TABLE IV (cont.)

BOTTOM SURFACE

ANGLE OF ATTACK = 4.2° $Re_c = 3.67 \times 10^6$

STATION	x/c	(inches)	η (inches)
1	0.00757		
2	0.11700	0.170	0.01136
3	0.17760	0.170	0.01970
4	0.24980	0.170	0.02320
5	0.32800	0.300	0.04040
6	0.41100	0.312	0.15900
7	0.43900	0.500	0.55500
8	0.58600	0.500	0.04360
9	0.67000	0.599	0.08400
10	0.75000	0.611	0.09210
11	0.82200	0.554	0.09980
12	0.91400	0.530	0.10720
WAKE	1.02300	0.870	0.14200

TABLE V

VELOCITY PROFILE IN THE WAKE

ANGLE OF ATTACK = 0.0° $RE_c = 3.67 \times 10^6$

y	h - hst (inches)	v/v
1.26	2.80	1.000
1.11	2.81	1.004
1.03	2.80	1.000
1.01	2.83	1.030
.86	2.74	0.989
.86	2.79	0.998
.82	2.75	0.991
.76	2.73	0.987
.64	2.62	0.967
.61	2.57	0.9581
.53	2.40	0.926
.51	2.44	0.933
.44	2.31	0.908
.36	2.08	0.862
.36	1.89	0.822
.32	1.93	0.8307
.26	1.57	0.749
.14	1.15	0.641
.11	1.00	0.597
.01	0.84	0.534
- .06	0.94	0.580
- .14	1.22	0.664
- .18	1.32	0.691
- .36	1.76	0.797
- .46	2.02	0.854
- .49	2.16	0.883
- .53	2.36	0.922
- .73	2.48	0.947
- .88	2.71	0.989
- .96	2.72	0.992
- .98	2.77	1.000
- .113	2.78	1.004
- .113	2.73	0.990
- .117	2.77	1.000
- .123	2.76	0.998

TABLE V (cont.)

VELOCITY PROFILE IN THE WAKE

ANGLE OF ATTACK = 0.0° $Re_c = 5.45 \times 10^6$

y	$h - h_{st}$ (inches)	v/v
0.90	6.00	1.0000
0.81	5.88	0.9899
0.76	5.81	0.9800
0.53	5.01	0.9590
0.46	4.65	0.8800
0.46	4.52	0.8680
0.41	4.22	0.8390
0.27	3.10	0.7190
0.24	3.17	0.7270
0.17	2.24	0.6100
-0.04	2.12	0.5950
-0.06	2.35	0.6260
-0.18	3.17	0.7270
-0.23	3.45	0.7580
-0.23	3.57	0.7710
-0.28	3.45	0.7580
-0.33	4.12	0.8300
-0.46	4.46	0.8630
-0.53	4.68	0.8830
-0.54	4.73	0.8880
-0.56	5.01	0.9130
-0.58	4.93	0.9070
-0.68	5.41	0.9500
-0.73	5.53	0.9600
-0.73	5.60	0.9660
-0.76	5.46	0.9510
-0.83	5.83	0.9860
-0.96	5.92	0.9930
-1.03	5.89	0.9900
-1.06	5.95	0.9960
-1.08	5.96	0.9970
-1.18	5.96	0.9970
-1.23	5.97	0.9980
-1.46	6.02	1.0000

Figure 1

Figure 1 shows the results of the experiment.

Figure 1 shows the results of the experiment.

Figure 1

Figure 1 shows the results of the experiment.

Figure 1

Figure 1 shows the results of the experiment.

Figure 1

Figure 1 shows the results of the experiment.

TABLE V (cont)

VELOCITY PROFILE IN THE WAKE

ANGLE OF ATTACK = 2° $Re_c = 3.67 \times 10^6$

y	h - hat (inches)	v/V
1.41	2.79	1.0000
1.23	2.77	0.9965
1.16	2.68	0.9808
1.03	2.73	0.9889
1.02	2.73	0.9889
0.83	2.58	0.9620
0.74	2.44	0.9350
0.66	2.01	0.8490
0.58	2.02	0.8500
0.52	1.96	0.8340
0.51	1.95	0.8360
0.44	1.72	0.7850
0.33	1.67	0.7260
0.26	1.28	0.6770
0.24	1.22	0.6590
0.16	0.98	0.6190
0.08	0.83	0.5690
0.04	0.88	0.5860
0.02	0.81	0.5620
0.01	0.75	0.5441
-0.06	0.89	0.5890
-0.17	1.31	0.6850
-0.24	1.66	0.7720
-0.26	1.66	0.7720
-0.42	2.12	0.8690
-0.46	2.03	0.8710
-0.49	2.19	0.8870
-0.56	2.40	0.9280
-0.74	2.67	0.9780
-0.84	2.74	0.9910
-0.96	2.75	0.9930
-0.98	2.79	1.0000
-1.17	2.76	0.9980
-1.26	2.79	1.0000
-1.34	2.77	0.9980

TABLE VI

SURFACE VELOCITY PROFILES

ANGLE OF ATTACK = 0.0° $Re_c = 3.67 \times 10^6$ TOP SURFACE

<u>STATION 1</u>		<u>STATION 3</u>		<u>STATION 4</u>		<u>STATION 5</u>	
v/V	y	v/V	y	v/V	y	v/V	y
0.990	0.03	0.995	0.05	0.983	0.05	0.964	0.05
0.703	0.015	0.999	0.10	0.998	0.10	0.9945	0.10
0.889	0.12	1.000	0.17	0.999	0.17	0.9995	0.17
0.999	0.33	0.999	0.25	0.9985	0.25	0.9995	0.25
1.000	0.37	0.999	0.41	0.999	0.41	0.9995	0.41
1.000	0.69	0.999	0.68	1.00	0.68	1.0000	0.68
1.000	0.80	0.999	0.71	1.00	0.71	1.0000	0.71
1.000	0.90	0.999	0.87	1.00	0.87	1.0000	0.87
1.000	1.00	0.999	0.91	1.00	0.91	1.0000	0.91

<u>STATION 6</u>		<u>STATION 7</u>		<u>STATION 8</u>		<u>STATION 9</u>	
v/V	y	v/V	y	v/V	y	v/V	y
0.8591	0.05	0.7457	0.05	0.5891	0.002	0.5616	0.02
0.9612	0.10	0.8837	0.10	0.8106	0.16	0.8349	0.20
0.9889	0.17	0.955	0.17	0.9072	0.26	0.9154	0.32
0.9965	0.25	0.993	0.25	0.9839	0.40	0.9803	0.45
0.9965	0.41	0.9965	0.41	0.9970	0.50	0.9945	0.53
0.9970	0.68	0.9970	0.68	0.9995	0.68	1.00	0.72
0.9965	0.71	0.9970	0.71	0.9995	0.80	1.00	0.84
0.9975	0.87	0.9965	0.87	0.9985	0.89	1.00	0.94
1.00	0.91	1.00	0.91	1.00	1.000	1.00	1.04
				0.999	1.25	1.00	1.32
				0.9985	1.58	1.00	1.61

TABLE VI (cont)

SURFACE VELOCITY PROFILES

ANGLE OF ATTACK = 0.0° $Re_c = 3.67 \times 10^6$ TOP SURFACE

<u>STATION 10</u>		<u>STATION 11</u>		<u>STATION 12</u>	
v/V	y	v/V	y	v/V	y
0.5263	0.020	0.5301	0.02	0.4733	0.02
0.7635	0.180	0.7810	0.20	0.7880	0.23
0.8660	0.285	0.8712	0.30	0.9044	0.38
0.9455	0.420	0.9439	0.44	0.9434	0.52
0.9752	0.480	0.9721	0.52	0.9829	0.60
1.0000	0.690	1.0000	0.72	0.9995	0.80
1.0000	0.800	1.0000	0.73	0.9995	0.91
1.0000	0.900	1.0000	0.94	0.9990	1.02
1.0000	1.010	1.0000	1.03	1.0000	1.10
1.0000	1.310	1.0000	1.32	0.9985	1.34
1.0000	1.600	1.0000	1.62	0.9990	1.65

BOTTOM SURFACE

<u>STATION 1</u>		<u>STATION 2</u>		<u>STATION 3</u>		<u>STATION 4</u>	
v/V	y	v/V	y	v/V	y	v/V	y
0.853	0.025	0.658	0.030	0.6750	0.03	0.618	0.02
0.970	0.100	0.978	0.190	0.9150	0.13	0.869	0.15
0.996	0.110	0.996	0.320	0.9975	0.24	0.983	0.26
0.999	0.200	0.996	0.430	0.9975	0.38	0.998	0.40
0.999	0.340	0.996	0.550		0.50	0.997	0.51
0.999	0.670	0.998	0.720	1.0000	0.65	0.999	0.68
0.999	0.800	0.998	0.825	1.0000	0.78	0.999	0.80
	0.890	0.997	0.930	1.0000	0.88	0.997	0.89
1.000	1.000	1.000	1.020	1.0000	0.98	1.000	1.00

TABLE VI (cont)

SURFACE VELOCITY PROFILES

ANGLE OF ATTACK = 0.0° $RE_c = 3.67 \times 10^6$ BOTTOM SURFACE

<u>STATION 5</u>		<u>STATION 6</u>		<u>STATION 7</u>		<u>STATION 8</u>	
v/V	y	v/V	y	v/V	y	v/V	y
0.597	0.02	0.598	0.02	0.597	0.03	0.715	0.120
0.838	0.16	0.745	0.16	0.749	0.14	0.781	0.200
0.955	0.27	0.913	0.27	0.864	0.25	0.877	0.310
0.998	0.41	0.987	0.40	0.950	0.39	0.960	0.450
0.999	0.51	0.998	0.51	0.992	0.50	0.978	0.525
1.000	0.68	1.000	0.67	1.003	0.65	1.001	0.720
1.000	0.81	1.000	0.80	1.003	0.78	1.001	0.850
0.999	0.96	1.000	0.89	1.001	0.89	1.000	0.940
1.000	1.00	1.000	1.00	1.003	0.98	1.002	1.050
		1.000	1.31	1.004	1.31	1.000	1.400
		1.000	1.61	1.001	1.60	1.000	1.670

<u>STATION 9</u>		<u>STATION 10</u>		<u>STATION 11</u>		<u>STATION 12</u>	
v/V	y	v/V	y	v/V	y	v/V	y
0.710	0.10	0.543	0.025	0.454	0.03	0.506	0.02
0.750	0.17	0.696	0.130	0.679	0.13	0.509	0.02
0.841	0.32	0.801	0.250	0.780	0.24	0.573	0.07
0.891	0.42	0.880	0.420	0.882	0.38	0.698	0.21
0.949	0.49	0.915	0.465	0.890	0.45	0.738	0.25
0.952	0.70	0.983	0.670	0.968	0.67	0.846	0.47
0.999	0.82	0.996	0.800	0.989	0.78	0.893	0.59
0.999	0.91	0.995	0.880	0.996	0.88	0.930	0.67
1.000	1.03	1.002	1.000	1.002	0.99	0.957	0.80
0.999	1.36	0.999	1.350	1.001	1.30	0.998	1.32
0.999	1.66	0.999	1.630	1.001	1.59	0.999	1.62

TABLE VI (cont.)

SURFACE VELOCITY PROFILES

ANGLE OF ATTACK = 2° $Re_c = 3.67 \times 10^6$ TOP SURFACE

<u>STATION 1</u>		<u>STATION 2</u>		<u>STATION 3</u>		<u>STATION 4</u>	
v/V	y	v/V	y	v/V	y	v/V	y
0.9160	0.01	0.6770	0.02	0.6510	0.02	0.615	0.02
0.9915	0.11	0.7690	0.01	0.8670	0.10	0.879	0.11
0.9871	0.06	0.9690	0.12	0.9270	0.15	0.909	0.16
0.9975	0.25	0.9995	0.21	0.9960	0.21	0.968	0.23
0.9970	0.10	0.9995	0.10	0.9990	0.30	1.000	0.37
0.9960	0.57	1.0000	0.56	0.9995	0.57	0.998	0.55
0.9960	0.68	0.9995	0.67	0.9995	0.69	0.998	0.65
0.9950	0.80	0.9995	0.79	1.0000	0.78	0.997	0.79
1.0000	0.88	1.0000	0.87		0.86	1.000	0.86

<u>STATION 5</u>		<u>STATION 6</u>		<u>STATION 7</u>		<u>STATION 8</u>	
v/V	y	v/V	y	v/V	y	v/V	y
0.6810	0.05	0.6600	0.01	0.5190	0.07	0.5580	0.03
0.8120	0.15	0.7860	0.13	0.7330	0.15	0.7250	0.11
0.9020	0.19	0.8370	0.17	0.8010	0.19	0.7850	0.15
0.9580	0.27	0.8950	0.25	0.8590	0.25	0.8130	0.23
0.9965	0.10	0.9760	0.39	0.9150	0.10	0.9300	0.37
1.0000	0.58	0.9975	0.56	0.9960	0.59	0.9790	0.55
1.0000	0.68	0.9975	0.67	0.9980	0.67	0.9980	0.65
0.9995	0.82	0.9995	0.80	0.9995	0.80	0.9995	0.79
1.0000	0.88	1.0000	0.86	1.0000	0.85	1.0000	1.00

TABLE VI (cont)

SURFACE VELOCITY PROFILES

ANGLE OF ATTACK = 2° $Re_c = 3.67 \times 10^6$ TOP SURFACE

<u>STATION 9</u>		<u>STATION 10</u>		<u>STATION 11</u>		<u>STATION 12</u>	
v/V	y	v/V	y	v/V	y	v/V	y
0.527	0.03	0.548	0.03	0.5570	0.03	0.623	0.13
0.752	0.18	0.682	0.10	0.7270	0.18	0.758	0.30
0.800	0.23	0.731	0.16	0.8020	0.28	0.818	0.38
0.844	0.31	0.781	0.23	0.8760	0.42	0.884	0.53
0.919	0.43	0.857	0.35	0.9220	0.53	0.926	0.62
0.966	0.62	0.926	0.52	0.9770	0.72	0.977	0.80
0.995	0.73	0.973	0.64	0.9955	0.87	0.991	0.92
0.998	0.88	0.993	0.82	0.9980	0.92	0.994	1.00
1.000	1.08	1.000	0.96	1.0000	1.03	0.999	1.10
				0.9970	1.56	0.998	1.66
					2.25		2.30

BOTTOM SURFACE

<u>STATION 2</u>		<u>STATION 3</u>		<u>STATION 4</u>		<u>STATION 5</u>	
v/V	y	v/V	y	v/V	y	v/V	y
0.653	0.02	0.471	0.02	0.4380	0.02	0.6140	0.02
0.987	0.15	0.984	0.13	0.9800	0.13	0.9330	0.16
0.995	0.29	0.984	0.28	0.9950	0.24	0.9925	0.29
0.995	0.40	0.995	0.43	0.9950	0.40	0.9950	0.40
0.996	0.50		0.51	0.9960	0.49	0.9960	0.51
0.999	0.68	1.000	0.69	0.9980	0.66	0.9985	0.69
0.998	0.84	0.9975	0.83	0.9965	0.82	0.9975	0.83
0.999	0.90	1.0000	0.88	0.9995	0.89	0.9985	0.91
1.000	1.00	1.0000	1.00	1.0000	1.00	1.0000	1.01

TABLE VI (cont)

SURFACE VELOCITY PROFILES

ANGLE OF ATTACK = 2° $Re_c = 3.67 \times 10^6$ BOTTOM SURFACE

<u>STATION 6</u>		<u>STATION 7</u>		<u>STATION 8</u>		<u>STATION 9</u>	
v/V	y	v/V	y	v/V	y	v/V	y
0.6240	0.02	0.5600	0.02	0.8006	0.08	0.6020	0.02
0.8540	0.15	0.8220	0.13	0.8200	0.16	0.7580	0.15
0.9630	0.23	0.9260	0.25	0.9120	0.27	0.8540	0.26
0.9955	0.38	0.9890	0.41	0.9010	0.40	0.9420	0.40
0.9955	0.48	0.9935	0.50	0.9940	0.53	0.9790	0.50
0.9980	0.68	0.9980	0.69	0.9980	0.70	0.9975	0.71
0.9970	0.80	0.9980	0.84	0.9970	0.85	0.9975	0.82
0.9990	0.88	0.9990	0.90	0.9985	0.93	0.9980	0.88
1.0000	1.00	1.0000	1.01	1.0000	1.02	1.0000	1.01

<u>STATION 10</u>		<u>STATION 11</u>		<u>STATION 12</u>	
v/V	y	v/V	y	v/V	y
0.6620	0.05	0.682	0.05	0.5010	0.04
0.7440	0.15	0.750	0.15	0.7220	0.13
0.8350	0.24	0.828	0.24	0.8030	0.22
0.9171	0.38	0.905	0.38	0.9140	0.36
0.9620	0.48	0.954	0.48	0.9490	0.48
0.9970	0.67	0.995	0.67	0.9920	0.64
0.9980	0.82	0.999	0.82	0.9975	0.75
0.9990	0.88	1.000	0.88	1.0000	0.86
1.0000	1.00	1.000	1.00	1.0000	0.95
		1.000	1.00		

(total 20 items)

Approximate frequency distribution

For a total of 100

For a total of 100

Frequency distribution

Frequency

Frequency

Frequency

Frequency

100

100

100

100

100

100

100

100

100

100

100

100

100

100

100

100

100

100

100

100

100

100

100

100

100

100

100

100

100

100

100

100

100

100

100

100

100

100

100

100

100

100

100

100

100

100

100

100

100

100

100

100

100

100

100

100

100

100

100

100

100

100

100

100

100

100

100

100

100

100

100

100

100

100

100

100

100

100

100

100

100

100

100

100

100

100

100

100

100

100

100

100

TABLE VI (cont.)

SURFACE VELOCITY PROFILES

ANGLE OF ATTACK = 0.0° $Re_c = 5.45 \times 10^6$ TOP SURFACE

<u>STATION 1</u>		<u>STATION 4</u>		<u>STATION 6</u>		<u>STATION 8</u>	
v/V	y	v/V	y	v/V	y	v/V	y
0.9930	0.030	0.9340	0.085	0.7090	0.03	0.7310	0.060
0.7970	0.015	0.8770	0.060	0.9540	0.14	0.8470	0.130
0.9975	0.120	0.9750	0.120	0.9910	0.19	0.9180	0.160
0.9980	0.330	0.9985	0.220	0.9970	0.31	0.9860	0.295
0.9980	0.370	0.9995	0.370	0.9975	0.44	0.9975	0.425
0.9990	0.690	1.0000	0.700	0.9985	0.70	0.9990	0.670
0.9990	0.800	1.0000	0.810	0.9985	0.80	0.9990	0.800
0.9975	0.900	0.9995	0.900	0.9990	0.90	0.9990	0.900
1.0000	1.000			1.0000	1.00	1.0000	0.980

<u>STATION 10</u>		<u>STATION 12</u>	
v/V	y	v/V	y
0.5820	0.02	0.5130	0.02
0.7350	0.13	0.5600	0.24
0.7930	0.17	0.8600	0.34
0.8870	0.31	0.9210	0.45
0.9560	0.44	0.9750	0.60
0.9990	0.68	0.9995	0.80
0.9995	0.80	1.0000	0.90
0.9990	0.90	0.9985	1.02
1.0000	0.99	1.0000	1.11

TABLE VI (cont.)

SURFACE VELOCITY PROFILES

ANGLE OF ATTACK = 0.0° $Re_\rho = 5.45 \times 10^6$ BOTTOM SURFACE

<u>STATION 1</u>		<u>STATION 4</u>		<u>STATION 6</u>		<u>STATION 8</u>	
v/V	y	v/V	y	v/V	y	v/V	y
0.8030	0.03	0.617	0.02	0.6620	0.03	0.6950	0.08
0.9760	0.10	0.806	0.08	0.7560	0.10	0.7440	0.13
0.9980	0.11	0.906	0.15	0.8210	0.15	0.8020	0.19
0.9985	0.20	0.994	0.30	0.9470	0.29	0.8900	0.31
	0.33	0.999	0.42	0.9890	0.44	0.9580	0.44
0.9990	0.66	0.999	0.67	1.0000	0.67	0.9985	0.72
0.9990	0.80	0.999	0.78	0.9995	0.80	0.9985	0.83
0.9980	0.88	0.999	0.87	0.9995	0.88	0.9985	0.93
1.0000	0.98	1.000	0.97	1.0000	0.98	1.0000	1.02

<u>STATION 10</u>		<u>STATION 12</u>	
v/V	y	v/V	y
0.5620	0.025	0.175	0.02
0.6820	0.090		
0.7310	0.130	0.622	0.11
0.7420	0.260	0.734	0.21
0.9010	0.410	0.790	0.33
0.9800	0.650	0.898	0.58
0.9925	0.760	0.936	0.67
0.9960	0.870	0.964	0.80
1.0000	0.950	0.985	0.89
0.9980	1.300	1.000	0.30
0.9970	1.570	0.999	1.55

TABLE VII
PRESSURE COEFFICIENTS

BOTTOM SURFACE				ANGLE OF ATTACK = 0.0°	
STATIC READINGS FOR RAKE				$Re_c = 3.67 \times 10^6$	
STATION	h stat	h stat m	hs-hm	q_{∞}	$\frac{h_{st}-h_{mst}}{q_{\infty}}$
1	+2.52	+1.42	-1.10	11.74	-0.09370
2	+2.20	+1.38	-0.82	11.77	-0.06890
3	+2.10	+1.35	-0.75	11.78	-0.06370
4	+1.95	+1.31	-0.64	11.76	-0.05440
5	+1.82	+1.25	-0.57	11.80	-0.04830
6	+1.80	+1.28	-0.52	11.72	-0.04430
7	+1.55	+1.29	-0.26	11.78	-0.02208
8	+1.56	+1.25	-0.31	11.80	-0.02628
9	+1.27	+1.17	-0.10	11.75	-0.00851
10	+1.12	+1.18	+0.06	11.84	+0.00507
11	+0.86	+1.08	+0.22	11.74	+0.01874
12	-0.04	+0.86	+0.90	11.78	+0.07640

h stat and h stat m in inches of oil spg. 0.827 on inclined manometer.

q_{∞} = dynamic head read on indirect reading manometer.

spg. 0.806 converted to same scale as inclined manometer.

+ indicates inches above datum on inclined manometer.

- indicates inches below datum on inclined manometer.

Table 1 Summary of results

Variable	Model 1			Model 2	
	Mean	SD	95% CI	Mean	SD
Variable 1	10.2	2.1	9.8 - 10.6	10.5	2.2
Variable 2	15.3	3.4	14.5 - 16.1	15.8	3.5
Variable 3	20.1	4.2	19.5 - 20.7	20.3	4.3
Variable 4	25.4	5.1	24.8 - 26.0	25.6	5.2
Variable 5	30.7	6.0	30.1 - 31.3	30.9	6.1
Variable 6	35.9	7.2	35.3 - 36.5	36.1	7.3
Variable 7	40.2	8.5	39.6 - 40.8	40.4	8.6
Variable 8	45.5	9.8	44.9 - 46.1	45.7	9.9
Variable 9	50.8	11.1	50.2 - 51.4	51.0	11.2
Variable 10	55.1	12.4	54.5 - 55.7	55.3	12.5
Variable 11	60.4	13.7	59.8 - 61.0	60.6	13.8
Variable 12	65.7	15.0	65.1 - 66.3	65.9	15.1

Continuous variables are listed with their mean and standard deviation. Categorical variables are listed with their frequency and percentage. The data were analyzed using SPSS version 25.0. The results are presented in Table 1.

Continuous variables are listed with their mean and standard deviation. Categorical variables are listed with their frequency and percentage. The data were analyzed using SPSS version 25.0. The results are presented in Table 1.

TABLE VII (cont.)

PRESSURE COEFFICIENTS

TOP SURFACE

ANGLE OF ATTACK = 0.00°

STATIC READINGS FOR CASE

 $Re_c = 3.67 \times 10^6$

STATION	h_{stat}	h_{static}	$h_s - h_{sc}$	q_{sc}	$\frac{h_{st} - h_{sc}}{q_{sc}}$
1	+2.31	+1.30	-1.01	11.78	-0.0856
2					
3	+3.32	+1.30	-2.02	11.78	-0.1715
4	+3.47	+1.29	-2.18	11.75	-0.1855
5	+3.60	+1.31	-2.29	11.75	-0.1950
6	+3.60	+1.23	-2.37	11.85	-0.2000
7	+3.30	+1.10	-2.20	11.76	-0.1871
8	+3.45	+1.20	-2.25	11.75	-0.1915
9	+3.62	+1.18	-2.44	11.75	-0.2076
10	+3.40	+1.09	-2.31	11.70	-0.1974
11	+3.20	+1.10	-2.10	11.70	-0.1795
12	+2.74	+1.08	-1.66	11.75	-0.1412

TABLE VII (cont)

PNEUMATIC COEFFICIENTS

BOTTOM SURFACE

ANGLE OF ATTACK = 2.0°

READINGS FROM WAKE STATIC PROBE

 $q_\infty = 3.67 \times 10^6$

STATION	h stat	h stat w	h _{st} -h _{sw}	q _{sw}	$\frac{h_{st}-h_{sw}}{q_\infty}$
1					
2	-0.45	+1.00	+1.45	11.86	0.1223
3	+0.10	+1.00	+0.90	11.80	0.0762
4	+0.25	+1.00	+0.75	11.85	0.0633
5	+0.37	+1.00	+0.63	11.85	0.0532
6	+0.50	+1.00	+0.50	11.85	0.0422
7	+0.49	+0.98	+0.49	11.86	0.0413
8	+0.58	+0.98	+0.40	11.86	0.0337
9	+0.45	+0.87	+0.32	11.85	0.0270
10	+0.30	+0.89	+0.59	11.85	0.0498
11	+1.25	+1.25	+0.71	11.90	0.0622
12	+1.25	+1.25	+1.25	11.95	0.1046

Appendix 1: Data Summary 2012-2013 Season

Table 1: Summary of Data by Site and Date

Site	Date	Time	Temperature (°C)	Humidity (%)	Wind Speed (m/s)
Site 1	2012-01-01	08:00	15.2	65.0	2.5
Site 1	2012-01-01	12:00	18.5	55.0	3.0
Site 1	2012-01-01	16:00	16.0	60.0	2.0
Site 1	2012-01-02	08:00	14.0	70.0	1.5
Site 1	2012-01-02	12:00	17.0	60.0	2.5
Site 1	2012-01-02	16:00	15.0	65.0	2.0
Site 1	2012-01-03	08:00	16.0	55.0	3.0
Site 1	2012-01-03	12:00	19.0	45.0	3.5
Site 1	2012-01-03	16:00	17.0	50.0	2.5
Site 1	2012-01-04	08:00	15.0	60.0	2.0
Site 1	2012-01-04	12:00	18.0	50.0	3.0
Site 1	2012-01-04	16:00	16.0	55.0	2.5
Site 1	2012-01-05	08:00	14.0	65.0	1.5
Site 1	2012-01-05	12:00	17.0	55.0	2.5
Site 1	2012-01-05	16:00	15.0	60.0	2.0
Site 1	2012-01-06	08:00	16.0	50.0	3.0
Site 1	2012-01-06	12:00	19.0	40.0	3.5
Site 1	2012-01-06	16:00	17.0	45.0	2.5
Site 1	2012-01-07	08:00	15.0	55.0	2.0
Site 1	2012-01-07	12:00	18.0	45.0	3.0
Site 1	2012-01-07	16:00	16.0	50.0	2.5
Site 1	2012-01-08	08:00	14.0	60.0	1.5
Site 1	2012-01-08	12:00	17.0	50.0	2.5
Site 1	2012-01-08	16:00	15.0	55.0	2.0
Site 1	2012-01-09	08:00	16.0	45.0	3.0
Site 1	2012-01-09	12:00	19.0	35.0	3.5
Site 1	2012-01-09	16:00	17.0	40.0	2.5
Site 1	2012-01-10	08:00	15.0	50.0	2.0
Site 1	2012-01-10	12:00	18.0	40.0	3.0
Site 1	2012-01-10	16:00	16.0	45.0	2.5
Site 1	2012-01-11	08:00	14.0	55.0	1.5
Site 1	2012-01-11	12:00	17.0	45.0	2.5
Site 1	2012-01-11	16:00	15.0	50.0	2.0
Site 1	2012-01-12	08:00	16.0	40.0	3.0
Site 1	2012-01-12	12:00	19.0	30.0	3.5
Site 1	2012-01-12	16:00	17.0	35.0	2.5
Site 1	2012-01-13	08:00	15.0	45.0	2.0
Site 1	2012-01-13	12:00	18.0	35.0	3.0
Site 1	2012-01-13	16:00	16.0	40.0	2.5
Site 1	2012-01-14	08:00	14.0	50.0	1.5
Site 1	2012-01-14	12:00	17.0	40.0	2.5
Site 1	2012-01-14	16:00	15.0	45.0	2.0
Site 1	2012-01-15	08:00	16.0	35.0	3.0
Site 1	2012-01-15	12:00	19.0	25.0	3.5
Site 1	2012-01-15	16:00	17.0	30.0	2.5
Site 1	2012-01-16	08:00	15.0	30.0	2.0
Site 1	2012-01-16	12:00	18.0	20.0	3.0
Site 1	2012-01-16	16:00	16.0	25.0	2.5
Site 1	2012-01-17	08:00	14.0	35.0	1.5
Site 1	2012-01-17	12:00	17.0	25.0	2.5
Site 1	2012-01-17	16:00	15.0	30.0	2.0
Site 1	2012-01-18	08:00	16.0	20.0	3.0
Site 1	2012-01-18	12:00	19.0	15.0	3.5
Site 1	2012-01-18	16:00	17.0	20.0	2.5
Site 1	2012-01-19	08:00	15.0	15.0	2.0
Site 1	2012-01-19	12:00	18.0	10.0	3.0
Site 1	2012-01-19	16:00	16.0	15.0	2.5
Site 1	2012-01-20	08:00	14.0	20.0	1.5
Site 1	2012-01-20	12:00	17.0	10.0	2.5
Site 1	2012-01-20	16:00	15.0	15.0	2.0
Site 1	2012-01-21	08:00	16.0	10.0	3.0
Site 1	2012-01-21	12:00	19.0	5.0	3.5
Site 1	2012-01-21	16:00	17.0	10.0	2.5
Site 1	2012-01-22	08:00	15.0	5.0	2.0
Site 1	2012-01-22	12:00	18.0	0.0	3.0
Site 1	2012-01-22	16:00	16.0	5.0	2.5
Site 1	2012-01-23	08:00	14.0	10.0	1.5
Site 1	2012-01-23	12:00	17.0	5.0	2.5
Site 1	2012-01-23	16:00	15.0	10.0	2.0
Site 1	2012-01-24	08:00	16.0	5.0	3.0
Site 1	2012-01-24	12:00	19.0	0.0	3.5
Site 1	2012-01-24	16:00	17.0	5.0	2.5
Site 1	2012-01-25	08:00	15.0	0.0	2.0
Site 1	2012-01-25	12:00	18.0	0.0	3.0
Site 1	2012-01-25	16:00	16.0	5.0	2.5
Site 1	2012-01-26	08:00	14.0	10.0	1.5
Site 1	2012-01-26	12:00	17.0	5.0	2.5
Site 1	2012-01-26	16:00	15.0	10.0	2.0
Site 1	2012-01-27	08:00	16.0	5.0	3.0
Site 1	2012-01-27	12:00	19.0	0.0	3.5
Site 1	2012-01-27	16:00	17.0	5.0	2.5
Site 1	2012-01-28	08:00	15.0	0.0	2.0
Site 1	2012-01-28	12:00	18.0	0.0	3.0
Site 1	2012-01-28	16:00	16.0	5.0	2.5
Site 1	2012-01-29	08:00	14.0	10.0	1.5
Site 1	2012-01-29	12:00	17.0	5.0	2.5
Site 1	2012-01-29	16:00	15.0	10.0	2.0
Site 1	2012-01-30	08:00	16.0	5.0	3.0
Site 1	2012-01-30	12:00	19.0	0.0	3.5
Site 1	2012-01-30	16:00	17.0	5.0	2.5
Site 1	2012-01-31	08:00	15.0	0.0	2.0
Site 1	2012-01-31	12:00	18.0	0.0	3.0
Site 1	2012-01-31	16:00	16.0	5.0	2.5
Site 2	2012-01-01	08:00	16.0	60.0	2.0
Site 2	2012-01-01	12:00	19.0	50.0	2.5
Site 2	2012-01-01	16:00	17.0	55.0	2.0
Site 2	2012-01-02	08:00	15.0	65.0	1.5
Site 2	2012-01-02	12:00	18.0	55.0	2.5
Site 2	2012-01-02	16:00	16.0	60.0	2.0
Site 2	2012-01-03	08:00	17.0	50.0	2.5
Site 2	2012-01-03	12:00	20.0	40.0	3.0
Site 2	2012-01-03	16:00	18.0	45.0	2.5
Site 2	2012-01-04	08:00	16.0	55.0	2.0
Site 2	2012-01-04	12:00	19.0	45.0	2.5
Site 2	2012-01-04	16:00	17.0	50.0	2.0
Site 2	2012-01-05	08:00	15.0	60.0	1.5
Site 2	2012-01-05	12:00	18.0	50.0	2.5
Site 2	2012-01-05	16:00	16.0	55.0	2.0
Site 2	2012-01-06	08:00	17.0	45.0	2.5
Site 2	2012-01-06	12:00	20.0	35.0	3.0
Site 2	2012-01-06	16:00	18.0	40.0	2.5
Site 2	2012-01-07	08:00	16.0	50.0	2.0
Site 2	2012-01-07	12:00	19.0	40.0	2.5
Site 2	2012-01-07	16:00	17.0	45.0	2.0
Site 2	2012-01-08	08:00	15.0	55.0	1.5
Site 2	2012-01-08	12:00	18.0	45.0	2.5
Site 2	2012-01-08	16:00	16.0	50.0	2.0
Site 2	2012-01-09	08:00	17.0	40.0	2.5
Site 2	2012-01-09	12:00	20.0	30.0	3.0
Site 2	2012-01-09	16:00	18.0	35.0	2.5
Site 2	2012-01-10	08:00	16.0	45.0	2.0
Site 2	2012-01-10	12:00	19.0	35.0	2.5
Site 2	2012-01-10	16:00	17.0	40.0	2.0
Site 2	2012-01-11	08:00	15.0	50.0	1.5
Site 2	2012-01-11	12:00	18.0	40.0	2.5
Site 2	2012-01-11	16:00	16.0	45.0	2.0
Site 2	2012-01-12	08:00	17.0	35.0	2.5
Site 2	2012-01-12	12:00	20.0	25.0	3.0
Site 2	2012-01-12	16:00	18.0	30.0	2.5
Site 2	2012-01-13	08:00	16.0	40.0	2.0
Site 2	2012-01-13	12:00	19.0	30.0	2.5
Site 2	2012-01-13	16:00	17.0	35.0	2.0
Site 2	2012-01-14	08:00	15.0	45.0	1.5
Site 2	2012-01-14	12:00	18.0	35.0	2.5
Site 2	2012-01-14	16:00	16.0	40.0	2.0
Site 2	2012-01-15	08:00	17.0	30.0	2.5
Site 2	2012-01-15	12:00	20.0	20.0	3.0
Site 2	2012-01-15	16:00	18.0	25.0	2.5
Site 2	2012-01-16	08:00	16.0	30.0	2.0
Site 2	2012-01-16	12:00	19.0	20.0	2.5
Site 2	2012-01-16	16:00	17.0	25.0	2.0
Site 2	2012-01-17	08:00	15.0	35.0	1.5
Site 2	2012-01-17	12:00	18.0	25.0	2.5
Site 2	2012-01-17	16:00	16.0	30.0	2.0
Site 2	2012-01-18	08:00	17.0	20.0	2.5
Site 2	2012-01-18	12:00	20.0	15.0	3.0
Site 2	2012-01-18	16:00	18.0	20.0	2.5
Site 2	2012-01-19	08:00	16.0	15.0	2.0
Site 2	2012-01-19	12:00	19.0	10.0	2.5
Site 2	2012-01-19	16:00	17.0	15.0	2.0
Site 2	2012-01-20	08:00	15.0	20.0	1.5
Site 2	2012-01-20	12:00	18.0	10.0	2.5
Site 2	2012-01-20	16:00	16.0	15.0	2.0
Site 2	2012-01-21	08:00	17.0	10.0	2.5
Site 2	2012-01-21	12:00	20.0	5.0	3.0
Site 2	2012-01-21	16:00	18.0	10.0	2.5
Site 2	2012-01-22	08:00	16.0	5.0	2.0
Site 2	2012-01-22	12:00	19.0	0.0	2.5
Site 2	2012-01-22	16:00	17.0	5.0	2.0
Site 2	2012-01-23	08:00	15.0	10.0	1.5
Site 2	2012-01-23	12:00	18.0	5.0	2.5
Site 2	2012-01-23	16:00	16.0	10.0	2.0
Site 2	2012-01-24	08:00	17.0	5.0	2.5
Site 2	2012-01-24	12:00	20.0	0.0	3.0
Site 2	2012-01-24	16:00	18.0	5.0	2.5
Site 2	2012-01-25	08:00	16.0	0.0	2.0
Site 2	2012-01-25	12:00	19.0	0.0	2.5
Site 2	2012-01-25	16:00	17.0	5.0	2.0
Site 2	2012-01-26	08:00	15.0	10.0	1.5
Site 2	2012-01-26	12:00	18.0	5.0	2.5
Site 2	2012-01-26	16:00	16.0	10.0	2.0
Site 2	2012-01-27	08:00	17.0	5.0	2.5
Site 2	2012-01-27	12:00	20.0	0.0	3.0
Site 2	2012-01-27	16:00	18.0	5.0	2.5
Site 2	2012-01-28	08:00	16.0	0.0	2.0
Site 2	2012-01-28	12:00	19.0	0.0	2.5
Site 2	2012-01-28	16:00	17.0	5.0	2.0
Site 2	2012-01-29	08:00	15.0	10.0	1.5
Site 2	2012-01-29	12:00	18.0	5.0	2.5
Site 2	2012-01-29	16:00	16.0	10.0	2.0
Site 2	2012-01-30	08:00	17.0	5.0	2.5
Site 2	2012-01-30	12:00	20.0	0.0	3.0
Site 2	2012-01-30	16:00	18.0	5.0	2.5
Site 2	2012-01-31	08:00	16.0	0.0	2.0
Site 2	2012-01-31	12:00	19.0	0.0	2.5
Site 2	2012-01-31	16:00	17.0	5.0	2.0

TABLE VII (cont)

PRESSURE COEFFICIENTS

TOP SURFACE

ANGLE OF ATTACK = 2.0°

READINGS FROM THE RAKE STATIC PROBE

 $q_{\infty} = 3.67 \times 10^6$

STATION	h_{stat}	h_{static}	$h_a - h_{\infty}$	q_{∞}	$\frac{h_a - h_{\infty}}{q_{\infty}}$
1	+5.38	+1.20	-4.18	11.81	-0.354
2	+4.70	+1.25	-3.45	11.95	-0.3052
3	+4.20	+0.68	-3.52	11.71	-0.2995
4	+4.19	+0.68	-3.51	11.85	-0.2960
5	+4.10	+0.70	-3.40	11.84	-0.2870
6	+3.78	+0.60	-3.18	11.80	-0.2661
7	+3.71	+0.53	-3.18	11.80	-0.2692
8	+3.58	+0.62	-2.96	11.84	-0.2500
9	+3.50	+0.65	-2.85	11.85	-0.2405
10	+3.27	+0.65	-2.62	11.76	-0.2225
11	+3.38	+0.99	-2.39	11.82	-0.2020
12	+2.73	+1.09	-1.64	11.85	-0.1385

January 2018 Intermediate Algebra

Student Name: _____
 Date: _____

Page: _____

Score: _____

Problem	Answer	Score	Comments	Grade	Points
1. Simplify: $3x^2 + 5x - 2x^2 + 4x - 7$	$x^2 + 9x - 7$	2			
2. Simplify: $4x^3 - 2x^2 + 3x - 1 + x^3 - 5x^2 + 2x + 6$	$5x^3 - 7x^2 + 5x + 5$	3			
3. Simplify: $2x^2 + 3x - 4x^2 + 5x - 1$	$-2x^2 + 8x - 1$	2			
4. Simplify: $3x^2 + 4x - 2x^2 + 5x - 3$	$x^2 + 9x - 3$	2			
5. Simplify: $5x^3 - 2x^2 + 3x - 1 + x^3 - 5x^2 + 2x + 6$	$6x^3 - 7x^2 + 5x + 5$	3			
6. Simplify: $2x^2 + 3x - 4x^2 + 5x - 1$	$-2x^2 + 8x - 1$	2			
7. Simplify: $3x^2 + 4x - 2x^2 + 5x - 3$	$x^2 + 9x - 3$	2			
8. Simplify: $5x^3 - 2x^2 + 3x - 1 + x^3 - 5x^2 + 2x + 6$	$6x^3 - 7x^2 + 5x + 5$	3			
9. Simplify: $2x^2 + 3x - 4x^2 + 5x - 1$	$-2x^2 + 8x - 1$	2			
10. Simplify: $3x^2 + 4x - 2x^2 + 5x - 3$	$x^2 + 9x - 3$	2			
11. Simplify: $5x^3 - 2x^2 + 3x - 1 + x^3 - 5x^2 + 2x + 6$	$6x^3 - 7x^2 + 5x + 5$	3			
12. Simplify: $2x^2 + 3x - 4x^2 + 5x - 1$	$-2x^2 + 8x - 1$	2			

TABLE VII (cont)

PRESSURE COEFFICIENTS

BOTTOM SURFACE

ANGLE OF ATTACK = 2.0°

PRESSURES FROM STATIC TAPS

 $q_\infty = 3.67 \times 10^6$

STATION	h_{stat}	h_{static}	$h_s - h_{st}$	q_{st}	$\frac{h_s - h_{st}}{q_{st}}$
1	+2.26	-0.10	+2.66	11.85	+0.22610
2	+0.18	+0.90	+0.72	11.85	+0.06080
3	+0.51	+0.90	+0.39	11.85	+0.03290
4	+0.60	+0.90	+0.30	11.85	+0.02530
5	+0.68	+0.90	+0.22	11.85	+0.01860
6	+0.78	+0.90	+0.12	11.85	+0.01010
7	+0.87	+0.90	+0.03	11.85	+0.002531
8	+1.21	+0.90	-0.31	11.85	-0.026200
9					
10	+0.75	+0.90	+0.15	11.85	+0.012670
11	+0.79	+0.90	+0.11	11.85	+0.009280
12	+0.37	+0.90	+0.53	11.85	+0.044700
13A	-0.68	+0.37	+1.05	11.85	+0.089700
13B	-0.81	+0.33	+1.17	11.85	+0.099600

Table 1. Summary of results

Regression results

Model 1: OLS regression

Model 2: OLS regression

Model 3: OLS regression

Model 4: OLS regression

Variable	Model 1	Model 2	Model 3	Model 4	Model 5
Constant	1.234	1.234	1.234	1.234	1.234
X1	0.567	0.567	0.567	0.567	0.567
X2	0.123	0.123	0.123	0.123	0.123
X3	0.789	0.789	0.789	0.789	0.789
X4	0.456	0.456	0.456	0.456	0.456
X5	0.234	0.234	0.234	0.234	0.234
X6	0.987	0.987	0.987	0.987	0.987
X7	0.345	0.345	0.345	0.345	0.345
X8	0.678	0.678	0.678	0.678	0.678
X9	0.101	0.101	0.101	0.101	0.101
X10	0.543	0.543	0.543	0.543	0.543
X11	0.876	0.876	0.876	0.876	0.876
X12	0.210	0.210	0.210	0.210	0.210
X13	0.765	0.765	0.765	0.765	0.765
X14	0.432	0.432	0.432	0.432	0.432
X15	0.901	0.901	0.901	0.901	0.901
X16	0.321	0.321	0.321	0.321	0.321
X17	0.654	0.654	0.654	0.654	0.654
X18	0.198	0.198	0.198	0.198	0.198
X19	0.521	0.521	0.521	0.521	0.521
X20	0.854	0.854	0.854	0.854	0.854
X21	0.287	0.287	0.287	0.287	0.287
X22	0.710	0.710	0.710	0.710	0.710
X23	0.401	0.401	0.401	0.401	0.401
X24	0.934	0.934	0.934	0.934	0.934
X25	0.367	0.367	0.367	0.367	0.367
X26	0.690	0.690	0.690	0.690	0.690
X27	0.123	0.123	0.123	0.123	0.123
X28	0.556	0.556	0.556	0.556	0.556
X29	0.889	0.889	0.889	0.889	0.889
X30	0.201	0.201	0.201	0.201	0.201
X31	0.734	0.734	0.734	0.734	0.734
X32	0.467	0.467	0.467	0.467	0.467
X33	0.900	0.900	0.900	0.900	0.900
X34	0.312	0.312	0.312	0.312	0.312
X35	0.645	0.645	0.645	0.645	0.645
X36	0.178	0.178	0.178	0.178	0.178
X37	0.511	0.511	0.511	0.511	0.511
X38	0.844	0.844	0.844	0.844	0.844
X39	0.277	0.277	0.277	0.277	0.277
X40	0.710	0.710	0.710	0.710	0.710
X41	0.401	0.401	0.401	0.401	0.401
X42	0.934	0.934	0.934	0.934	0.934
X43	0.367	0.367	0.367	0.367	0.367
X44	0.690	0.690	0.690	0.690	0.690
X45	0.123	0.123	0.123	0.123	0.123
X46	0.556	0.556	0.556	0.556	0.556
X47	0.889	0.889	0.889	0.889	0.889
X48	0.201	0.201	0.201	0.201	0.201
X49	0.734	0.734	0.734	0.734	0.734
X50	0.467	0.467	0.467	0.467	0.467
X51	0.900	0.900	0.900	0.900	0.900
X52	0.312	0.312	0.312	0.312	0.312
X53	0.645	0.645	0.645	0.645	0.645
X54	0.178	0.178	0.178	0.178	0.178
X55	0.511	0.511	0.511	0.511	0.511
X56	0.844	0.844	0.844	0.844	0.844
X57	0.277	0.277	0.277	0.277	0.277
X58	0.710	0.710	0.710	0.710	0.710
X59	0.401	0.401	0.401	0.401	0.401
X60	0.934	0.934	0.934	0.934	0.934
X61	0.367	0.367	0.367	0.367	0.367
X62	0.690	0.690	0.690	0.690	0.690
X63	0.123	0.123	0.123	0.123	0.123
X64	0.556	0.556	0.556	0.556	0.556
X65	0.889	0.889	0.889	0.889	0.889
X66	0.201	0.201	0.201	0.201	0.201
X67	0.734	0.734	0.734	0.734	0.734
X68	0.467	0.467	0.467	0.467	0.467
X69	0.900	0.900	0.900	0.900	0.900
X70	0.312	0.312	0.312	0.312	0.312
X71	0.645	0.645	0.645	0.645	0.645
X72	0.178	0.178	0.178	0.178	0.178
X73	0.511	0.511	0.511	0.511	0.511
X74	0.844	0.844	0.844	0.844	0.844
X75	0.277	0.277	0.277	0.277	0.277
X76	0.710	0.710	0.710	0.710	0.710
X77	0.401	0.401	0.401	0.401	0.401
X78	0.934	0.934	0.934	0.934	0.934
X79	0.367	0.367	0.367	0.367	0.367
X80	0.690	0.690	0.690	0.690	0.690
X81	0.123	0.123	0.123	0.123	0.123
X82	0.556	0.556	0.556	0.556	0.556
X83	0.889	0.889	0.889	0.889	0.889
X84	0.201	0.201	0.201	0.201	0.201
X85	0.734	0.734	0.734	0.734	0.734
X86	0.467	0.467	0.467	0.467	0.467
X87	0.900	0.900	0.900	0.900	0.900
X88	0.312	0.312	0.312	0.312	0.312
X89	0.645	0.645	0.645	0.645	0.645
X90	0.178	0.178	0.178	0.178	0.178
X91	0.511	0.511	0.511	0.511	0.511
X92	0.844	0.844	0.844	0.844	0.844
X93	0.277	0.277	0.277	0.277	0.277
X94	0.710	0.710	0.710	0.710	0.710
X95	0.401	0.401	0.401	0.401	0.401
X96	0.934	0.934	0.934	0.934	0.934
X97	0.367	0.367	0.367	0.367	0.367
X98	0.690	0.690	0.690	0.690	0.690
X99	0.123	0.123	0.123	0.123	0.123
X100	0.556	0.556	0.556	0.556	0.556

TABLE VIII

SAMPLE CALCULATION OF NOMINAL THICKNESS UNDER

STRESSWAVE MULTIPLIER

TOP SURFACE

ANGLE OF ATTACK = 0.0°

STATION 1

 $W = 3.67 \times 10^6$

Z	$y/$	v/v	$1 - v/v$	$v/v(1 - v/v)$	W	$f(\theta)$
.031	1.0	.992	.008	.00796	1	.00796
.306	0.9	.989	.011	.01057	1	.01318
.272	0.8	.981	.019	.01563	2	.03726
.238	0.7	.960	.040	.05440	1	.22560
.204	0.6	.870	.130	.1131	2	.22620
.170	0.5	.783	.217	.1691	1	.67640
.136	0.4	.676	.324	.2180	2	.13600
.0102	0.3	.610	.390	.2379	1	.95160
.0068	0.2	.490	.510	.2499	2	.19980
.0031	0.1	.250	.750	.1875	1	.75000
	0.0	0	0	0	1	0

$$\theta = \frac{f(\theta)_{station}}{3} = \frac{(1)(3.8512)}{3} = .128373$$

$$\theta = \theta / \dots \theta = (.128373)(.031) = .0039655$$

$$H = \theta / \theta = \frac{.0100}{.0039655} = 2.290$$

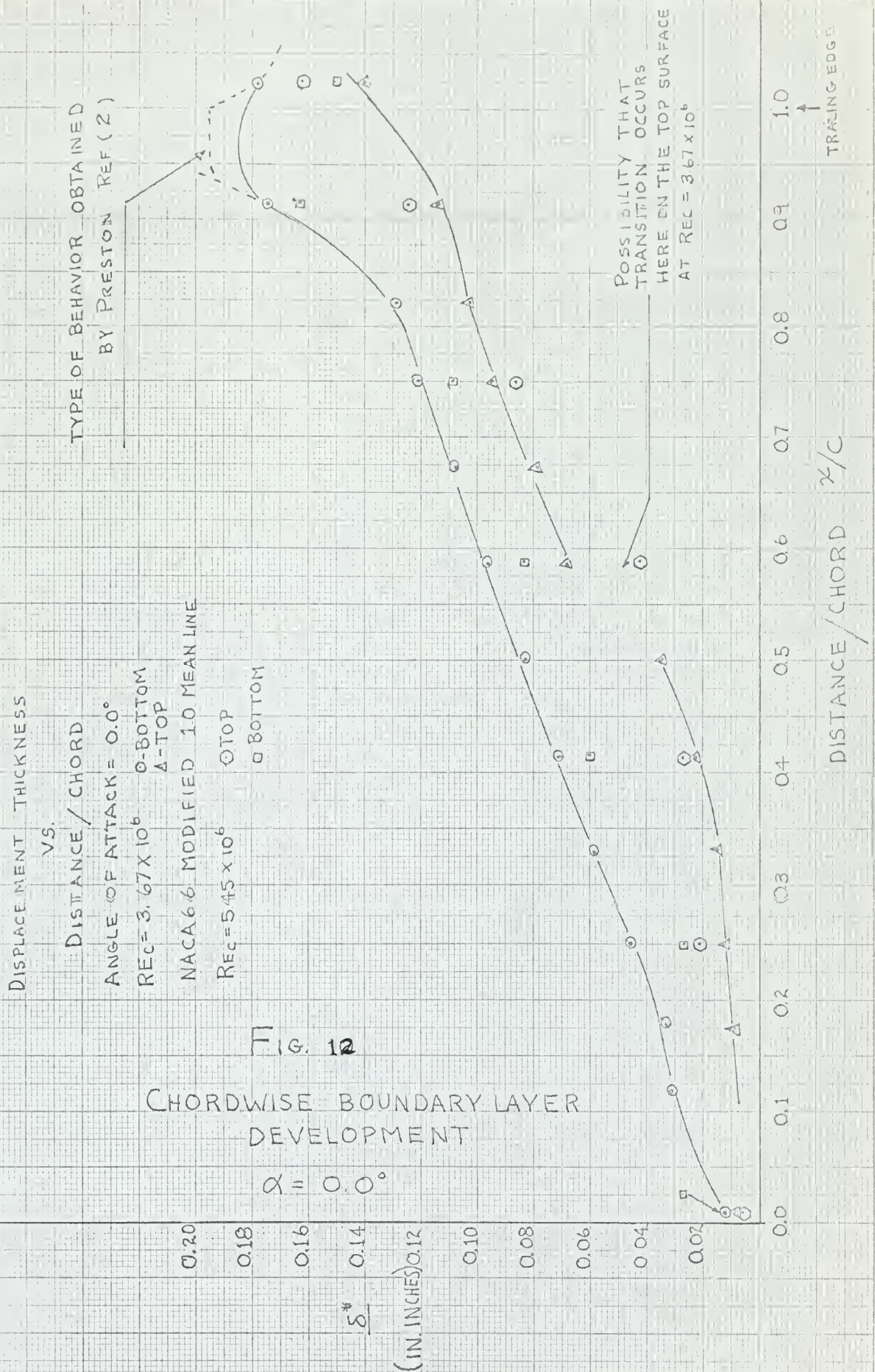
APPENDIX

TABLE 1. SUMMARY OF DATA FOR THE STUDY

TABLE 1. SUMMARY OF DATA FOR THE STUDY

Study 1: Summary of Data		Study 2: Summary of Data				
Age	Sex	Height (cm)	Weight (kg)	Age	Sex	Height (cm)
18-24	M	175.0	75.0	25-34	M	175.0
25-34	F	165.0	60.0	35-44	F	165.0
35-44	M	175.0	75.0	45-54	M	175.0
45-54	F	165.0	60.0	55-64	F	165.0
55-64	M	175.0	75.0	65-74	M	175.0
65-74	F	165.0	60.0	75-84	F	165.0
75-84	M	175.0	75.0	85-94	M	175.0
85-94	F	165.0	60.0	95-104	F	165.0
105-114	M	175.0	75.0	115-124	M	175.0
125-134	F	165.0	60.0	135-144	F	165.0
145-154	M	175.0	75.0	155-164	M	175.0
165-174	F	165.0	60.0	175-184	F	165.0
185-194	M	175.0	75.0	195-204	M	175.0
205-214	F	165.0	60.0	215-224	F	165.0
225-234	M	175.0	75.0	235-244	M	175.0
245-254	F	165.0	60.0	255-264	F	165.0
265-274	M	175.0	75.0	275-284	M	175.0
285-294	F	165.0	60.0	295-304	F	165.0
305-314	M	175.0	75.0	315-324	M	175.0
325-334	F	165.0	60.0	335-344	F	165.0
345-354	M	175.0	75.0	355-364	M	175.0
365-374	F	165.0	60.0	375-384	F	165.0
385-394	M	175.0	75.0	395-404	M	175.0
405-414	F	165.0	60.0	415-424	F	165.0
425-434	M	175.0	75.0	435-444	M	175.0
445-454	F	165.0	60.0	455-464	F	165.0
465-474	M	175.0	75.0	475-484	M	175.0
485-494	F	165.0	60.0	495-504	F	165.0
505-514	M	175.0	75.0	515-524	M	175.0
525-534	F	165.0	60.0	535-544	F	165.0
545-554	M	175.0	75.0	555-564	M	175.0
565-574	F	165.0	60.0	575-584	F	165.0
585-594	M	175.0	75.0	595-604	M	175.0
605-614	F	165.0	60.0	615-624	F	165.0
625-634	M	175.0	75.0	635-644	M	175.0
645-654	F	165.0	60.0	655-664	F	165.0
665-674	M	175.0	75.0	675-684	M	175.0
685-694	F	165.0	60.0	695-704	F	165.0
705-714	M	175.0	75.0	715-724	M	175.0
725-734	F	165.0	60.0	735-744	F	165.0
745-754	M	175.0	75.0	755-764	M	175.0
765-774	F	165.0	60.0	775-784	F	165.0
785-794	M	175.0	75.0	795-804	M	175.0
805-814	F	165.0	60.0	815-824	F	165.0
825-834	M	175.0	75.0	835-844	M	175.0
845-854	F	165.0	60.0	855-864	F	165.0
865-874	M	175.0	75.0	875-884	M	175.0
885-894	F	165.0	60.0	895-904	F	165.0
905-914	M	175.0	75.0	915-924	M	175.0
925-934	F	165.0	60.0	935-944	F	165.0
945-954	M	175.0	75.0	955-964	M	175.0
965-974	F	165.0	60.0	975-984	F	165.0
985-994	M	175.0	75.0	995-1004	M	175.0
1005-1014	F	165.0	60.0	1015-1024	F	165.0
1025-1034	M	175.0	75.0	1035-1044	M	175.0
1045-1054	F	165.0	60.0	1055-1064	F	165.0
1065-1074	M	175.0	75.0	1075-1084	M	175.0
1085-1094	F	165.0	60.0	1095-1104	F	165.0
1105-1114	M	175.0	75.0	1115-1124	M	175.0
1125-1134	F	165.0	60.0	1135-1144	F	165.0
1145-1154	M	175.0	75.0	1155-1164	M	175.0
1165-1174	F	165.0	60.0	1175-1184	F	165.0
1185-1194	M	175.0	75.0	1195-1204	M	175.0
1205-1214	F	165.0	60.0	1215-1224	F	165.0
1225-1234	M	175.0	75.0	1235-1244	M	175.0
1245-1254	F	165.0	60.0	1255-1264	F	165.0
1265-1274	M	175.0	75.0	1275-1284	M	175.0
1285-1294	F	165.0	60.0	1295-1304	F	165.0
1305-1314	M	175.0	75.0	1315-1324	M	175.0
1325-1334	F	165.0	60.0	1335-1344	F	165.0
1345-1354	M	175.0	75.0	1355-1364	M	175.0
1365-1374	F	165.0	60.0	1375-1384	F	165.0
1385-1394	M	175.0	75.0	1395-1404	M	175.0
1405-1414	F	165.0	60.0	1415-1424	F	165.0
1425-1434	M	175.0	75.0	1435-1444	M	175.0
1445-1454	F	165.0	60.0	1455-1464	F	165.0
1465-1474	M	175.0	75.0	1475-1484	M	175.0
1485-1494	F	165.0	60.0	1495-1504	F	165.0
1505-1514	M	175.0	75.0	1515-1524	M	175.0
1525-1534	F	165.0	60.0	1535-1544	F	165.0
1545-1554	M	175.0	75.0	1555-1564	M	175.0
1565-1574	F	165.0	60.0	1575-1584	F	165.0
1585-1594	M	175.0	75.0	1595-1604	M	175.0
1605-1614	F	165.0	60.0	1615-1624	F	165.0
1625-1634	M	175.0	75.0	1635-1644	M	175.0
1645-1654	F	165.0	60.0	1655-1664	F	165.0
1665-1674	M	175.0	75.0	1675-1684	M	175.0
1685-1694	F	165.0	60.0	1695-1704	F	165.0
1705-1714	M	175.0	75.0	1715-1724	M	175.0
1725-1734	F	165.0	60.0	1735-1744	F	165.0
1745-1754	M	175.0	75.0	1755-1764	M	175.0
1765-1774	F	165.0	60.0	1775-1784	F	165.0
1785-1794	M	175.0	75.0	1795-1804	M	175.0
1805-1814	F	165.0	60.0	1815-1824	F	165.0
1825-1834	M	175.0	75.0	1835-1844	M	175.0
1845-1854	F	165.0	60.0	1855-1864	F	165.0
1865-1874	M	175.0	75.0	1875-1884	M	175.0
1885-1894	F	165.0	60.0	1895-1904	F	165.0
1905-1914	M	175.0	75.0	1915-1924	M	175.0
1925-1934	F	165.0	60.0	1935-1944	F	165.0
1945-1954	M	175.0	75.0	1955-1964	M	175.0
1965-1974	F	165.0	60.0	1975-1984	F	165.0
1985-1994	M	175.0	75.0	1995-2004	M	175.0
2005-2014	F	165.0	60.0	2015-2024	F	165.0
2025-2034	M	175.0	75.0	2035-2044	M	175.0
2045-2054	F	165.0	60.0	2055-2064	F	165.0
2065-2074	M	175.0	75.0	2075-2084	M	175.0
2085-2094	F	165.0	60.0	2095-2104	F	165.0
2105-2114	M	175.0	75.0	2115-2124	M	175.0
2125-2134	F	165.0	60.0	2135-2144	F	165.0
2145-2154	M	175.0	75.0	2155-2164	M	175.0
2165-2174	F	165.0	60.0	2175-2184	F	165.0
2185-2194	M	175.0	75.0	2195-2204	M	175.0
2205-2214	F	165.0	60.0	2215-2224	F	165.0
2225-2234	M	175.0	75.0	2235-2244	M	175.0
2245-2254	F	165.0	60.0	2255-2264	F	165.0
2265-2274	M	175.0	75.0	2275-2284	M	175.0
2285-2294	F	165.0	60.0	2295-2304	F	165.0
2305-2314	M	175.0	75.0	2315-2324	M	175.0
2325-2334	F	165.0	60.0	2335-2344	F	165.0
2345-2354	M	175.0	75.0	2355-2364	M	175.0
2365-2374	F	165.0	60.0	2375-2384	F	165.0
2385-2394	M	175.0	75.0	2395-2404	M	175.0
2405-2414	F	165.0	60.0	2415-2424	F	165.0
2425-2434	M	175.0	75.0	2435-2444	M	175.0
2445-2454	F	165.0	60.0	2455-2464	F	165.0
2465-2474	M	175.0	75.0	2475-2484	M	175.0
2485-2494	F	165.0	60.0	2495-2504	F	165.0
2505-2514	M	175.0	75.0	2515-2524	M	175.0
2525-2534	F	165.0	60.0	2535-2544	F	165.0
2545-2554	M	175.0	75.0	2555-2564	M	175.0
2565-2574	F	165.0	60.0	2575-2584	F	165.0
2585-2594	M	175.0	75.0	2595-2604	M	175.0
2605-2614	F	165.0	60.0	2615-2624	F	165.0
2625-2634	M	175.0	75.0	2635-2644	M	175.0
2645-2654	F	165.0	60.0	2655-2664	F	165.0
2665-2674	M	175.0	75.0	2675-2684	M	175.0
2685-2694	F	165.0	60.0	2695-2704	F	165.0
2705-2714	M	175.0	75.0	2715-2724	M	175.0
2725-2734	F	165.0	60.0	2735-2744	F	165.0
2745-2754	M	175.0	75.0	2755-2764	M	175.0
2765-2774	F	165.0	60.0	2775-2784	F	165.0
2785-2794	M	175.0	75.0	2795-2804	M	175.0
2805-2814	F	165.0	60.0	2815-2824	F	165.0
2825-2834	M	175.0	75.0	2835-2844	M	175.0
2845-2854	F	165.0	60.0	2855-2864	F	165.0
2865-2874	M	175.0	75.0	2875-2884	M	175.0
2885-2894	F	165.0	60.0	2895-2904	F	165.0
2905-2914	M	175.0	75.0	2915-2924	M	175.0
2925-2934	F	165.0	60.0	2935-2944	F	165.0
2945-2954	M	175.0	75.0	2955-2964	M	175.0
2965-2974	F	165.0	60.0	2975-2984	F	165.0
2985-2994	M	175.0	75.0	2995-3004	M	175.0
3005-3014	F	165.0	60.0	3015-3024	F	165.0
3025-3034	M	175.0	75.0	3035-3044	M	175.0
3045-3054	F	165.0	60.0	3055-3064	F	165.0
3065-3074	M	175.0	75.0	3075-3084	M	175.0
3085-3094	F	165.0	60.0	3095-3104	F	165.0
3105-3114	M	175.0	75.0	3115-3124	M	175.0
3125-3134	F	165.0	60.0	3135-3144	F	165.0
3145-3154	M	175.0	75.0	3155-3164	M	175.0
3165-3174	F	165.0	60.0	3175-3184	F	165.0
3185-3194	M	175.0	75.0	3195-3204	M	175.0
3205-3214	F	165.0	60.0	3215-3224	F	165.0
3225-3234	M	175.0	75.0	3235-3244	M	175.0
3245-3254	F	165.0	60.0	3255-3264	F	165.0
3265-3274	M	175.0	75.0	3275-3284	M	175.0
3285-3294	F	165.0	60.0	3295-3304	F	165.0
3305-3314	M	175.0	75.0			

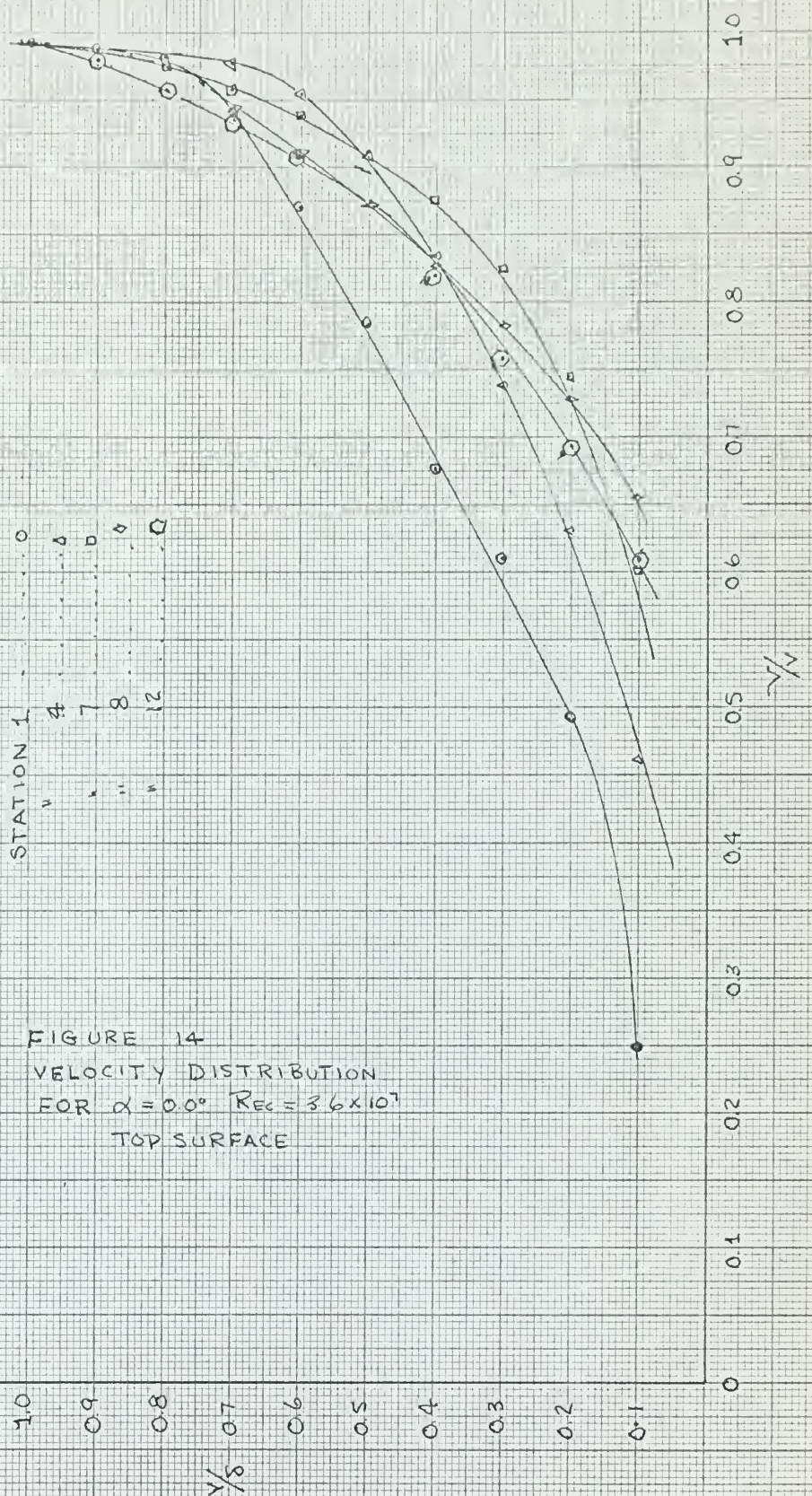
APPENDIX 3
CHARTS OF DATA



PLOT OF V/V VERSUS Y/δ
 FOR NOMINAL $\alpha = 0.0^\circ$
 $Re = 3.61 \times 10^6$
 TOP SURFACE

STATION 1	0
"	4
"	7
"	8
"	12
"	Q

FIGURE 14
 VELOCITY DISTRIBUTION
 FOR $\alpha = 0.0^\circ$ $Re = 3.6 \times 10^7$
 TOP SURFACE



PLOT OF V/V_∞ VERSUS Y/δ

FOR NOMINAL $\alpha = 0.0^\circ$

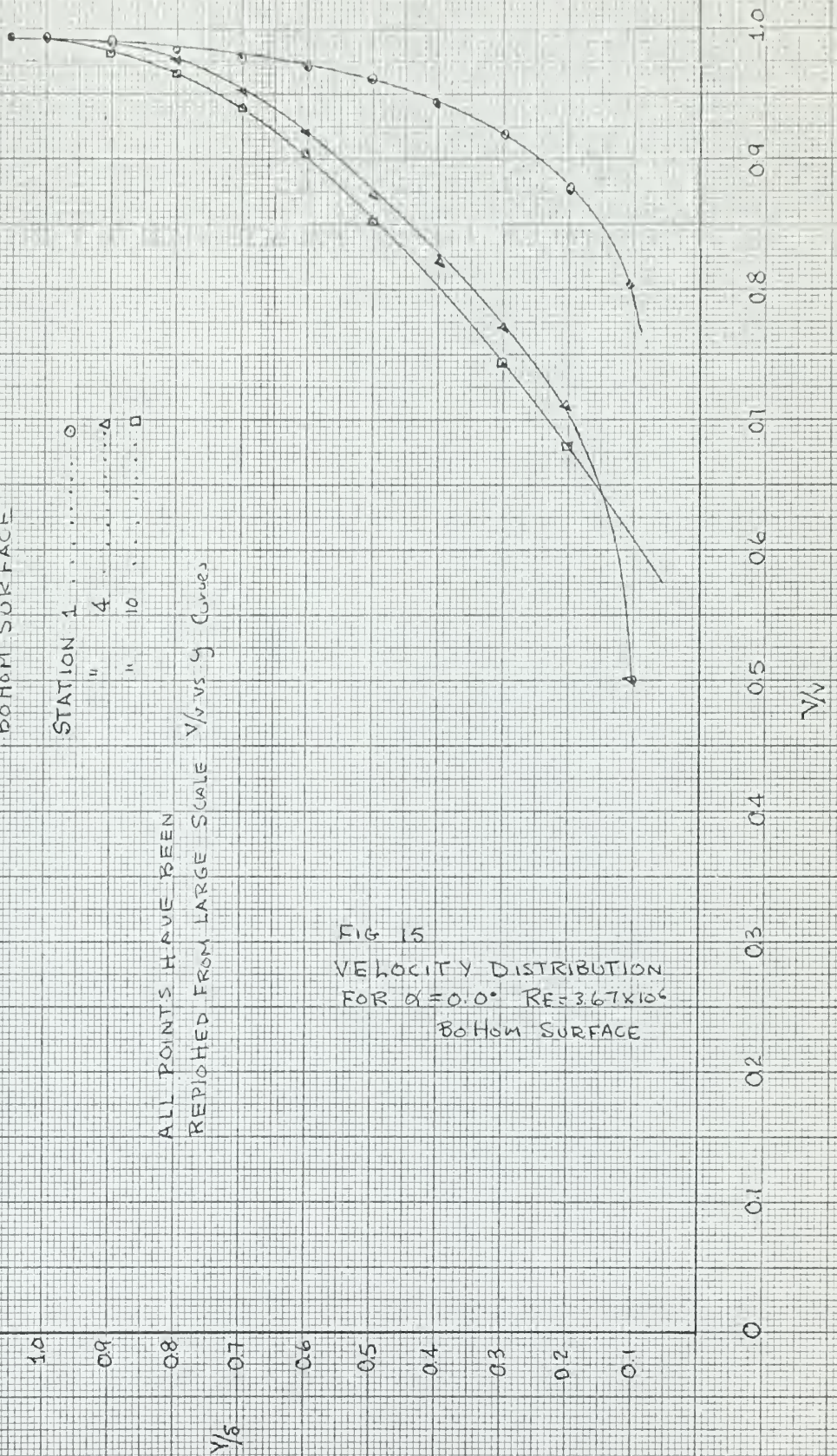
$Re = 3.67 \times 10^6$

BOTTOM SURFACE

STATION 1 0
 " 4 Δ
 " 10 \square

ALL POINTS HAVE BEEN
 REPOSITIONED FROM LARGE SCALE
 V/V_∞ VS y CURVES

FIG 15
 VELOCITY DISTRIBUTION
 FOR $\alpha = 0.0^\circ$ $Re = 3.67 \times 10^6$
 BOTTOM SURFACE



PLOT OF V/V_∞ VERSUS Y/δ
 FOR NOMINAL $\alpha = 2.0^\circ$
 $Re = 3.67 \times 10^6$

TOP SURFACE

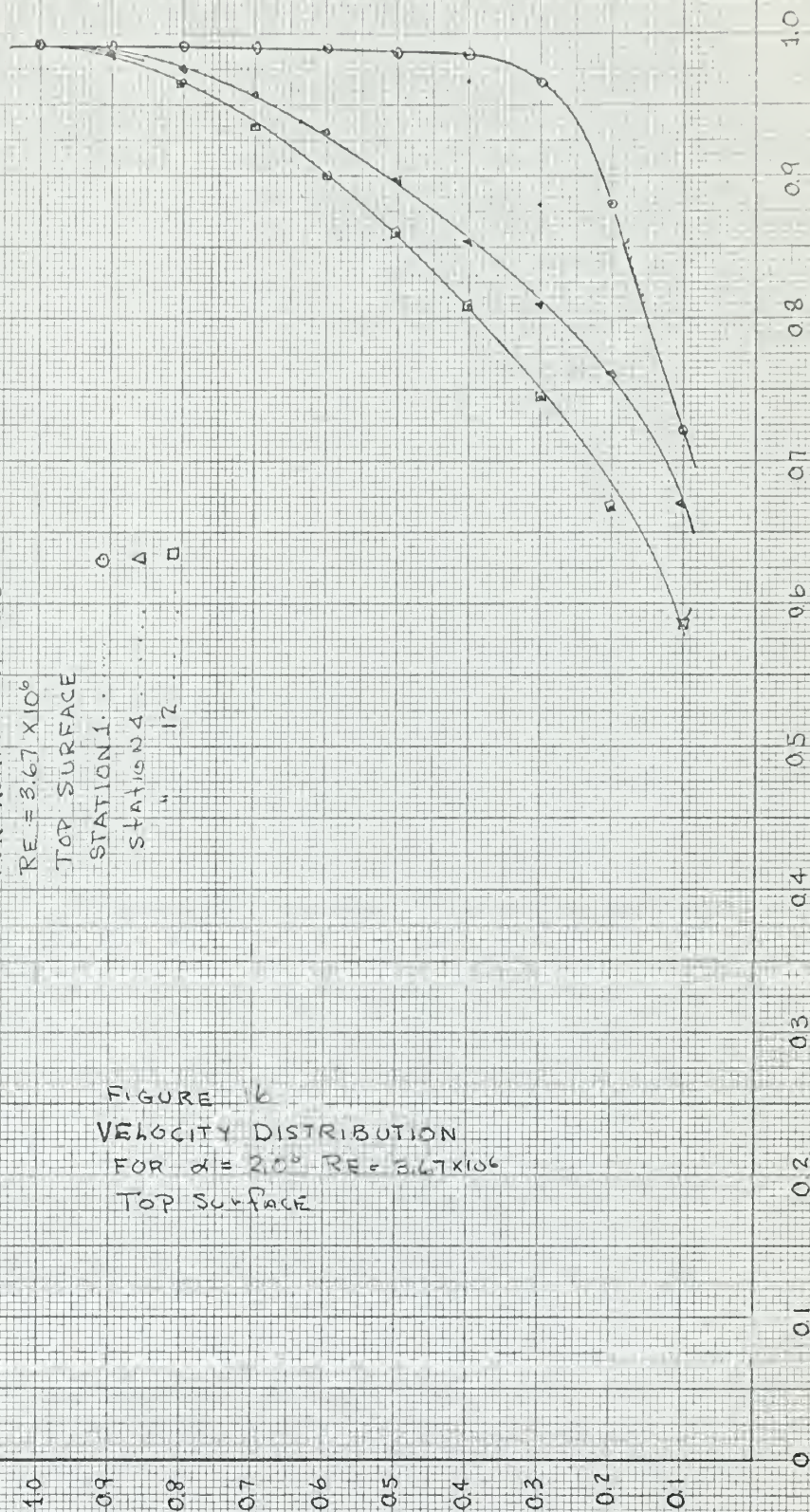
STATION 1

STATION 2

" 12

○
 △
 □

FIGURE 16
 VELOCITY DISTRIBUTION
 FOR $\alpha = 2.0^\circ$ $Re = 3.67 \times 10^6$
 TOP SURFACE



PLOT OF y/δ VERSUS y/δ

FOR

NOMINAL ANGLE OF ATTACK = 2.0°

$Re_c = 3.67 \times 10^6$ BOTTOM SURFACE

STATION 2

" 6

" 8

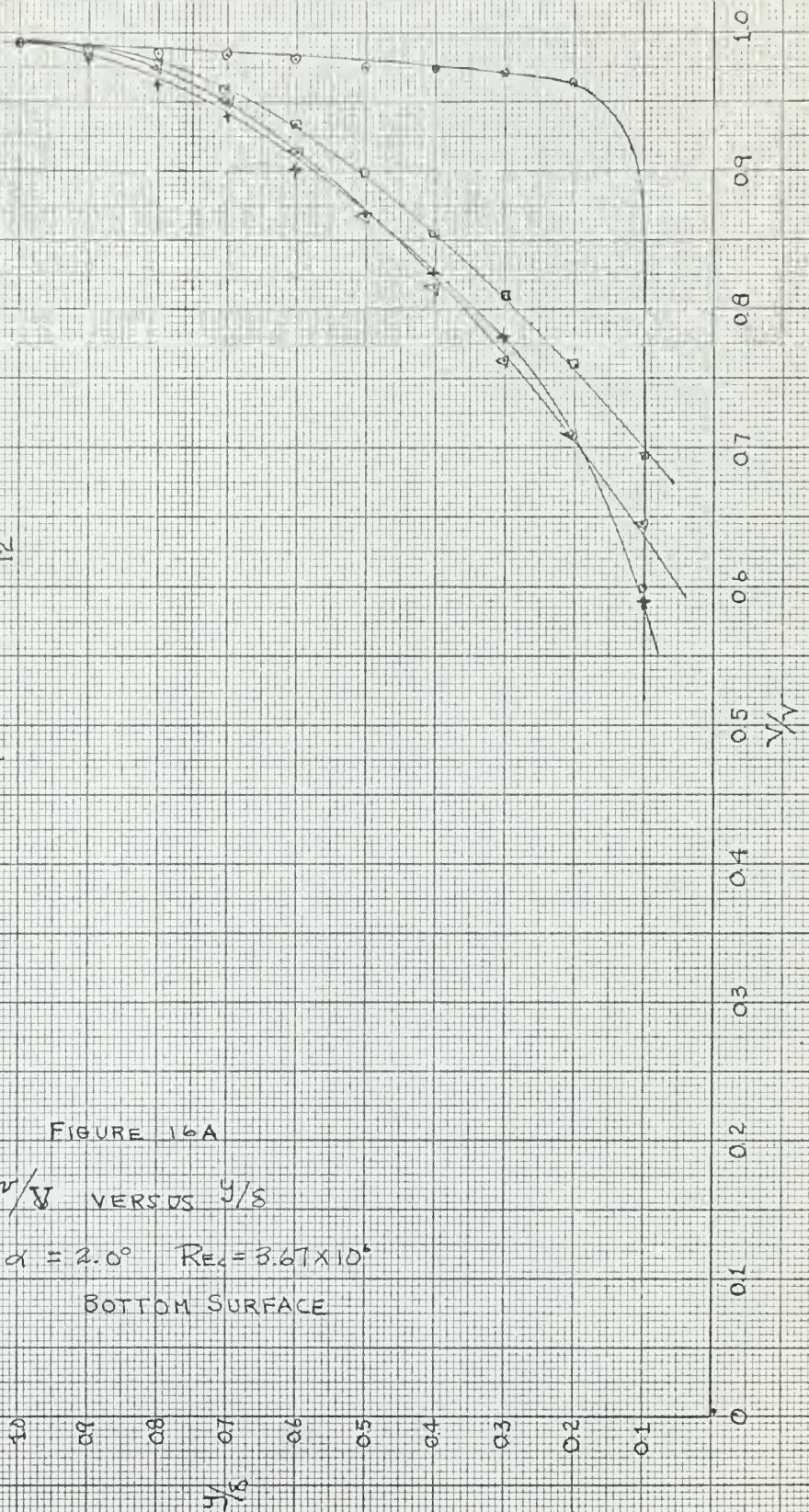
" 12

FIGURE 16A

v/δ VERSUS y/δ

$\alpha = 2.0^\circ$ $Re_c = 3.67 \times 10^6$

BOTTOM SURFACE



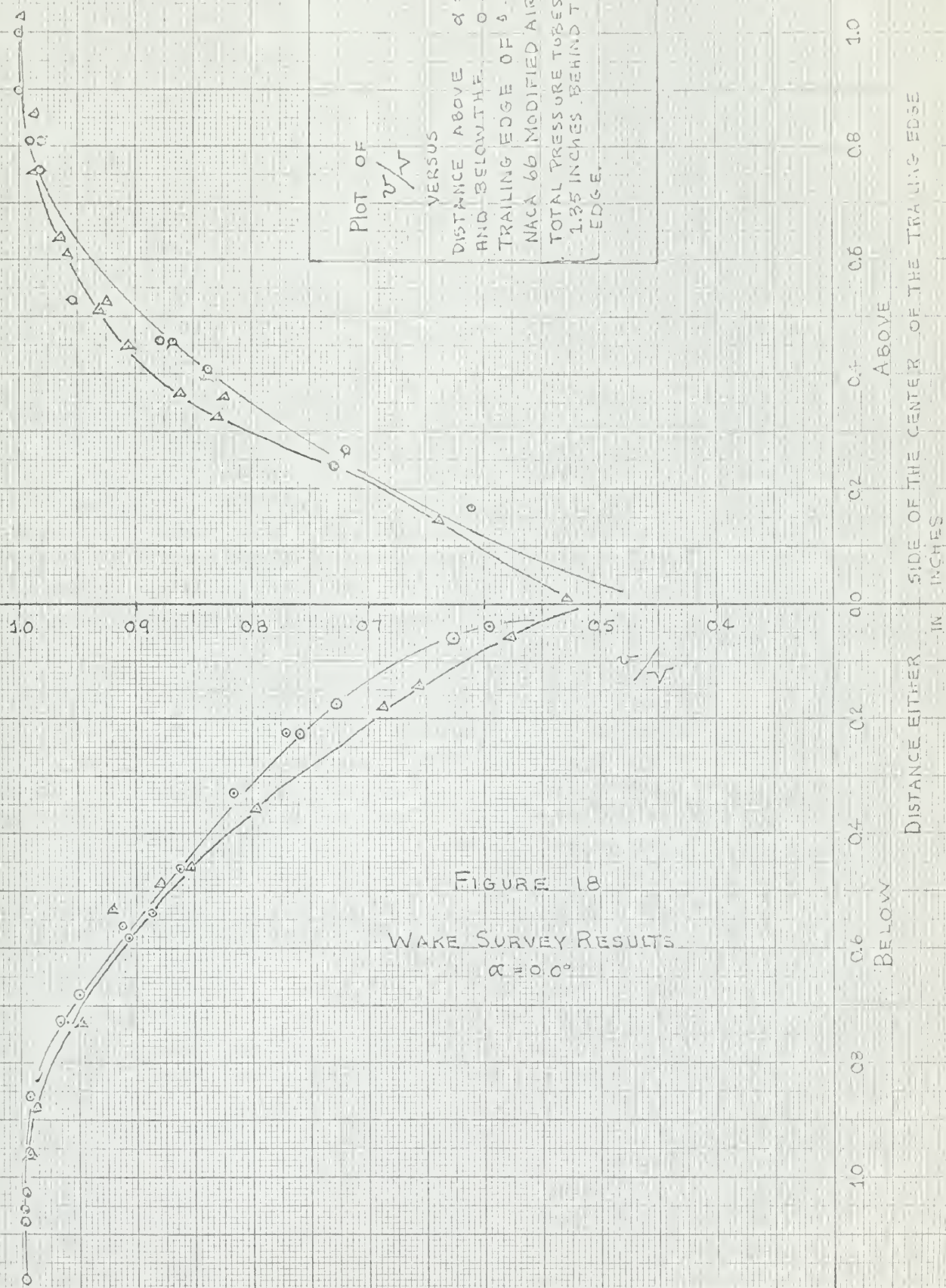
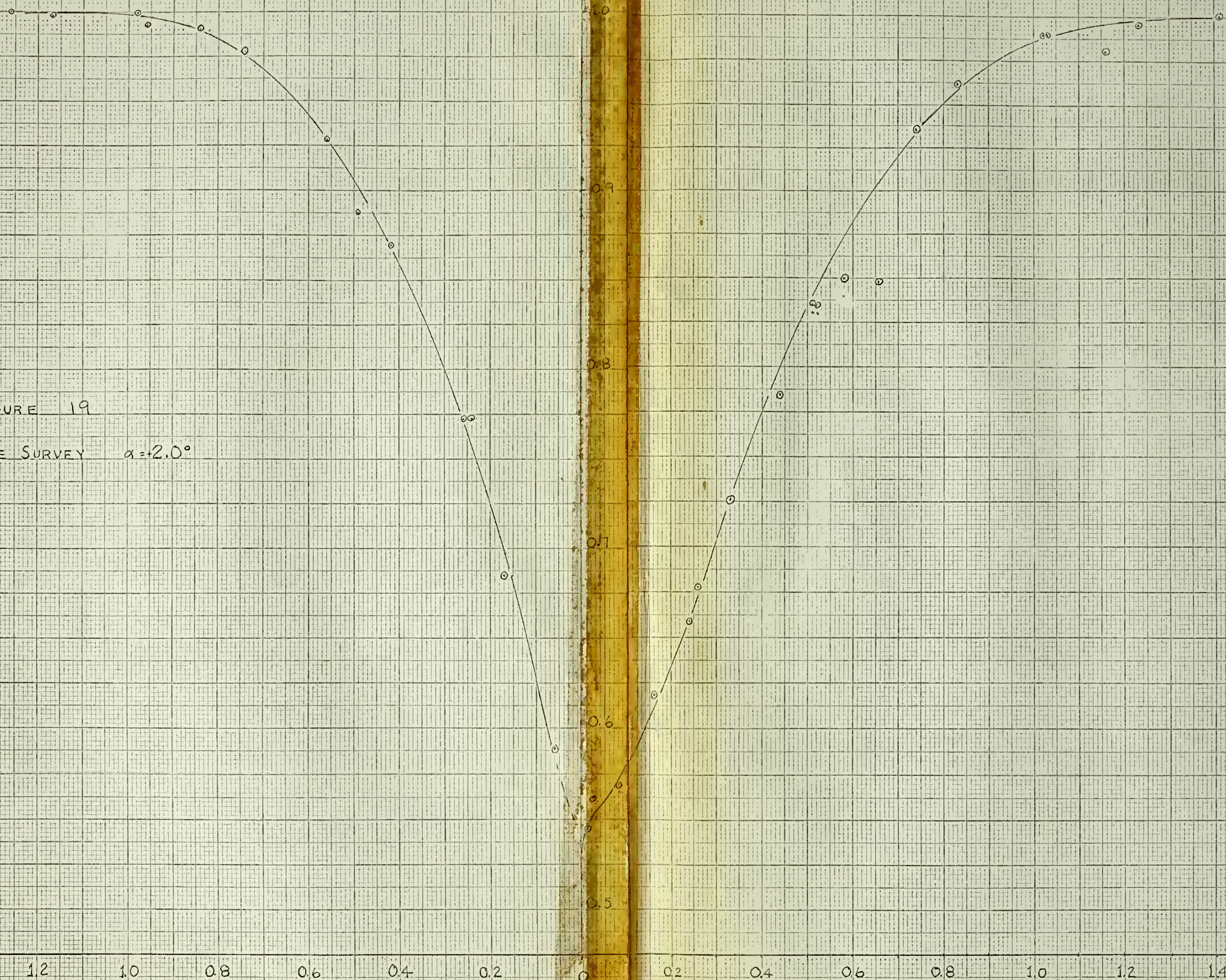


FIGURE 19
WAKE SURVEY $\alpha = 2.0^\circ$

1.6 1.4 1.2 1.0 0.8 0.6 0.4 0.2 0 0.2 0.4 0.6 0.8 1.0 1.2 1.4 1.6

1.0
0.9
0.8
0.7
0.6
0.5





PRESSURE COEFFICIENT
VERSUS

FRACTION OF CHORD

$Re = 3.67 \times 10^6$ $\alpha = 0.0^\circ$

MODIFIED NACA 66 FOIL

Δ - PRESSURES MEASURED USING SURFACE TAPS

\circ - PRESSURES MEASURED USING STATIC TUBE ON RAKE 1.1 INCHES ABOVE SURFACE

BOTTOM SURFACE

TOP SURFACE

FIGURE 20

EXPERIMENTAL PRESSURE
DISTRIBUTION ALONG CHORD
 $\alpha = 0.0^\circ$ $Re = 3.6 \times 10^6$

0.2

0.1

0

-0.1

-0.2

$\frac{P - P_\infty}{\frac{1}{2} \rho V_\infty^2}$

10.0

9.0

8.0

7.0

6.0

5.0

4.0

3.0

2.0

1.0

PRESSURE COEFFICIENT
VERSUS
FRACTION OF CHORD LENGTH

$Re_c = 3.67 \times 10^6$ $\alpha = 0.0^\circ$

MODIFIED NACA 66 AIRFOIL
TOP SURFACE ONLY

NOTE: ALL READINGS TAKEN FROM
SURFACE STATIC TAPS WITH
THE BOUNDARY LAYER RAKE
IN VARIOUS POSITIONS AS FOLLOW:

SYMBOL	RAKE STA.
□	3
○	4
△	5
●	6
◊	9

X/L (FRACTION OF CHORD LENGTH)

FIG 21

TOP SURFACE PRESSURES
WITH THE RAKE IN PLACE

$\frac{P - P_\infty}{\frac{1}{2} \rho V_\infty^2}$

0.1

-0.1

-0.2

-0.3

-0.3

0

0.1

0.2

0.3

0.4

0.5

0.6

0.7

0.8

0.9

1.0

1.1

1.2

1.3

1.4

1.5

1.6

1.7

1.8

1.9

2.0

2.1

2.2

2.3

2.4

2.5

2.6

2.7

2.8

2.9

3.0

3.1

3.2

3.3

3.4

3.5

3.6

3.7

3.8

3.9

4.0

4.1

4.2

4.3

4.4

4.5

4.6

4.7

4.8

4.9

5.0

5.1

5.2

5.3

5.4

5.5

5.6

5.7

5.8

5.9

6.0

6.1

6.2

6.3

6.4

6.5

6.6

6.7

6.8

6.9

7.0

7.1

7.2

7.3

7.4

7.5

7.6

7.7

7.8

7.9

8.0

8.1

8.2

8.3

8.4

8.5

8.6

8.7

8.8

8.9

9.0

9.1

9.2

9.3

9.4

9.5

9.6

9.7

9.8

9.9

10.0

10.1

10.2

10.3

10.4

10.5

10.6

10.7

10.8

10.9

11.0

11.1

11.2

11.3

11.4

11.5

11.6

11.7

11.8

11.9

12.0

12.1

12.2

12.3

12.4

12.5

12.6

12.7

12.8

12.9

13.0

13.1

13.2

13.3

13.4

13.5

13.6

13.7

13.8

13.9

14.0

14.1

14.2

14.3

14.4

14.5

14.6

14.7

14.8

14.9

15.0

15.1

15.2

15.3

15.4

15.5

15.6

15.7

15.8

15.9

16.0

16.1

16.2

16.3

16.4

16.5

16.6

16.7

16.8

16.9

17.0

17.1

17.2

17.3

17.4

17.5

17.6

17.7

17.8

17.9

18.0

18.1

18.2

18.3

18.4

18.5

18.6

18.7

18.8

18.9

19.0

19.1

19.2

19.3

19.4

19.5

19.6

19.7

19.8

19.9

20.0

20.1

20.2

20.3

20.4

20.5

20.6

20.7

20.8

20.9

21.0

21.1

21.2

21.3

21.4

21.5

21.6

21.7

21.8

21.9

22.0

22.1

22.2

22.3

22.4

22.5

22.6

22.7

22.8

22.9

23.0

23.1

23.2

23.3

23.4

23.5

23.6

23.7

23.8

23.9

24.0

24.1

24.2

24.3

24.4

24.5

24.6

24.7

24.8

24.9

25.0

25.1

25.2

25.3

25.4

25.5

25.6

25.7

25.8

25.9

26.0

26.1

26.2

26.3

26.4

26.5

26.6

26.7

26.8

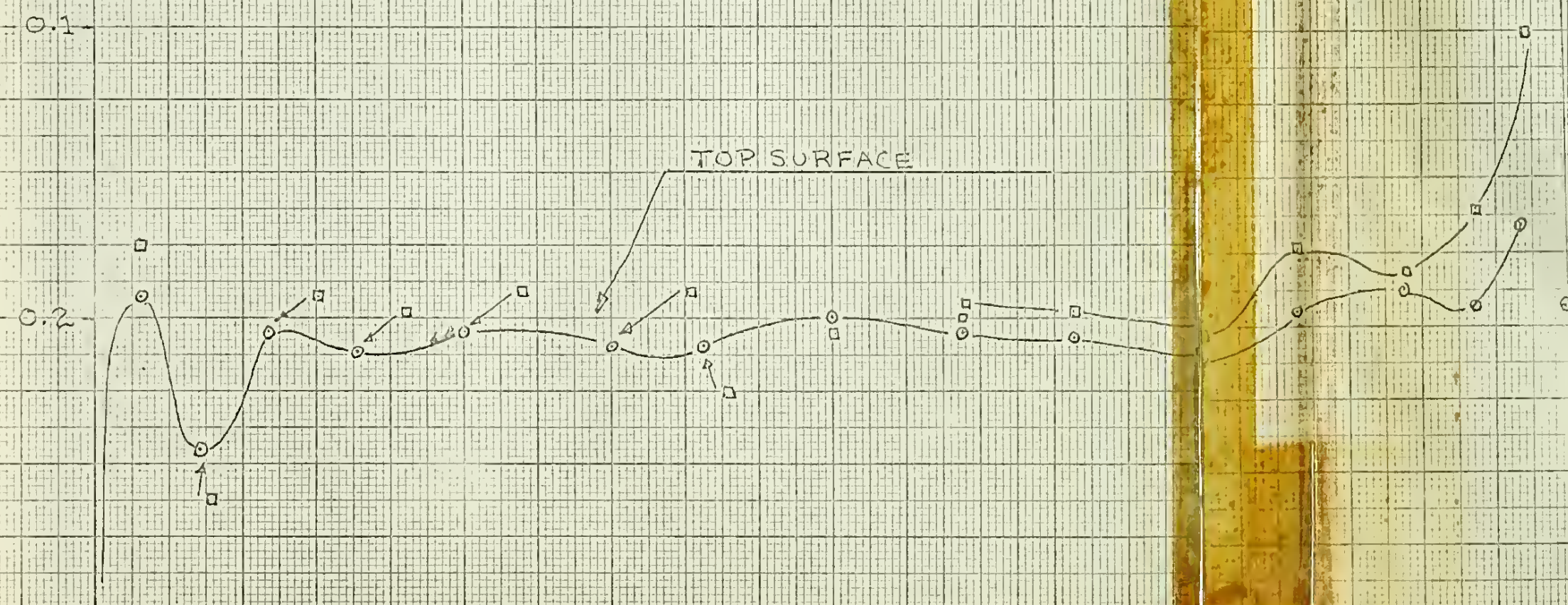
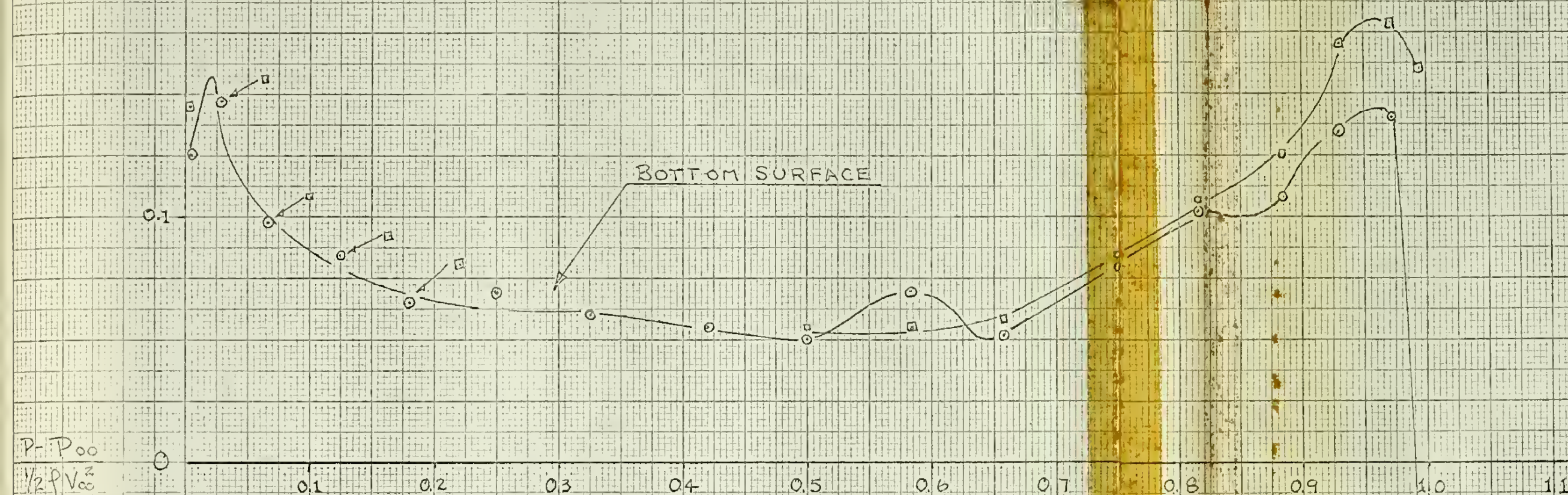
26.9

FIGURE 22 PRESSURE COEFFICIENT VS CHORD
POTENTIAL FLOW

PRESSURE COEFFICIENT
VERSUS
CHORDWISE DISTANCE/CHORD
FOR A MODIFIED NACA 66 FOIL
NOMINAL ANGLE OF ATTACK = 0.0°
 $Re = 3.67 \times 10^6$

RESULTS OF POTENTIAL FLOW:

\circ AROUND FOIL CORRECTED FOR $\delta^* + \alpha$
 \square AROUND ORIGINAL FOIL

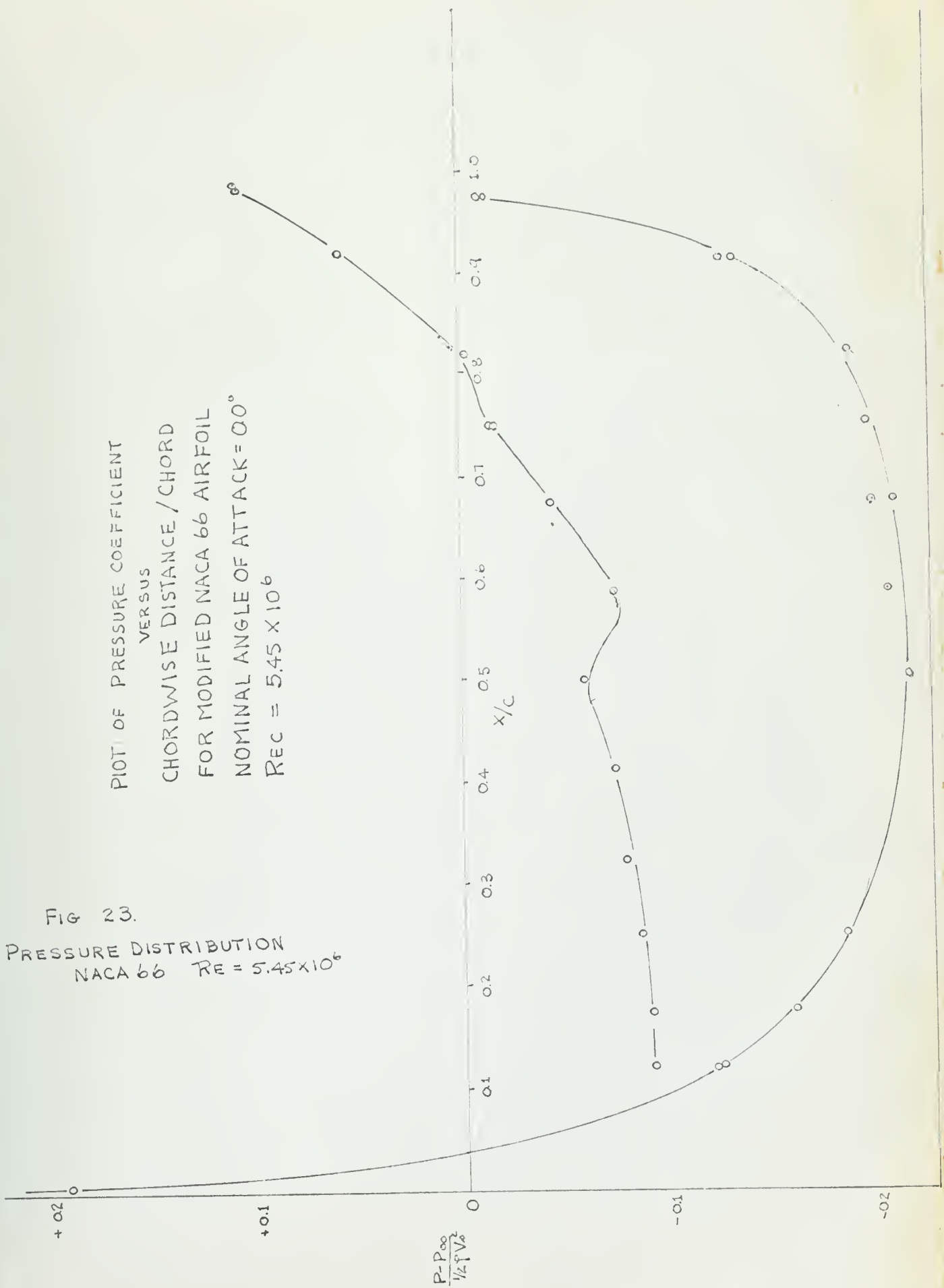


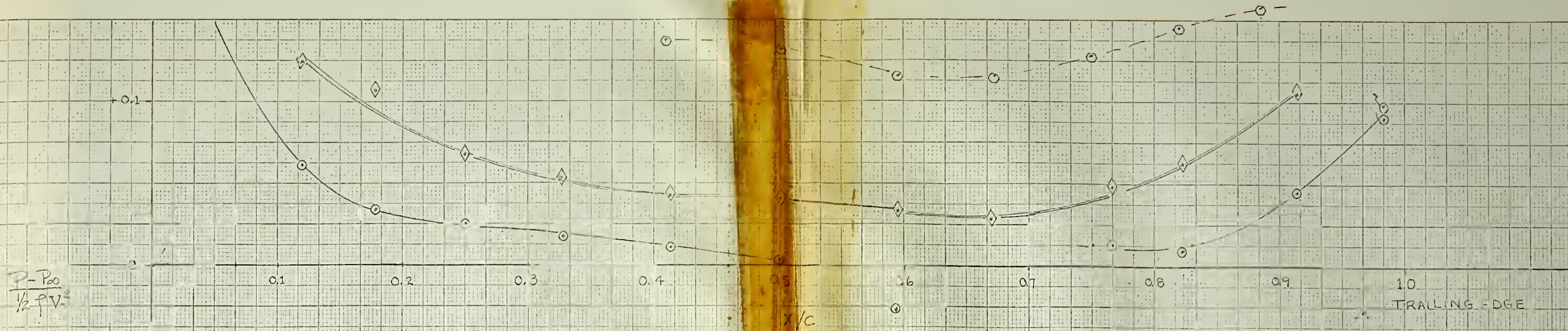


PLOT OF PRESSURE COEFFICIENT
 VERSUS
 CHORDWISE DISTANCE / CHORD
 FOR MODIFIED NACA 66 AIRFOIL
 NOMINAL ANGLE OF ATTACK = 00°
 $Re = 5.45 \times 10^6$

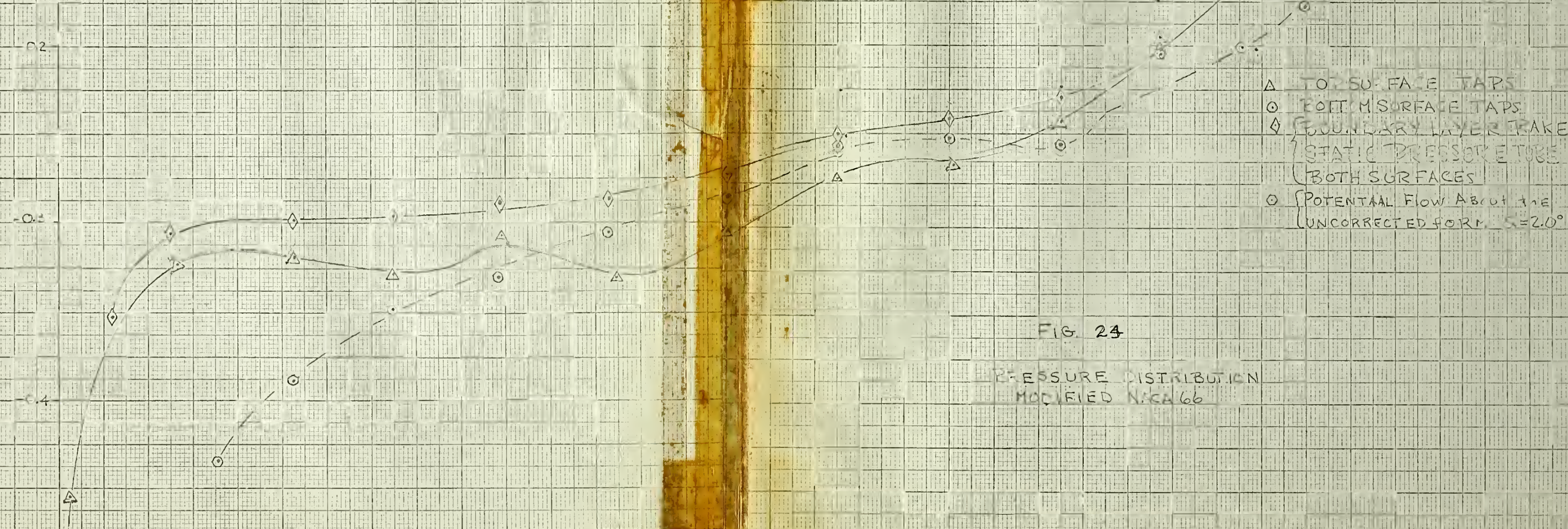
FIG 23.

PRESSURE DISTRIBUTION
 NACA 66 $Re = 5.45 \times 10^6$





PLOT OF PRESSURE COEFFICIENT
VERSUS
CHORDWISE DISTANCE/CHORD LENGTH
FOR A MODIFIED NACA-66 FOIL
NOMINAL ANGLE OF ATTACK = 2.0°
 $Re_c = 3.67 \times 10^6$ $Cl = 0.3335$ MEASURED



- Δ TOP SURFACE TAPS
- \circ BOTTOM SURFACE TAPS
- \diamond BOUNDARY LAYER TAP
- $\{$ STATIC PRESSURE TUBE
- $\{$ BOTH SURFACES
- \circ $\{$ POTENTIAL FLOW ABOUT THE
- $\{$ UNCORRECTED FORM $\alpha = 2.0^\circ$

FIG. 24

PRESSURE DISTRIBUTION
MODIFIED NACA 66



$$\frac{P - P_{\infty}}{\frac{1}{2} \rho V^2}$$

0.1

0.2

0.3

0.4

0.5

0.6

0.7

0.8

0.9

1.0

 x/c

PLOT OF PRESSURE COEFFICIENT

VERSUS

CHORDWISE DISTANCE / CHORD LENGTH

FOR NACA 66 MODIFIED $\alpha = 2.0^\circ$ $Re = 3.67 \times 10^6$

POTENTIAL THEORY RESULTS FOR

 $\alpha = 1.956^\circ$ FORM CORRECTED FOR δ^* AND LAMINAR $\alpha = 1.200^\circ$ " " " " " " $\alpha = 1.200^\circ$ UNCORRECTED

FIG. 25

POTENTIAL FLOW PRESSURE
COEFFICIENTS NOMINAL $\alpha = 2.0^\circ$

TOP SURFACE

SHAPE FACTOR AND MOMENTUM THICKNESS
VERSUS

CHORDWISE DISTANCE / CHORD

FOR $\alpha = 0.0^\circ$

$Re_c = 5.45 \times 10^6$

TOP SURFACE ONLY

Δ - SHAPE FACTOR H

\circ - MOMENTUM THICKNESS



FIG 26

SHAPE FACTOR AND
MOMENTUM THICKNESS
VS.
CHORD

APPENDIX C

COMPUTER OUTPUTS

NON-DIMENSIONAL GEOMETRIC COEFFICIENTS

EDWARDS	ACA 66 MODIFIED IN INVISCID FLOW
AREA	= .022638
XBAR	= .474175
YBAR	= .009703
I(X,ABT LE)	= .000004
I(Y,ABT LE)	= .006391
I(XBAR)	= .000001
I(YBAR)	= .001301

thesE254

Prediction of boundary layer effects on



3 2768 001 90353 7

DUDLEY KNOX LIBRARY